Role of MICOS for mitochondrial morphology and function

Dissertation

for the award of the degree "Doctor rerum naturalium"

at the Georg-August-University Göttingen

within the doctoral program "Molecular Medicine"

of the Georg-August University School of Science (GAUSS)

submitted by

Tobias Müller

born in Alfeld (Leine)

Göttingen, 2019

Members of the Thesis Committee

Prof. Dr. Peter Rehling (Supervisor and First Referee)	University Medical Center Göttingen Institute for Cellular Biochemistry Göttingen, Germany
PD Dr. Olaf Jahn (Second Referee)	Proteomics Max-Planck Institute for Experimental Medicine Göttingen, Germany
Prof. Dr. Michael Meinecke	University Medical Center Göttingen Institute for Cellular Biochemistry Göttingen, Germany

Additional Members of the Examination Board

Prof. Dr. Stefan Jakobs	Department of Nanobiophotonics Max-Planck Institute for Biophysical Chemistry Göttingen, Germany
Dr. Alexander Stein	Membrane Protein Biochemistry Max-Planck Institute for Biophysical Chemistry Göttingen, Germany
Prof. Dr. Ralph Kehlenbach	University Medical Center Göttingen Institute for Molecular Biology Göttingen, Germany

Affidativ

Herewith I declare that I prepared my dissertation **"Role of MICOS for mitochdondrial morphology and function"** on my own and with no other sources and aids than quoted.

Göttingen, March 2019

Part of this thesis will be communicated in the following publication:

Callegari S., Müller T., Schulz C., Lenz C., Jans D. C., Wissel M., Opazi F., Rizzoli S. O., Jakobs S., Urlaub H., Rehling P., Deckers M. (2019). A MICOS-TIM22 association promotes mitochondrial carrier import in human mitochondria. *Journal of Molecular Biology* (submitted)

Acknowledgements

First of all I would like to thank my supervisor **Peter Rehling** for the opportunity to work in such an interesting and challenging field, for his relentless support throughout the project and his patience with me.

Furthemore **Michael Meinecke** and **Olaf Jahn** for being part of my thesis committee and interesting and constructive discussions during committee meetings. In addition **Ralph Kehlenbach**, **Stefan Jakobs** and **Henning Urlaub** for joining my extended examination board.

A very special gratitude to **Markus Deckers** for his never-ending support and cascade of ideas to forward this project. Various scientific and personal discussions together with his patience in frustrating moments were deeply appreciated.

A big thanks to my collaborators who provided essential data for this work. **Daniel C. Jans** and **Stefan Jakobs** for electron microscopy pictures and **Christof Lenz, Thierry Wasselin, Henning Urlaub** and **Monika Raabe** for the Mass-Spectrometry analysis and dealing with the various problems that occurred on the way to the final dataset.

Special thanks to all current and past members of the department. **Markus** and **Sylvie** for correcting my manuscript, dealing with my language skills and a nice collaboration on a wonderful publication. **Mirjam** for always making me laugh and lighten up many dark days and providing a plethora of evenings with nice food and good company. **Ridhima**, without whom I wouldn't have survived many frustrating lab days and was always providing cheer ups, food, tea, manuscript proof reading and great Doctor Who and Merlin moments. My labmates **Bettina**, **Abhishek**, **Natasha**, **Lioba** and **Magnus** in addition to various great students for creating a unique and crazy working environment. Special thanks to **David, Flo, Matt, Alex, Kathi, Moritz, Sabine, Frank, Cong, Arpita, Martina, Christin, 3x Lisa, Lena, Hussein, Rosi, Petra**

and so many more for enduring me the last couple of years in the lab.

People, who are more family than friends and supported me all my way along, the **Dödels** inclusive attachments, the **Knusperkäfer** and last but not least my whole **Hammer Style group**. I would not have managed without anyone of you!

Last and most importantly, **my family**. They supported me throughout all obstacles without questions and complain and no words can describe my gratefulness.

Contents

Abstract

Mitochondria are highly dynamic organelles with a distinct morphological membrane ultrastructure. The mayor protein complex responsible for the formation and maintenance of the inner mitochondrial membrane is the mitochondrial contact site and cristae organizing system (MICOS). This complex consists of 6 constituents in *Saccharomyces cerevisiae* and 7 in the mammalian system, with Mic60 and Mic10 being the core components. MICOS has been predominantly investigated in *S. cerevisiae* and studies in human cells have focussed mainly on MIC60.

In this study, a CRISPR/CAS9 mediated MIC10 knock-out cell-line was generated and further characterized. Herby MIC10 could be identified to be essential for forming and maintaining proper mitochondrial morphology in mammalian cells. However, the loss of inner membrane ultrastructure did not have an impact on mitochondrial function and health.

To better understand MICOS function in human, two different proximity biotinylation approaches were undertaken and compared to determine novel interaction partners. The first approach involved using an enhanced ascorbate C peroxidase APEX fused to MIC10 and the second approach made use of a promiscuous biotin ligase BioID2. The usage of the BioID2 enzyme proved to be more suitable since it already produced a distinct set of mutual interaction partners together with already known interaction partners. On the other hand, the active labelling reagent using the APEX enzyme proved to be more reactive than anticipated and would need a more thorough control system to identify background labelling.

Recent findings reported a connection between MICOS via Mic60 and protein translocation through the TOM complex and the MIA-pathway (von der Malsburg et al., 2011). In this study, a spatial connection between MICOS and the TIM23 complex mediated via Mic60 could be found. Performing import studies in two different yeast strains with impaired inner membrane ultrastructure *mic10*Δ and *atp20*Δ revealed, that independent from MICOS, proper inner mitochondrial membrane morphology is essential for efficient precursor protein translocation via the TIM23-complex. In contrast to the mammalian system, carrier import via the TIM22 complex was verified to be independent of morphological alterations in yeast, thus further confirming the immense evolutionary divergence between the human and yeast TIM22 carrier translocase.

1. Introduction

1.1. The eukaryotic cell

The basic building block of each living organism is the cell. They can be divided into two major groups, prokaryotic cells, which are usually single-celled organisms and eukaryotic cells, which can either be single-celled or be part of multicellular organisms (Palade, 1964).

The different types of organelles in the cell lead to a compartmentalization of the cell, which allows to physical separate many different biological processes from each other and enlarges the internal membrane surface. This benefits vital biochemical processes, which take place in or on membrane surfaces. For example, the lipid metabolism is catalysed mostly by membrane-bound enzymes, also, oxidative phosphorylation and photosynthesis both require a membrane to couple the transport of protons to the ATP synthesis. Furthermore, enclosed compartments, which are separated from the cytosol are created, thereby providing the cell with functionally specialized aqueous space. This way, processes with different requirements can take place simultaneously. Moreover, anabolic and metabolic reactions like glycolysis and gluconeogenesis can be separated from each other, in that regard eliminating the danger of futile cycles. Due to the semi-permeable nature of cellular membranes, specific transport mechanisms for both charged and uncharged molecules are necessary to achieve a specialized aqueous environment within each organelle .

The largest organelle in the cell is the nucleus where the key synthesis of DNA and RNA takes place. Connected to the outer nuclear membrane is the tubular network of the largest cellular organelle termed endoplasmic reticulum. Bound to its cytosolic surface, the ribosomes of the ER are responsible for the synthesis of soluble proteins as well as proteins being destined to be integrated into a membranes, The majority of these proteins are intended for either to the extracellular space or other compartments within the cell. Further organelles inside the cells are lysosomes. This vesicles play an important role during autophagy for the degradation of defective intracellular organs as well as in the demolition of particles and macromolecules that had been uptaken by the cell during endocytosis (heterophagy) by harbouring the the essential enzymes

required for the digestion of these particles. Small, membrane-enclosed organelles called peroxisomes are involved in multitudes of metabolic reactions.

Although a variation of abundance and special properties can occur depending on the specialized function of the cell, the basic functions of each membrane-enclosed organelle are executed similarly in each cell type. The position of the different organelles within the cytosol variates from condensed as in case of the Golgi apparatus, which is exclusively located close to the nucleus, to expanded like the ER, whose tubular network spread through the whole cytosol.

These characteristic locations are evoked by interactions between organelles and the cytoskeleton. Furthermore, the cytoskeleton is involved in intracellular transport, cell motility, mitosis and meiosis. These functions are provided by microtubules and actin filaments, which are part of the cytoskeletal network. Microtubules consist of a polymer of the protein tubulin, which can be rapidly assembled or disassembled depending on the needs of the cell. In order to reposition cellular compartments, chemical energy has to be converted into mechanical energy. This is achieved by specific interaction of the three mechanochemical proteins myosin, dynesin and kinesin (Lamond, 2002).

1.2. Mitochondria

Mitochondria play a major role in cellular energy metabolism. For example, they can use oxygen as a terminal electron acceptor for the production of adenosin triphosphate (ATP) by oxidative phosphorylation (Saraste, 1999). Furthermore, mitochondria are essential even for organisms that do not respire due to their role in the iron sulphur cluster biogenesis, which are essential cofactors for many enzmyes (Lill, 2009). Because of its role in signalling, mitochondria also play a role in apoptosis. A key checkpoint during programmed cell death is the release of cytochrome c from mitochondria, leading to the formation of the apoptosome (Wang & Youle, 2009). Moreover, at least parts of essential metabolic pathways like the tricarboxylic acid (TCA) cycle or the urea cycle take place in mitochondria and they are also involved in β-oxidation and amino acid synthesis. Due to there essential role in energy production, mitochondrial malfunction can be cause of several diseases.

1.2.1. Structure and dynamics of mitochondria

Mitochondria have been proved to be present as a connected network rather than single entities (Friedman & Nunnari, 2014). Furthermore, mitochondria are highly dynamic organelles, the whole mitochondrial network undergoes permanent fission and fusion to satisfy the metabolic parts of the cell, to separate damaged parts for mitophagy (Mueller & Reski, 2015) and to distribute mitochondria during cell division (Mishra & Chan, 2014).

Due to their dual origin, mitochondria still contain their own genome, although during evolution most of the original α-proteobacterial DNA was lost or transferred to the nucles (Gabaldón & Huynen, 2004). Located in the mitochondrial matrix, the mitochondrial DNA encodes for 8 proteins in yeast an 13 in the mammalian system, additionally to tRNAs and rRNAs for them mitochondrial translation machinery. Biogenesis of mitochondrial encoded proteins takes place at ribosomes attached to the inner mitochondrial membrane, due to the fact that most proteins encoded on the mitochondrial genome are highly hydrophobic and are cotranslationally inserted into the inner mitochondrial membrane (M. Ott & Herrmann, 2010).

The internal matrix is surrounded by two phospholipid membranes (Hackenbrock, 1968), which are distinctively different in appearance and biochemical function due to their endosymbiotic origin (Fig. 1.1). The outer membrane (OM) originates from the host cell, whereas the inner mitochondrial membrane (IMM) originates from the membrane of a proteobacterium (Gray, Burger, & Lang, 1999). The surrounding OM is relatively permeable for ions and metabolites due to the presence of the β-barrel protein porin (VDAC in higher eukaryotes), which is the most abundant protein in the OM (Benz, 1994). However, recent studies revelead novel channel proteins that are selective for either anions or cations, implying a more regulatory role of the OM in terms of metabolite flux (Krüger et al., 2017). In contrast, the IMM is highly selective. It forms a diffusion barrier for ions, proteins and metabolites, contains a number of transmembrane transport systems and is also the protein richest membrane known (Simbeni, Pon, Zinser, Paltauf, & Daum, 1991). This is important for maintaining a proton gradient, built up by the mitochondrial respiratory chain using electrons derived from catabolic reactions and used as a driving force for generating ATP out of ADP and P_i by the F_1F_0ATPase (Martin, Mahlke, & Pfanner, 1991; Saraste, 1999).

The inner membrane of mitochondria displays a unique morphology due to its formation of sub-compartments. The inner boundary membrane (IBM) is in proximity to the OM. Furthermore, the IMM forms large invaginations, called the mitochondrial

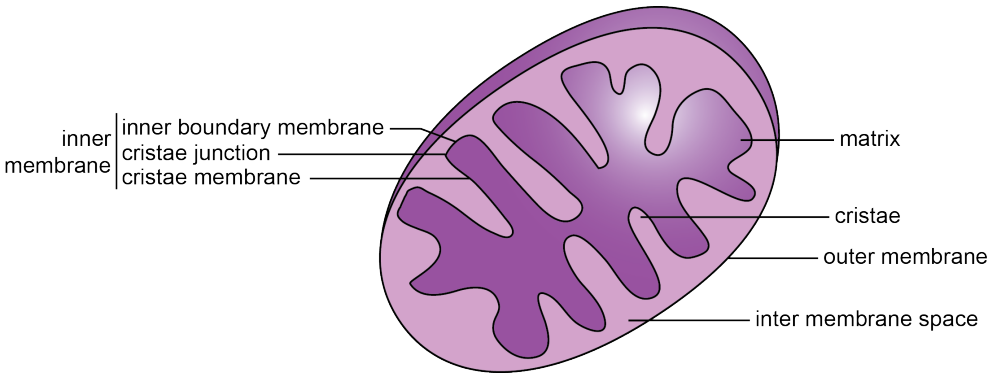

Figure 1.1.: Schematic cross-section of a mitochondrion.
Outer and inner mitochondrial membranes separate two distinct aqueous compartments: intermembrane space and matrix. The inner membrane forms invaginations (cristae), that significantly increase the total inner mitochondrial membrane surface.

cristae, which are connected to the IBM by tubular openings, the cristae junctions. The distribution of proteins in the IM appears not evenly, but instead organize into functionally distinct subcompartments (Werner & Neupert, 1972; Vogel, Bornhövd, Neupert, & Reichert, 2006).

1.2.2. Mitochondrial oxidative phosphorylation

The mitochondrion is the main energy-producing organelle in the eukaryotic cell. It converts energy of reducing equivalents (NADH, $FADH_2$) into the form of macroergic ATP bonds. Five different enzyme complexes (I-V) forming the OXPHOS machinery are the driving force in this process and are located in the IMM.

Four enzyme complexes (I-IV) transfer electrons to acceptor molecules and pump protons from the matrix to the IMS, thereby generating a proton gradient. The last enzyme complex, complex V or F_1F_oATPase, uses this proton gradient to generate ATP from ADP and P_i. All enzymes involved are composed of multiple subunits of different genetic origin. Assembly of these complexes is a multistep process that requires numerous assembly factors and a sophisticated regulation mechanism. There are two ways for electrons to enter the electron transport chain. The first is to be transferred from NADH, through complex I (NADH:ubiquinone oxidoreductase), to ubiquinone. The second is a transfer of electrons from succinate to complex II (succinate:ubiqiunone oxidoreductase) from which they are subsequently passed on to ubiquinone. Electrons travel from ubiqiunone through complex III (ubiquinol:ferricytochrome *c* oxidoreductase) to cytochrome *c* and, finally, passing complex IV (cytochrome *c* oxidase) to reach oxygen. Only electron

transfer through complex II is not coupled with proton pumping to the IMS.

The first proton-pumping complex in the respiratory chain is complex I or NADH dehydrogenase. During transfer of two electrons from NADH, four protons from the matrix are pumped to the IMS. One molecule of FMN and several iron-sulfur clusters participate in the redox reactions catalyzed by complex I (Weiss, Friedrich, Hofhaus, & Preis, 1991). In *S. cerevisiae*, this type of multiprotein enzyme is missing, therefore not assembled monomeric enzymes undertake this work. This enzymes have a single nuclear-encoded subunit and do not possess a proton-pumping function (Lenaz & Genova, 2010).

Complex II (succinat dehydrogenase, SDH) is highly conserved among all aerobic organisms and is a membrane-bound enzyme of the Krebs cycle that catalyses the oxidation of succinate to fumarate and transfers electrons to ubiquinone. It is also the only complex of the respiratory chain that does not contain structural subunits encoded in the mitochondrial genome. SDH is considered to be the smallest enzyme of the respiratory chain and transfers two electrons to ubiquinone without the need of pumping them to the IMS (Hatefi, 1985; Lenaz & Genova, 2010).

An essential part of the respiratory chain is ubiquinone. Reduced by complexes I and II and oxidized by complex III during electron transfer, ubiquinone is a small hydrophilic mobile electron carrier (Genova & Lenaz, 2011). It exists in three oxidation states: fully oxidized (ubiquinone), semiquinone (ubisemiquinone) and fully reduced (ubiquinol). Ubiquinol passes on its electrons to complex II (ubiquinol-cytochrome *c* oxidoreductase) (Hatefi, 1985). Only one of its 10 different subunits in yeast, cytochrome *b*, is encoded by the mitochondrial genome (Tzagoloff, 1995).

The electrons are passed on to another mobile electron carrier, cytochrome *c*. Cytochrome *c* belongs to the cytochrome protein family, however, in contrast to its other members, it is hydrophilic and loosely associated with the inner mitochondrial membrane. The main function of this protein is to shuttle electrons between complex II and IV of the respiratory chain (Volkov & van Nuland, 2012).

The next enzyme in the respiratory chain is the heme-copper oxygen reductase (cytochrome *c* oxidase, COX), or complex IV. By pumping protons across the IM, it transfers electrons from cytochrome *c* to molecular oxygen, thereby generating water (Capaldi, 1990). Complex IV consists of 11 - 14 subunits, of which the three subunits Cox1, Cox2 and Cox3 are mitochondrially encoded (Mick, Fox, & Rehling, 2011; Balsa et al., 2012).

The generated proton gradient of the respiratory chain is used by the F_1F_o ATPase (complex V) to hydrolyse ATP from ADP and P_i in an exergonic process (Martin et al., 1991). The respiratory chain complexes are preferentially located in the cristae mem-

branes, whereas presequence protein translocases are enriched in the inner boundary membrane (Vogel et al., 2006). This leads to an increased efficiency of ATP generation and simultaneously to a closer contact of translocating complexes to the OM. The F_1F_oATPase is a multisubunit enzyme (Collinson et al., 1994; Boyer, 1997) which can be divided into the membrane-spanning F_o subcomplex responsible for H^+ translocation, and the F_1 domain containing the catalytic sites for ATP synthesis (Boyer, 1997; Fillingame & Divall, 1999; Velours et al., 2000). Whereas the enzymatic function of the F_1F_oATPase has been extensively investigated, recent studies revealed a second important role of the F_1F_oATPase in organization of the inner mitochondrial membrane (Giraud et al., 2002; Paumard et al., 2002; Gavin, Prescott, Luff, & Devenish, 2004; Thomas et al., 2008; Velours, Dautant, Salin, Sagot, & Br e thes, 2009; De los Rios Castillo et al., 2011). It is believed that this complex is critical for the formation and stabilization of the cristae tip by promoting positive curvature of the inner membrane.

The F_1F_oATPase occurs predominantly as a monomer or a homodimer (Arnold, Pfeiffer, Neupert, Stuart, & Sch a gger, 1998; Nijtmans, Taanman, Muijsers, Speijer, & Van den Bogert, 1998; Wittig, Velours, Stuart, & Schägger, 2008). However, various organisms were found to contain in addition higher oligomeric forms of the F_1F_oATPase homodimer (Eubel, 2003; Krause, Reifschneider, Goto, & Dencher, 2005; Thomas et al., 2008; De los Rios Castillo et al., 2011). The membrane curvature in the cristae tips is induced by the formation of ribbons of the $_1F_o$ATPase homodimers (Strauss, Hofhaus, Schröder, & Kühlbrandt, 2008; Rabl et al., 2009; Davies et al., 2011). Essential for the dimerization of the F_1F_oATPase are the small membrane proteins Atp20 (subunit g) and Atp21 (subunit e; Tim11) which have a characteristic glycin-rich region.

1.3. Mitochondrial protein import

The mitochondrial proteasome comprises about 1000 (yeast) to 1500 (human) different proteins (Sickmann et al., 2003; Perocchi et al., 2006; Pagliarini et al., 2008). However, only 1% of these are encoded in the mitochondrial genome. The majority is encoded in the nuclear genome and synthesized on ribosomes in the cytosol (Komiya, 1997). Therefore, a sophisticated import and distribution mechanism is needed to transport proteins to their destined location (Chacinska, Koehler, Milenkovic, Lithgow, & Pfanner, 2009; Becker, Böttinger, & Pfanner, 2012). To ascertain correct sub-mitochondrial localisations, they contain different targeting signals, recognized by specific receptors in the OM.

The imported proteins can be separated into proteins containing a cleavable N-terminal amphiphatic α-helix (presequence), internal hydrophobic motifs or N- and C-terminal signals that do not undergo processing (Chacinska et al., 2009; Dudek, Rehling, & van der Laan, 2013; Sjuts, Soll, science, & 2017, n.d.; Endo, Yamano, & Kawano, 2011). To ensure correct translocation, a plethora of different import machineries are present in mitochondria to maintain mitochondrial functions and dynamics (Fig. 1.2).

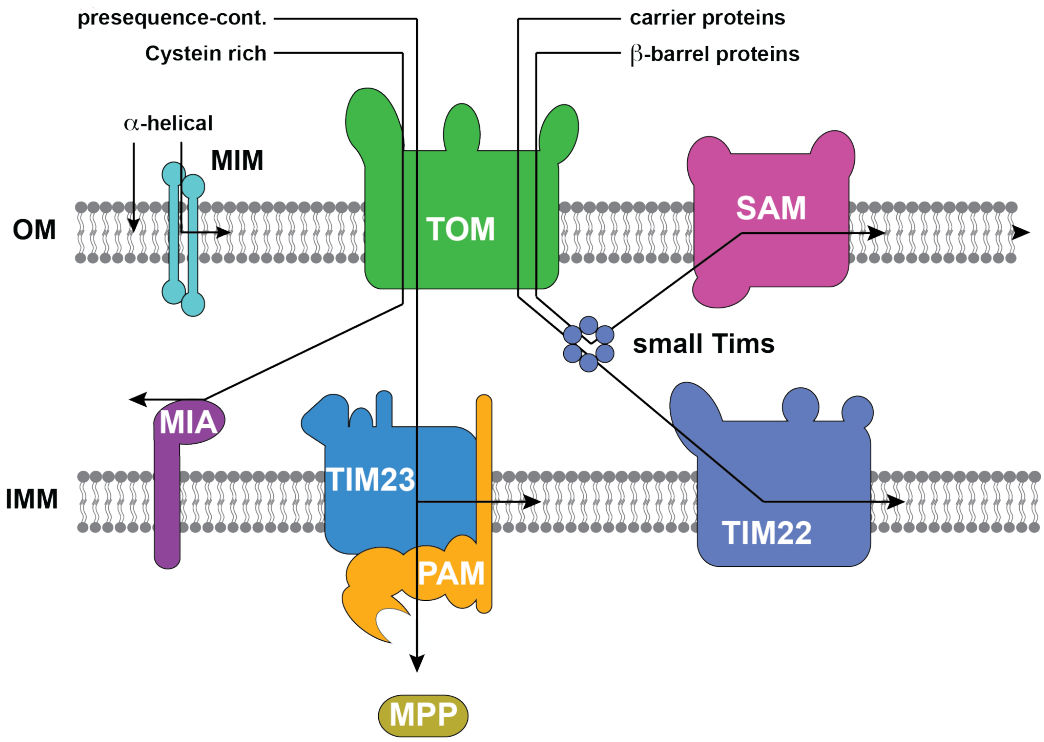

Figure 1.2.: Overview of the transport machinery in mitochondria.
Nearly all proteins have to pass the translocase of the outer membrane (TOM) complex, from where they follow different pathways. β-barrel proteins are shielded by small TIM chaperones in the IMS and transported to the sorting and assembly (SAM) complex. For some IMS proteins, oxidative folding by the mitochondrial intermembrane space assembly (MIA) is coupled to import. Transport across the IMM is potential dependent. Transmembrane proteins of the carrier family are bound by small TIM proteins and sorted into the inner membrane by the TIM22 complex. The presequence translocase of the inner membrane TIM23 mediates the transport of presequence containing proteins (presequence-cont.) into the IMM and the matrix. Additionally, transport into the matrix requires the association of the presequence translocase associated motor complex (PAM). Cleavage of the presequences in the matrix is supported by the mitochondrial processing peptidase (MPP).

1.3.1. Translocase of the outer membrane: The TOM complex

Ions and metabolites can freely diffuse through the outer mitochondrial membrane by passing pores of the voltage-dependent anion channel (VDAC)-porin superfamily. Proteins however are mainly transported into mitochondria through the TOM complex (Mokranjac & Neupert, 2015). It consists of the main channel Tom40 (Kiebler et al., 1990; Lackey et al., 2014) and three receptor proteins Tom20, Tom22 and Tom70 (Brix, Dietmeier, & Pfanner, 1997). The protein-conducting channel is formed by three copies of Tom40 (Model, Meisinger, & Kühlbrandt, 2008; Shiota et al., 2015) but is not only able to act as a passive channel but can furthermore bind to hydrophobic parts of the precursor, thus preventing aggregation (Esaki et al., 2003). Tom20 is responsible for initial presequence recognition and bind the hydrophobic surface of of the presequence (Abe et al., 2000), whereas Tom22 binds to the positively charged surface of the presequence (Shiota, Mabuchi, Tanaka-Yamano, Yamano, & Endo, 2011). Its IMS domain is assisting in the handover of precursor from the TOM complex to the TIM23 complex by binding soluble presequences, additionally to its essential role in TOM oligomerisation (van Wilpe et al., 1999). Hydrophobic proteins are recognized by Tom70 (Schlossmann, Dietmeier, Pfanner, & Neupert, 1994). Chaperones of the Hsp70 family bind to hydrophobic proteins in the aqueous cytosol and are recognized by the cytosolic domain of Tom70 (Schlossmann et al., 1994). Moreover, it could be shown that Tom70 plays a role in presequence binding (Melin et al., 2015) and recognition of internal MTS (matrix targeting signal)-like signals (iMTS-Ls) (Backes et al., 2018). Further constituents are the proteins Tom5, Tom6 and Tom7, who are essential for assembly, stability and the dynamics of the TOM complex (Wiedemann & Pfanner, 2017). However, an assortment of α-helical proteins are not imported via the TOM-complex but utilize the MIM complex. Its constituents are Mim1 and Mim2 and form together a 200 kDa complex (Dimmer & Rapaport, 2012; Popov-Celeketić, Waizenegger, & Rapaport, 2008). Substrates bind via their transmembrane segment to Mim1, which forms oligomers with the help of GXXXG/A motifs. Substrates of the MIM complex are for example Tom20, Tom70 and the outer membrane protein Ugo1 (Hulett et al., 2008; Papic, Krumpe, Dukanovic, Dimmer, & Rapaport, 2011) and are inserted into the outer membrane without a protein-aqueous pore.

1.3.2. The SAM complex

Mitochondria have their origin in Gram-negative bacteria, thus they contain mainly β-barrel proteins in the outer membrane. Prime examples are the channel proteins Porin/VDAC, Tom40 and Sam50 itself. Proteins of this pathway are recognized by a β-hairpin motif at the very C-Terminus, consisting of two adjacent β-strands (Jores et al., 2016). The core component of the sorting and assembly machinery (SAM complex) is the channel Sam50 together with two peripheral proteins Sam35 and Sam37 (Wiedemann & Pfanner, 2017). Substrates of the SAM complex are recognized by Tom20 and are translocated across the OM by the TOM-complex. To avoid aggregation, small soluble TIM chaperons bind to the hydrophobic patches of the imported protein in the IMS (Curran, Leuenberger, Oppliger, & Koehler, 2002; S. C. Hoppins & Nargang, 2004; Wiedemann et al., 2004) before they are inserted into the OM via Sam50. In the mammalian system however the process is still unclear (Kang, Fielden, & Stojanovski, 2018). SAM50 itself is highly conserved (Paschen et al., 2003) but no clear homologues for Sam35 and Sam37 are identified so far. Evidence suggests that the Metaxins MTX1 and MTX2 fulfil the role in human cells (Kozjak-Pavlovic et al., 2007). Additionally to forming a complex with SAM50, MTX1 was also found to be involved in cristae structure maintenance and OXPHOS assembly (Huynen, Mühlmeister, Gotthardt, Guerrero-Castillo, & Brandt, 2016).

1.3.3. The MIA pathway transport into the intermembrane space

Proteins located in the intermembrane space often contain characteristic cystein motifs (i.e. CX_3C or CX_9C) which are able to form disulfid bonds and serve as targeting signals (Dudek et al., 2013). Furthermore, the import signal includes two hydrophobic residues in close proximity which are recognized by Mia40, one of the components of the MIA complex. In yeast, MIA is anchored into the IMM with the soluble domain facing the IMS whereas in mammalian cells it is a soluble intermembrane space protein itself, their function however is similar in both organisms (Chacinska et al., 2004, 2008; Hofmann et al., 2005). The cystein residues of the substrates are kept in a reduced state while crossing the outer membrane, after recognition of Mia40 it oxidizes their substrates and aids in the correct formation of disulfid bonds and folding of the protein (Gornicka et al., 2014; Milenkovic et al., 2009; Sideris et al., 2009). After releasing the substrate, Mia40 is reoxidized by another key component of the MIA pathway, Erv1 (ALR in human) (Chacinska et al., 2004; Daithankar, Farrell, & Thorpe, 2009; Kang et al., 2018; Rissler

et al., 2005).

1.3.4. Carrier import via the TIM22 complex

Metabolite carries like the ADP/ATP carrier (AAC) or phosphate carrier (PiC) typically consist of 6 transmembrane domains, shielded by cytosolic chaperones to prevent misfolding (Young, Hoogenraad, & Hartl, 2003). But also four transmembrane spanning translocase components Tim23, Tim22 and Tim17 are known substrates of the TIM22-complex (Curran et al., 2002). The precursor proteins are recognized via internal targeting signals by Tom70 and handover through the IMS is mediated by small TIM chaperons to prevent misfolding of the proteins (Davis, Alder, Jensen, & Johnson, 2007). The core component in yeast is the channel Tim22, whereas Tim54 is responsible for recruitment of the chaperone complex (Wagner, Mick, & Rehling, 2009) and Tim18 and Sdh3 are responsible for assembly of the TIM22 complex. Interestingly, Sdh3 displays dual localization not only in the TIM22 complex, but also in complex II of the respiratory chain (Gebert et al., 2011).

In the mammalian system however, the complex consists of TIM22, TIM29, TIM10B and AGK, thus being the most evolutionary diverged translocase with having two metazoan specific components (Wiedemann & Pfanner, 2017; Kang et al., 2018). Whereas neither Tim54 and Tim18 are conserved in human, the recently found TIM29 is responsible for assembling the TIM22 complex (Callegari et al., 2016; Kang et al., 2016). In addition, TIM29 mediates membrane insertion of TIM22 substrates and forms a contact site to the outer membrane via interaction with the TOM complex. The second metazoan specific constituent AGK is a lipid kinase associated with Sengers syndrome, but also stabilizes the TIM22 complex independent of its kinase function and mediates import of various carrier proteins (Kang et al., 2017; Vukotic et al., 2017).

1.3.5. Importing presequence proteins via the TIM23 complex

Nearly 70 % of proteins are targeted via N-terminal targeting signals called presequences to the inner mitochondrial membrane or the matrix (Vögtle et al., 2009). Import is mediated by the TIM23-complex, thus being by far the most important import pathway. Presequence can vary significantly in length, although they are typically 15-55 amino acids long, form an amphipatic α-helix with net positive charge and are usually cleaved off after import by the matrix processing peptidase (MPP) (Hawlitschek et al., 1988). Translocation across the inner mitochondrial membrane is membrane potential driven

and reliant on the overall positiv charge of the presequence (Martin et al., 1991), although recent studies also revealed an impact of the mature protein form on the membrane potential dependency (Schendzielorz et al., 2017).

Presequence containing proteins are recognized by the $TIM23^{CORE}$ complex. After passing the TOM-complex, the N-terminus of the imported protein is handed over to the protein conducting pore of $TIM23^{CORE}$, thus generating a TOM-TIM23 supercomplex (Dudek et al., 2013). For proteins sorted into the IMM, Mgr2 recrutes Tim21 to the $TIM23^{CORE}$ to form the $TIM23^{SORT}$ complex and lateral releases the precursor into the IMM after arresting the imported protein due to downstream hydrophobic stop transfer signals (Bohnert et al., 2010; Bömer et al., 1997; Glick, Beasley, & Schatz, 1992; van der Laan et al., 2007).

Soluble proteins of the mitochondrial matrix are also translocated via $TIM23^{CORE}$. However, in contrast to lateral sorted proteins, membrane potential is not sufficient for full matrix import (Dudek et al., 2013). To ensure complete translocation, the presequence translocase associated import motor (PAM) is recruited to the $TIM23^{CORE}$ and mediates matrix import by providing additional inward-directed force on the incoming protein by Hsp70-mediated hydrolysis of ATP (Schulz, Schendzielorz, & Rehling, 2015).

1.4. Mitochondrial dynamics and inner mitochondrial membrane morphology

Mitochondria form highly ramified tubular networks that can extend through nearly the whole cytosol and are remarkably dynamic (Nunnari & Suomalainen, 2012). Each mitochondria itself exhibits a ultrastructure of high complexity, with the outer membrane enclosing the whole mitochondria and thus shielding it from the rest of the cell, whereas the inner mitochondrial membrane forms patches of highly specialized membrane regions and concentrating distinct interacting protein complexes in a close spatial manner to enhance the efficiency of mitochondrial function.

1.4.1. The ATP synthase stabilizes cristae tips

The most important role in this ultrastructure fill the tubular invaginations within the mitochondrial matrix called cristae. They predominantly harbour the complexes of the oxidative phosphorylation machinery OXPHOS which generates ATP via the F_1F_O-ATPase. Because of their spatial restriction due to a fusion barrier created by the

cristae junctions, they can be found in high concentration in this regions (Gilkerson, Selker, & Capaldi, 2003; Frey & Mannella, 2000; Mannella, 2006). The inner boundary membrane (IBM) is close to the outer membrane and can be described as flat, whereas the connection between cristae and IBM, termed cristae junction, is a region with a high degree of curvature. The size and shape of cristae is vastly dynamic and adapts to the energetic needs of the cell (Fawcett, 1981). The mitochondria of *S.cerevisiae* for example contain only a few small cristae when grown under fermentable condition, thus relying on ATP production via glycolysis in the cytosol. Whereas yeast grown in media containing a non-fermentable carbon source produce more proteins of the OXPHOS, hence the inner membrane expands and cristae becoming bigger (Renken et al., 2002). Well established key players in stabilizing the cristae tip are the dimers and oligomers of the F_1F_O-ATPase. Fundamental for this membrane shaping is the ability to form dimers, which is mediated by highly conserved glycine-rich GXXXG motifs (Arnold et al., 1998; Arselin et al., 2003; Saddar & Stuart, 2005; Wagner et al., 2009) that can also be found in various other oligomerizating proteins (Alavian et al., 2014; Barbot et al., 2015; Bohnert et al., 2015; Demishtein-Zohary, Marom, Neupert, Mokranjac, & Azem, 2015). Depletion of the ATP synthase or inhibition of dimerisation led to a lack of cristae tips (Paumard et al., 2002), thus confirming the dual role of the protein complex. Surprsingly, despite their importance for normal cristae morphology maintenance, ablation of dimerization units in the ATP synthase although displaying reduced membrane potential and respirational activity, did not lead to immediate cell death (Bornhövd, Vogel, Neupert, & Reichert, 2006; Boyle, Roucou, Nagley, Devenish, & Prescott, 1999). Furthermore, the highly curved cristae junctions seem to be unaffected upon the loss of F_1F_O-ATPase dimers, indicating that although the ATP synthase dimers are necessary for physiological cristae membrane morphology, the formation and stabilization of cristae junctions is performed by other proteins.

1.4.2. Regulation of cristae junctions

The large dynamine-like GTPAse Mgm1 in yeast and OPA1 in mammalian cells were originally identified as part of the mitochondrial fission and fusion machinery (Cipolat, Martins de Brito, Dal Zilio, & Scorrano, 2004; Meeusen et al., 2006; Wong et al., 2003). However, ablation of Mgm1/OPA1 led to an reduction and widening of cristae junctions (Amutha & Pain, 2003; Olichon et al., 2003; Sesaki, Southard, Yaffe, & Jensen, 2003), whereas an overexpression is reducing the diameter of the cristae junctions and is believed to have an anti-apoptotic effect (Cipolat et al., 2006; Frezza et al., 2006; Olichon et al.,

2003). OPA1 forms high molecular weight complexes which are located at the cristae junctions and preventing protein and metabolite diffusion from the cristae to the IBM and vice versa (Frezza et al., 2006). Recent studies could show, that on the other hand Mgm1/OPA1 is not strictly required for the formation of cristae junctions (Barrera, Koob, Dikov, Vogel, & Reichert, 2016).

1.4.3. The Mitochondrial Contact site and cristae Organizing System MICOS

A vast step towards unveiling the mechanisms of cristae and cristae junction formation and maintenance was done by revealing the evolutionary conserved mitochondrial contact site and cristae organizing system MICOS (John et al., 2005; Rabl et al., 2009; Harner et al., 2011; S. Hoppins et al., 2011; von der Malsburg et al., 2011; Alkhaja et al., 2012; Bohnert et al., 2015). MICOS is a approximately 700-1200 kDa complex, consistent of 5 annotated homologues constituents in yeast hand human (Mic60, Mic19, Mic10, Mic26, Mic27), two metazoan specific proteins (MIC13, MIC25) and on protein only found in yeast (Mic12) (Fig. 1.3). However, the exact stoichiometry of the complex is not known.

Depletion of either one of the two core components Mic60 or Mic10 resulted in a drastic reduction of cristae junctions, the consecutive alteration of inner mitochondrial membranes led to lamellar like stacks of the inner membrane in the matrix (John et al., 2005; von der Malsburg et al., 2011; Harner et al., 2011; S. Hoppins et al., 2011; Alkhaja et al., 2012). In mammalian cells, MICOS was found to interact with the SAM complex and together with DNAJC11 forming the mitochondrial intermembrane space bridging complex (MIB) (Darshi et al., 2011; C. Ott et al., 2012; Xie, Marusich, Souda, Whitelegge, & Capaldi, 2007). The MICOS complex can be divided into two subcomplexes, the MIC60 subcomplex (MIC60, MIC19, MIC25) and the MIC10 subcomplex (MIC13, MIC10, MIC26, MIC27).

1.4.3.1. The MIC60 subcomplex

MIC60 is one of the major proteins of the MICOS complex with the human MIC60 being on an evolutionary scale one of the oldest. Homologues could be found in α-proteobacteria which are presumed to be the ancestors of mitochondria (Huynen et al., 2016; Muñoz-Gómez et al., 2015). It exists in two isoforms and is preferentially localized at the cristae junctions (Jans et al., 2013) and forms a subcomplex together with MIC19

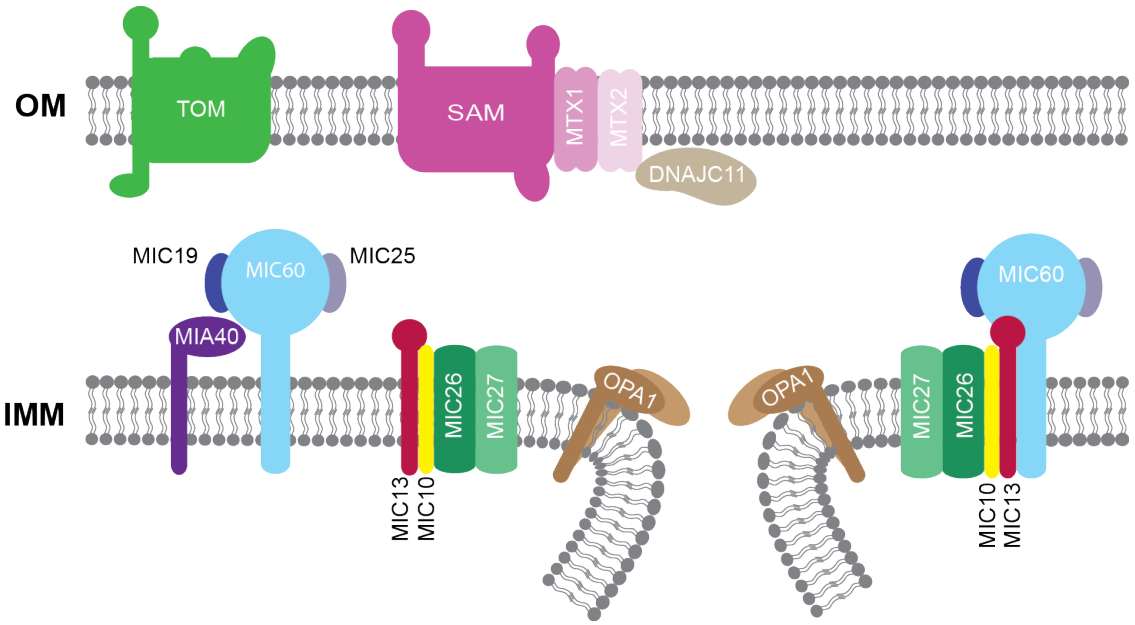

Figure 1.3.: The constituents of the MICOS complex.
The mammalian MICOS complex (hypothetical model) with its five integral inner membrane proteins (MIC10, MIC13, MIC26, MIC27, MIC60) and one peripheral inner membrane proteins MIC19 and MIC25. MICOS is thought to interact with different complexes of the protein translocase machinery and is vital for maintaining the unique morphology of the inner membrane.

and MIC25. The exact mechanism on how MIC60 influences membrane morphology is still unknown, although overexpression if Mic60 in yeast led to highly branched cristae membranes, thus suggesting a direct involvement in cristae shaping (Bohnert et al., 2015; Rabl et al., 2009). Recent *in vitro* studies revealed that purified yeast Mic60 demonstrated membrane bending ability, thus suggesting a direct mechanistical influence of yeast Mic60 on membrane morphology (Tarasenko et al., 2017). Kock-down of the human MIC60 strongly decreased the protein levels of other MICOS constituents as well as amounts of SAM complex constituents (C. Ott, Dorsch, Fraunholz, Straub, & Kozjak-Pavlovic, 2015). Furthermore it negatively effected the amount of OPA1 (Ding et al., 2015) and even mitochondrial fission and fusion proteins (Li et al., 2016) were decreased. The mitochondrial proteas Yme1L is likely to be involved in the homeostasis of MIC60 (Li et al., 2016). In addition, MIC60 was found to have a role in lipid trafficking in plants via MIC60 mediated contact sites (Michaud et al., 2016). Mitochondria membrane biogenesis requires lipid trafficking between different organelles, thus this finding adds an essential physiological role of contact sites.

A further constituent of this subcomplex is MIC19, a 26 kDa soluble protein in the IMS with a characteristic coiled-coil helix coiled coil helix (CHCH) domain which har-

bour two cystein rich CX_9C motifs. This CHCH domain acted as the binding site to MIC60 (Darshi et al., 2011) and it was recently found that MIC19 further interacts with components of the whole MICOS complex (Friedman, Mourier, Yamada, McCaffery, & Nunnari, 2015). Hence, MIC19 seem to be important for MICOS integrity and physically linking both subcomplexes. Deletion of MIC19 led to partial disruption of the MICOS complex and altered membrane morphology displayed by stacked cristae membranes in addition to a decreased OPA1 level (Darshi et al., 2011; Harner et al., 2011; S. Hoppins et al., 2011; von der Malsburg et al., 2011; Sakowska et al., 2015). Furthermore, it was found that MIC19 is able to be redox-regulated and its oxidation status has an influence on the MICOS complex (Sakowska et al., 2015) in addition to prevent MIC60 degradation via Yme1L (Li et al., 2016). This suggested that it is highly likely MIC19 influences the inner membrane morphology by regulating the MICOS complex by conducting the ratio between the sub-complexes rather than having a direct function of shaping membranes.

MIC25 belongs together with MIC19 to the CHCHD family of proteins and has no yeast homologue. Its structure resembles that of MIC19, however ablation of MIC25 only has a slight effect on inner mitochondrial ultrastructure and the levels of other MICOS components were unaffected (C. Ott et al., 2015). Interestingly, MIC25 is the only protein not affected in a MIC19 depletion, a simultaneous deletion however displays the same effects as a MIC19 single depletion (Li et al., 2016; C. Ott et al., 2015). This indicates that MIC25 is stabilized in the absence of MIC19, although a link to a function of MIC25 is yet to discover.

1.4.3.2. The MIC10 subcomplex

The second core component of the MICOS complex is a small hairpin-like protein called MIC10 and was identified due to its severe impact on inner mitochondrial ultrastructure upon deletion, simliar to ablation of MIC60, in addition to a strong growth defect in yeast cells, indicating the importance on cell viability (Harner et al., 2011; von der Malsburg et al., 2011; Alkhaja et al., 2012; van der Laan, Bohnert, Wiedemann, & Pfanner, 2012). *In vitro* studies proved that in yeast, Mic10 has membrane shaping abilities mediated by oligomerisation via its characteristic glycine-rich motifs (Barbot et al., 2015; Bohnert et al., 2015). Whether this mechanism is the same in mammalian cells is unknown so far. Recent studies found the dimeric form of the F_1F_O-ATPase interacting with yeast Mic10, but not Mic60. The mechanism behind this interaction though is still unknown. This suggested an even greater role of Mic10 in membrane architecture besides its own

membrane shaping ability.

Further constitutents of this subcomplex are two membrane integral proteins of the apolipoprotein family, MIC26 and MIC27. Although it was shown that they are components of the MICOS complex in human (C. Ott et al., 2015; Koob, Barrera, Anand, & Reichert, 2015b) and yeast (Harner et al., 2011; S. Hoppins et al., 2011; von der Malsburg et al., 2011), their exact function is unknown. In yeast, deletion of neither Mic26 nor Mic27 demonstrated a strong morphological phenotype (Harner et al., 2011; S. Hoppins et al., 2011; von der Malsburg et al., 2011), in mammalian cells downregulation of MIC27 likewise displayed only a mild alteration of inner mitochondrial ultrastructure (C. Ott et al., 2015) whereas the impact of a downregulation or depletion of human MIC26 is inconclusive (C. Ott et al., 2015; Koob et al., 2015b). Though in both organisms the effect of a loss of MIC26 is less severe than lower protein levels of MIC27. Recent studies revealed that in yeast as well as in human cells, MIC26 and MIC27 have an antagonizing role (Koob et al., 2015b; Rampelt et al., 2018). In yeast, Mic27 directly stabilizes the oligomerisation of Mic10 whereas higher levels of Mic26 exert a destabilizing effect on Mic10 oligomerisation (Rampelt, Zerbes, van der Laan, & Pfanner, 2016). In mammalian cells the interaction appear to happen in a more direct matter, overexpression of MIC26 led to a decrease in MIC27 amounts whereas its protein levels increased in a downregulation of MIC26 and vice versa (Koob, Barrera, Anand, & Reichert, 2015a). Both protein levels however positively correlate with protein levels of MIC10 in addition to tafazzin, a protein involved in cardiolipin biosynthesis. It is proposed, that both proteins are linked to cardiolipin metabolism, thus in protein complex stabilization via cardiolipin regiulation, since MIC27 is capable of binding cardiolipin (Weber et al., 2013) and MIC26 effects the levels of cardiolipin (Koob et al., 2015b).

Essential for the assembly of both subcomplex with each other is the human protein termed MIC13 (Guarani et al., 2015). It was demonstrated that downregulation of MIC13 alters inner mitochondrial membrane morphology and led to a reduction in protein levels of MIC10, MIC26 and MIC27, the MIC60 subcomplex however seemed to accumulate. Thus, MIC13 appears to act as a scaffold protein required for the assembly of the mature MICOS complex. The yeast Mic12 only appears to be distantly related to the human MIC13 to be a evident homologue (Huynen et al., 2016), although studies suggested that they fulfil a similar function (Zerbes, Höß, Pfanner, van der Laan, & Bohnert, 2016).

1.4.4. MICOS is connect to various mitochondrial processes

As previously described (chapter 1.4.3) it is well established that MICOS has a key role in forming and maintaining inner mitochondrial ultrastructure. In addition, various alterations of the MICOS complex were demonstrated to have an impact on a plethora of mitochondrial function.

Deletion of yeast Mic60 led to a decrease in protein import via the MIA pathway and β-barrel protein insertion into the outer membrane via SAM (von der Malsburg et al., 2011; Bohnert et al., 2012). In addition it was demonstrated in human cells that a knock-down of MIC60 dysregulated the mitochondrial fission and fusion and mitochondrial translation was impaired due to clustered mtDNA nucleoids (Li et al., 2016).

The endoplasmic-reticulum-mitochondria encounter structure (ERMES) is likely involved in lipid trafficking in yeast between the ER and mitochondria (S. E. Horvath & Daum, 2013; Osman, Voelker, & Langer, 2011; Tatsuta & Langer, 2017) and genetic interactions linked ERMES to the MICOS complex (S. Hoppins et al., 2011), thus suggesting an ER mitochondria organizing network (ERMIONE) which links biogenesis and transport of phospholipids to membrane architecture. Further findings supporting the role of MICOS in phosholipid metabolism linked MICOS to yeast tafazzin in remodelling cardiolipin (Harner et al., 2014), similar to human MIC26 (Koob et al., 2015b). In addition, MIC27 shows distinct cardiolipin binding abilities (Weber et al., 2013) and plant MIC60 demonstrated to be linked to lipid trafficking (Michaud et al., 2016). Although the exact mechanisms still need to be assessed, a clear trend of MICOS involvement in phospholipid biogenesis and trafficking is evident.

The importance of MICOS and the ensuing mitochondrial health can be further accentuated by involvement of MICOS in various diseases. A mutation in the MIC13 gene was found to be responsible for liver disease and severe neurological retardation (Gödiker et al., 2018). MIC60 has been shown to be either directly or indirectly involved in numerous diseases caused in various tissues like Down syndrome or Parkinson's disease in brain, diabetes mellitus in heart and liver, mtDNA related renal diseas in kidney and various forms of cancer (Feng, Madungwe, & Bopassa, 2018). In addition, Barth syndrome, caused by a mutation in the cardiolipin remodelling protein tafazzin, demonstrated altered levels of MICOS amounts (Chatzispyrou et al., 2018).

In conclusion, MICOS acts as a central organizer for mitochondrial membrane architecture and physiology. Several pathways and mitochondrial and cellular functions seem

to merge at cristae junctions, thus proper formation and maintenance is critical for cell and mitochondrial health. The mechanistic details of the various functions of MICOS are still vastly unknown and arduous to address since techniques need to be found to focus on one specific role without altering a vast number of different factors and rendering the obtained data inconclusive.

1.5. Aim of this study

The composition of the MICOS complex is well known and its impact on membrane morphology has been shown. Further function of the MICOS complex and its individual constituents are still in focus of ongoing research. The majority of studies investigating the role of MICOS was done in yeast so far. To further investigate function of the mammalian MICOS, one aim of this study was the generation a MIC10 knock-out cell line to verify MIC10 as a core component for the membrane shaping ability of MICOS in human cells. This cell line was used to investigate the functional connection between MICOS and further mitochondrial functions and protein-/ protein complexes.

In addition, a proximity labelling approach was established to investigate novel interaction partners of MICOS subunits. Therefore, different proximity biotinylation approaches were applied.

Studies of the MICOS complex in yeast revealed either a potential functional interaction between MICOS and the translocase in yeast or a connection of membrane morphology to protein translocation (von der Malsburg et al., 2011). Therefore, this study will analyze a functional relation between the TIM complexes and MICOS in yeast as well as in human. To investigate the interplay of MICOS and the translocase in yeast more thoroughly, the third part of this work focused on establishing a connection between MICOS and the different mitochondrial translocase complexes of the inner membrane as well as the functional connection between MICOS, inner mitochondrial membrane morphology and protein translocation in mitochondria.

2. Materials and Methods

2.1. Materials

2.1.1. Chemicals

Chemicals were used at analytical grade in this study and obtained from *AppliChem* (Darmstadt, Germany), *BD* (Heidelberg, Germany), *Bio-Rad* (Richmond, USA), *Merck*, *Novagen* and *Calbiochem* (Darmstadt, Germany), *Roth* (Karlsruhe, Germany), *Serva* (Heidelberg, Germany), *Sigma-Aldrich* (Taufkirchen, Germany), *Thermo Scientific* (Schwerte, Germany). The biotin phenol was synthesized by the Max Planck institute for biophysical chemistry, Göttingen.

Table 2.1.: List of chemicals

Chemical	Supplier
[^{35}S]-methionine	Hartmann Analytic
2-mercaptoethanol	Sigma-Aldrich
6-aminocaproic acid	Sigma-Aldrich
Acetic acid	Roth
Acetone	Roth
Acrylamid/bisacrylamide (37.5:1) solution	Merck
Acrylamid 2x crytallised	Roth
Agarose NEEO ultra-quality	Roth
Ammonium acetate	Merck
Ampicilin	AppliChem
Antimycine	Sigma-Aldrich
ATP	Roche
Avidin agarose	Thermo Scientific
Bacto Yeast Extract	BD
Bacto Agar	BD
Bacto Peptone	BD
Bacto Tryptone	BD
Bio-Rad Protein Assay	Bio-Rad

Table 2.1.: List of chemicals (continued)

Chemical	Supplier
Bis-Acrylamide	Roth
Bis-Tris Buffer grade	AppliChem
Bovine IgG	Bio-Rad
Bovine Serum Albumin	Sigmal-Aldrich
Bromophenol blue	Merck
Chloroform	Roth
Complete EDTA.free protease inhibitor mix	Roche
Coomassie Brilliant Blue G-250	Serva
Coomassie Brilliant Blue R-250	Serva
Copper(II)sulfate pentahydrate	Merck
Creatine kinase	Roche
Creatine phosphate	Roche
Deoxynucleotide triphoshphate mix (dNTPs)	New England Bio Labs
Digitonin	Calbiochem
DMSO	AppliChem
DNA ladder mix "Gene Ruler"	Thermo Scientific
DTT (1,4-dithiothretol)	Roth
EDTA (ethylendiamintetraacetic acid)	Roth
EGTA	Roth
Ethanol	Roth
Ethidium bromide 0.025%	Roth
GeneJuice	Merck
D(+)-Glucose	Roth
Glutamine	LifeTechnologies
Glycerol	Sigma-Aldrich
Glycine	Roth
HEPES	Roth
Herring sperm DNA	Roth
Hydrochloric acid 37%	Roth
IgG from human serum	Sigma-Aldrich
IgG protein standard	BioRad
Imidazole	Sigma-Aldrich
Immobilon-P PVDF membrane	Millipore/Merck
Lithium acetate	AppliChem
Magnesium acetate	Merck

Table 2.1.: List of chemicals (continued)

Chemical	Supplier
Magnesium chloride	Merck
Magnesium sulfate	Appplichem
Methanol	Roth
Methionine	Roth
MitoTracker Oragne CMTMRos	Thermo Scientific
MOPS	Sigma-Aldrich
NADH	Roche
Ni^{2+}-NTA agarose	Macherey Nagel
Olygomycin	Sigma-Aldrich
ortho-Phosphoric acid	Merck
OptiMem	LifeTechnologies
PEG-4000 (polyethylene glycol 4000)	Merck
Penicillin Streptomycine	LifeTechnologies
PMSF (polymethanesulfonylfluorid)	Roth
Potassium chloride	Roth
Potassium dihydrogen phosphate	Roth
Potassium hydrogen diphosphate	Roth
Protein A sepharose	GE Healthcare
Proteinase K	Roche
Roti-Quant	Roth
Saccharose	Roth
SDS (sodium dodecyl sulfate)	Serva
SDS-PAGE Protein Standard	Bio-Rad
Sodium chloride	Sigma-Aldrich
Sodium hydroxide	AppliChem
Sorbitol	Merck
Strep-Tactin agarose	IBA Science
Streptavidin agarose	Thermo Scientific
Streptavidin HRP	Dianova
Sucrose	Roth
TCA	Merck
TEMED (tetramethylethylenediamine)	Roth
Tetracycline hydrochloride	Sigma-Aldrich
Trehalose	Roth
Tris (tris(hydroxymethyl)aminomethane)	Roth

Table 2.1.: List of chemicals (continued)

Chemical	Supplier
Triton X-100	Sigma-Aldrich
Tween-20	Roth
Urea	Roth
Uridine	Sigma Aldrich
Valinomycin	Sigma-Aldrich
X-Ray films	Foma Bohemia (Czech Republic)
Yeast nitrogen base without amino acids	BD
Zymolyase 20 T	Seikagaku Biobusiness

2.1.2. Solutions

All solutions are given in 1x concentration and were prepared with desalted water. Yeast and bacteria medium and solutions for cellculture were autoclaved before use and kept under sterile conditions.

Table 2.2.: List of solutions

Solutions	Components
AVO mix	0.8 mM antmycin, 0.1 valinomycin, 2 mM oligomycin in ethanol
Blotting buffer	25 mM Tris, 192 mM glycine, 10% methanol
BN anode buffer	50 mM Bis-Tris/HCl pH 7.0
BN cathode buffer	50 mM tricine, pH 7.0, 15 mM Bis-Tris, with or without 0.02 % Coomassie Brilliant Blue G-250
BN gel buffer	66.67 mM 6-aminocaproic acid, 50 mM Bis-Tris/HCl 7.0
BN sample loading buffer	0.5 % Coomassie Brilliant Blue G-250, 50 mM 6-aminocaproic acid, pH 7.0
BN solubilzation buffer	1 % digitonin, 20 mM Tris/HCl pH 7.4, 0.1 mM EDTA pH 8.0, 50 mM NaCl, 10 % Glycerol, 1 mM PMSF
Carrier-DNA	herring sperm DNA (10 mg/mL) in TE buffer

Table 2.2.: List of solutions (continued)

Solutions	Components
Cell culture medium	DMEM (Dubelco's modified Eagle Medium) supplemented with 10 % (v/v) fetal calf serum (FCS), 1 mM sodium pyruvate, 2 mM L-gluatamine, 50 μg/mL uridin and with or without penicillin streptomycine (filtered)
Colloidal Coomassie Staining solution	0.1% (w/v) Coomassie Brilliant Blue G-250, 2% (w/v) phosphoric acid, 10% ammonium sulfate, 20% methanol
Coomassie staining solution	2.5 g/L Coomassie Brilliant Blue G-250, 40% ethanol, 10% acetic acid
Destaining solution	30% ethanol, 10% acetic acid
DTT buffer	10 mM DTT, 100 mM Tris/H_2SO_4 pH 9.4
EM buffer	10 mM MOPS-KOH pH 7.2, 1 mM EDTA
Import buffer	3 % fatty acid free bovine serum albumin, 250 mM sucrise, 80 mM KCl, 5 mM MgCl, 10 mM MOPS-KOH pH 7.2, 5 mM methionine, 2 mM NADH, with or without 100 μg/mL creatine kinase and 5 mM creatine phosphate
Homogenization buffer	0.6 M sorbitol, 10 mM Tris/HCl pH 7.4, 1 mM EDTA, 0.2% (w/v) fatty acid free BSA, 1 mM PMSF
LiAc/PEG	0.1 M Li-Acetate, 40% polyethylene glycol 400 in water, filtersterilized
LiAc-TE	0.1 M Li-Acetate, 10 mM Tris pH 8.0, 1 mM EDTA
LB medium	1% (w/v) tryptone, 0.5% (wt/v) yeast extract, 1% (wt/v) NaCl
PBS	137 mM NaCl, 2.7 mM KCl, 10 mM Na_2HPO_4, 1.8 mM KH_2PO_4
PMSF stock	0.2 M PMSF in ethanol
Resolving gel	14-16% acrylamide, 0.1 SDS, 80 mM Tris/HCl pH 6.8, 0.1% ammoniumperoxodisulfate, 0.05% TEMED
SEM buffer	250 mM sucrose, 10 mM MOPS-KOH pH 7.2, 1 mM EDTA

Table 2.2.: List of solutions (continued)

Solutions	Components
SDS sample buffer	10% glycerol, 2% SDS, 0.01% bromophenole blue, 60 mM Tris/HCl pH 6.8
SDS running buffer	25 mM Tris, 192 mM glycine, 0.1% SDS
Stacking gel	4% acrylamide, 0.1% SDS, 380 mM Tris/HCl pH 8.8, 0.1% ammoniumperoxodisulfate, 0.05% TEMED
SEM buffer	250 mM sucrose, 10 mM MOPS-KOH pH 7.2, 1 mM EDTA
TBS-T	50 mM Tris, 150 mM NaCl, 0.05% Tween-20
TE buffer	10 mM Tris pH 8.0, 1 mM EDTA
TAE buffer	40 mM Tris/acetate pH 8.0, 2 mM EDTA
TCA solution	72 % trichloroacetic acid in water
YPD medium	1 % yeast extract, 2 % peptone, 2 % glucose
YPG medium	1 % yeast extract, 2 % peptone, 3 % glycerol
Zymolyase buffer	1.2 M sorbitol, 20 mM K_3PO_4

2.1.3. Microorganism and cell lines

E. coli, *S. cerevisiae* and human strains used for expression and cloning are listed in Table 2.3.

Table 2.3.: List of strains

Strains	Genotype	Reference
XL1-blue (*E. coli*)		Stratagene
YPH499 (yeast)	MATa ura3-52 lys2-801_amber ade2-101_ochre trp1-Δ63 his3-Δ200 leu2-Δ1	Sikorski and Hieter (1989) Genetics 122 : 19 − 27
BY4741	MATa ura3−Δ0 his3-Δ1 leu2-Δ0 met15-Δ0	Euroscarf
*mic10*Δ	MATa ura3−Δ0 his3-Δ1 leu2-Δ0 met15-Δ0; mio10::kanMX4	Alkhaja et al. 2012
$Tim18^{ZZ}$	MATa ura3-52 lys2-801_amber ade2-101_ochre trp1-Δ63 his3-Δ200 leu2-Δ1, tim18::tim18-protAHIS3MX6	Rehling et al. 2002

Table 2.3.: List of strains (continued)

Strains	Genotype	Reference
Mic60^{EPEA}	MATa ura3-52 lys2-801_amber ade2-101_ochre trp1-Δ63 his3-Δ200 leu2-Δ1 mic60::MIC60-EPEA-HIS3MX6	This study
Flp-In T-Rex-293 (HEK293T-REx; human)		life technologies

2.1.4. Oligonucleotides and Plasmids

Table 2.4.: List of oligonucleotides

Purpose	Primers
oMD581	GCCGAATTCATGCTGGCCACCCGCGTGTTCAGC
SP6	TCTATAGTGTCACCTAAAT
oMD479	GTGGCGCGCTTAGGCATCAGCAAACCCAAGC
oMD490	ATATGTCAAAGAGCAGGAGCAGAAGGATCCA
oTM01	CACCGTGTCTGAGTCGGAGCTCGGC
oTM05	GGTGAGGAGGAAAGGCCTGGTCACG
oTM06	TTCCACTCAAGAGCTCTGCGACTCT

Table 2.5.: List of plasmids

Plasmid	Purpose
pcDNA5/FRT/TO	human expression plasmid
pcDNA5/FRT/TO-mitoAPEX	Expression of APEX in mitochondrial matrix
pcDNA5/FRT/TO-Mic10-APEX	Expression of MIC10-APEX
pcDNA3/FRT/TO-Mic10-BioID2	Expression of MIC10-BioID2
pYES2	yeast expression plasmid
pYES2-EPEA	Expression of Mic60-EPEA

2.1.5. Antibodies

Primary antibodies used in this study were generated by injection of peptides or purified proteins into rabbits. Goat anti-rabbit HRP conjugate (Dianova) was used as a secondary antibody.

2.1.6. Kits

Commercial kits used in this study together with suppliers are listed in Table 2.6. Kits were used and stored according to the manufactures' instructions.

Table 2.6.: List of Kits

Kits	Supplier
Complex IV Human Specific Activity Microplate Assay Kit	Thermo Scientific
FastDigest restriction enzymes	Fermentas/Thermo Scientific
Flexi®Rabbit reticulocyte Lysate System	Promega
KOD Hot Start DNA Polymerase	Novagen/Merck
TNT Quick coupled Transcription/Translation system	Promega
QIAamp DNA Mini Kit	Quagen
Wizard SV Gel and PCR Clean Up	Promega
Wizard SV Mini-Prep	Promega

2.1.7. Equipment

Laboratory equipment used in this study and suppliers are listed in Table 2.7.

Table 2.7.: List of Equipment

Product	Model	Supplier
Eletctrophoresis and blotting	EPS 601 power supply	GE Healthcare
	PowerPac HC Power supply	Bio-Rad
	Semi Dry Blotting Chamber	PEQLAB Biotechnologie
Centrifuges	5415R	Eppendorf
	5417R	Eppendorf
	5424	Eppendorf
	5804R	Eppendorf
	Sorvall RC 12BP	Thermo Scientific
	Sorvall RC6 Plus	Thermo Scientific
	Avanti J-26XP	Beckmann Coulter
Imaging	Agfa Curix 60 Developing machine	Agfa
	Amersham Typhoon PhosphorImager	GE Healthcare
	Autoradiography Storage Phosphor Screen	GE Healthcare
	Delta Vision Fluorescence Microscope	Applied Precision

Table 2.7.: List of Equipment (continued)

Product	Model	Supplier
	Fluorescence Scanner FLA-9000	Fujifilm
	V750 Pro	Epson
Other	Autoclave Systec DX-200	Systec
	Hoefer SE600 Ruby Blue native system	GE Healthcare
	Magnetic Stirrer MR 3001	Heidolph
	MilliQ water purification system	Millipore
	NanoVue Spectrophotometer	GE Healthcare
	pH-meter	InoLab
	Pipettes	Gilson
	Potter S glass-Teflon Homogenizer	Satorius AG
	Thermomixer Comfort	Eppendorf
	Vortex-Genie 2	Scienticic Industries

2.1.8. Software

Table 2.8.: Software used in this study

Software	Producer
ChemBioDraw Ultra 13.0	CambridgeSoft
ChemSketch 12.0	ACD Labs
DataGraph 4.3	Visual Data Tools, Inc.
Geneious Prime	Biomatters, Auckland, New Zealand
Fiji Image Processing	Johannes Schindelin, Albert Cardona, Mark Longair, Benjamin Schmid, and others
Illustrator CS5.3	Adobe Systems
ImageQuant TL	GE Healthcare
Microsoft Office 2013	Microsoft Corporations
mikTEX	Christian Schenk
Papers 3	Mekentosj, Aalsmeer, Netherlands
Photoshop CS5.1	Adobe Systems
Softworx Image Acquisition Software	Applied Precision, Bratislava, Slovakia
Texmaker	Pascal Brachet

2.2. Cell cultivation and isolation of mitochondria

2.2.1. Transformation of HEK-cells

For the transformation, HEK293T-REx cells were grown on a 6 well plate. To 100 μL Opti-MEM were added 5 μL Lipofectamine solution, 400 ng pcDNA5 and 1200 ng pOG44. The solution was mixed by pipetting and incubated for 20 min at RT to form the reagent complexes. 600 μL DMEM-medium were added and the solution was given drop-by-drop to the cells. After incubation for 3 h at 37 °C and 5% CO_2, 4 mL DMEM-medium were added and the cells grown for two days. Subsequently, selection was started by adding 2 mL fresh DMEM-medium with 4 μL hygromycin. After one week of selection, single cells were pipetted and grown on new wells in selective medium.

2.2.2. Isolation of human mitochondria

For isolation of human mitochondria (Mick et al., 2012), cells were grown on a 14 cm TC-plate. To start proteinbiosynthesis of modified proteins, the cells were induced for at least 12 h with tetracyclin (final concentration of 0.001 mg/mL). The medium was removed, the cells washed with 10 mL PBS and removed from the plate with 2x 5 mL PBS + 1 mM EDTA followed by centrifugation for 10 min at 1500 rpm and 4 °C. The pellets were resuspended in 2 mL cold THE-buffer containing 1% BSA and 1 mM PMSF. The cells were opened by 3 cycles of pottering 25x in a Potter S homogenizer, centrifugation for 10 min at 4000 g, keeping the supernatant and resuspending the pellet again in THE-buffer. The supernatant again was centrifuged for 5 min at 8000 g, transferred into new tubes and centrifuged for 10 min at 11000 g and the pellets were resuspended in 100 μL THE without BSA.

Using a 10% Bradford-based reagent Roti-Quant solution and Bovine IgG as a standard protein, the mitochondrial protein concentration was determined. Absorption at a wavelength of 595 nm was measured after 5 min of incubation using a GeneQuant 1300 Spectrophotometer. Isolated mitochondria were adjusted to 5 mg/mL in THE, flash frozen in liquid nitrogen and stored at -80°C.

2.2.3. Isolation of yeast mitochondria

For isolation of mitochondria as published (Meisinger, Pfanner, & Truscott, 2006), Yeast were grown at 30 °C in YPG medium to an OD_{600} of 2-3. Cells were pelleted and resuspended in buffer A (10 mM DTT, 100 mM Tris/H_2SO_4 pH 9.4) and incubated for

30 min at 30 °C. To remove the cell wall, cells were incubated after washing in zymolase buffer (20 mM KPO_4 pH 7.4, 1.2 M sorbitol and 0.57 mg/L zymolase) for 1 h at 30 °C and subsequently opened in cold homogenization buffer (600 mM sorbitol, 10 mM Tris/HCl pH 7.4, 1 g/L BSA, 1 mM PMSF and 1 mM EDTA) with a cell homogenizer. Differential centrifugation lead to a mitochondrial fraction, which was resuspended in SEM buffer and frozen in liquid nitrogen.

2.2.4. Transformation of *E. coli*

For transformation, frozen bacteria were thawed on ice, 100 ng of DNA was added and incubated for 10 min on ice. Then, bacteria were heat-shocked at 42 °C for 1 min and put back on ice for 1 min. Afterwards, 1 mL LB medium was added and bacteria were incubated for 1 h at 37 °C, 1000 rpm. After centrifugation for 1 min at 16000 g, the pellet was resuspended in 100 μL medium and plated out on LBamp plates.

2.2.5. Transformation of *Saccharomyces cerevisiae*

Yeast cells YPH499 were grown over night in 2x YPD Medium and harvested by centrifugation for 5 min at 4000 rpm. Subsequently, cells were washed 2x with 5 mL 0.1 M LiAc-TE buffer and were gathered in 2 mL buffer. To 50 μL of yeast cells were added 5 μL of Hering sperm DNA in TE buffer as carrier DNA, 1.5 μL of purified DNA or plasmid pYES2 and 300 μL of 0.1 M LiAc/PEG-4000 medium. After incubation for 30 min at 30 °C, 36 μL DMSO were added, the cells heat-shocked for 15 min at 41 ° and pelleted at 4000 rpm for 5 min. Cells were resuspended in 75 μL DNase free water and plated on seletive plaets and incubated at 30 °C.

2.2.6. Isolation of Yeast mitochondria

Mitochondria from yeast were isolated essentially as described before (Stojanovski, Pfanner, & Wiedemann, 2007). Yeast strains were grown in selective YNB-URA medium with 2% raffinose or 2% galactose to an OD_{600}=1.5-2.0 and pelleted for 15 min at 18 °C, 4000 rpm. Cells were washed with H_2O, pooled, re-pelleted and incubated at 30 °, 90 rpm in DTT buffer (2 mL per gram wet cell mass) for 30 min. After DTT treatment, cells were centrifuged at 18 °C for 8 min at 4000 rpm, washed with 1.2 M D(+)-Sorbitol and re-pelleted. Next, cells were resuspended in zymolyase buffer (7 mL per gram wet cell mass), 4 mg Zymolyase per gram wet cell mass in sorbitol was added and the yeast

was incubated at 90 rpm for 60 min at 30 °C. Afterwards, zymolyase treated cells were pelleted at 18 °C for 10 min at 3000 rpm and washed with 100 mL zymolyase buffer. Next, cells were resuspended in homogenization buffer in a volume of 7 mL/g of yeast and opened using a pre-cooled Potter S homogenizer at 700 rpm for 15 cycles. The homogenate was centrifuged at 4 °C for 5 min at 3000 rpm and the supernatant was collected and re-centrifuged at 4 °C for 10 min at 4000 rpm. Subsequently, mitochondria were pelleted at 4 °C for 15 min at 12000 rpm, pellets pooled in ice cold SEM containing 1 mM PMSF, re-centrifuged using the same conditions and resuspended in an appropriate amount of SEM buffer.

Using a 10% Bradford-based reagent Roti-Quant solution and Bovine IgGs as a standard protein, the mitochondrial protein concentration was determined. Absorption at a wavelength of 595 nm was measured after 5 min of incubation using a GeneQuant 1300 Spectrophotometer. Isolated mitochondria were adjusted to 10 mg/mL in SEM, flash frozen in liquid nitrogen and stored at -80°C.

2.3. Molecular biology methods

2.3.1. Isolation of plasmids from *E. coli*

A Wizard® Plus SV Minipreps DNA purification Kit (Promega) was used to isolate plasmids from *E. coli* strains according to the manual. Therefore, an overnight culture of bacteria harbouring the plasmid of interest were pelleted and resuspended in 250 μL resuspension buffer. Next, 250 μL of lysis buffer and 10 μL of alkaline protease were added and mixed by inverting for 4 times. Subsequently, 350 μL of neutralizing solution were added and the lysate was cleared by centrifugation for 10 min at 21000 g. The supernatant was loaded on columns and washed with 700 μL and 400 μL washing buffer supplemented with ethanol. Residual ethanol was removed by centrifugation of the columns without buffer and finally, DNA was eluted with 50 μL of DNase free water.

2.3.2. Polymerase chain reaction (PCR)

DNA fragments for molecular cloning and yeast transformation were amplified using KOD Hot Start DNA polymerase (Novagen) according to manufactures protocol. Each 50 μL reaction mix contained 200 ng of genomic DNA, 0.2 mM dNTP, 1 mM $MgSO_4$, 0.3 μM forward and reverse primers and 1 U KOD polymerase in 1x KOD reaction buffer. First, template DNA was denatured at 95 °C for 2 min. After this, 9 cycles of

polymerase chain reaction were performed. PCR products were analysed by agarose gel electrophoresis with ethidium bromide staining followed by exposure to UV light.

2.3.3. Agarose gel electrophoresis

For the visualization and purification of PCR products of different length, agarose gel electrophoresis was used. 1% agarose solution was freshly prepared by dissolving an appropriate amount of dry agarose in TAE buffer. The mixture was heated until agarose dissolved completely and then cooled to approximately 50 °C. Ethidium bromide was added to the final concentration of 1 mug/mL and solid gel was prepared. Samples were mixed with DNA loading dye, loaded on the solid gel and run at 8 V/cm. Separated DNA fragments were visualized by illuminating the gel with UV-light.

2.3.4. Gel purification of DNA

DNA was analysed on agarose gels, cut out and purified using the Wizard® SV Gel and PCR Clean-Up System Kit. For this, 10 μL membrane binding buffer per 10 mg excised gel was added and the gel was dissolved at 55 °C and 800 rpm for 10 min. The solution was than loaded on a column, incubated for 1 min and centrifuged for 1 min at 16000 g. Next, the columns were washed with 700 μL and 500 μL washing solution and dried for 2 min at 16000 g and for 5 min at 37 °C. The DNA was eluted with 50 μL DNase free water.

2.3.5. Molecular cloning

For cloning of DNA fragments into plasmids, Fast Digest restriction enzymes (Fermentas) were used as prescribed before (Sambrook & Russel, 2001). Therefore, the plasmid and the corresponding PCR product were digested with the respevtive FastDigest restriction enzyme (ThermoScientific). In 1x FastDigest buffer, 500 - 800 ng DNA were mixed with 1 μL of both restriction enzymes in a total reaction volume of 30 μL. After incubation for 30 min at 37 °C, digested fragments were purified as described before (see section 2.3.4). The ligation mix contained 5 μL digested plasmid, 10 μL digested insert, 4 μL DNA Ligation buffer and 1 μL T4 DNA Ligase (Rapid DNA Ligation Kit, Thermo Scientific) and was incuabted for 30 min at 22 °C. For bacterial expression, 10 μL of the mixture were transformed into competent E. coli XL1 cells (see section 2.2.4). Collected clones were confirmed by restriction digestion and sequencing (SeqLab, Göttingen).

2.4. Biochemical methods

2.4.1. Immunofluorescence of U_2OS-Cells

For microscoping the cells, an immunofluorescence protocol had to be done. Therefore, the cells were grown on a cover slip and transfected 24 h before. Cells were incubated for 20 min with MitoTracker Orange CMTMRos (Life Technologies). The slips were gently washed with PBS and incubated with 4% PFA in PBS for 20 min at 37 °C. After washing 5x with PBS they were incubated in 0.2% Triton X-100 for 20 min at rt. They were washed again 5x with PBS and incubated another 20 min at rt in 1% BSA and washed again 5x with PBS.

The samples were placed in a dark humid chamber and 40 μL of monoclonal anti-HA antibody were applied. After incubation for 1 h at rt and washing 5x with PBS 40 μL second antibody (AlexaFlour488 GαM 1:200 in PBS) were applied and incubated for another 30 min. The samples were washed 5x with PBS and 1x with H_2O. One drop DAPI/mowiol solution was applied on a glass slide and the cover slip put upside down onto the drop. After drying over night at rt in the dark the samples were stored at 4°C and analysed by fluorescence microscopy. Electron microscopy was performed as previously described (Richter et al., 2019).

2.4.2. Swelling of mitochondria

For swelling, aliquots of 2 x 11 μL and 1 x 5.5 μL mitochondria (10mg/mL) were prepared. In order to get fully intact mitochondria, 100 μL SEM-buffer were added to one 11 μL aliqout and split into 4 25 μL aliquots.

To prepare mitoplasts, 50 μL EM-buffer were added to the second 11 μL/g aliquot and gently pipetted 20 times, than another 50 μL EM-buffer were added and again followed by gently pipetting and aliquotation into 25 μL aliquots. This leads to a rupture of the outer mitochondrial membrane due to absence of an osmotic support. Subsequently, both samples were swollen for 25 min on ice and 0, 3, 6, or 9 μL proteinase K (1mg/mL) were added. After 10 min incubation on ice, 1.5 μL PMSF (0.2 M) were added to each sample to inhibit the proteinase and incubate again for 10 min on ice. The mitochondria and mitoplasts were spinned out for 10 min at 13.200 rpm and 4 °C and the pellets were resuspended in 30 μL 1x SDS sample buffer (+1% β-Mercaptoethanol and 1 mM PMSF).

To rupture both, the outer and inner mitochondrial membrane, 34.5 μL EM-buffer were added to the 5.5 μL aliquot, split into 2 x 20 μL and mixed with 0 or 9 μL proteinase

K. The samples were subjected to 3 x 20 sec indirect ultra sound pulses and 10 μL 4x SDS sample buffer were added. All samples were analysed by SDS-PAGE.

2.4.3. Affinity purifications

Isolated mitochondria were solubilized in buffer (20 mM Tris-HCl, pH 7.4, 100 mM NaCl, 0.5 mM EDTA, 10 % (w/v) glycerol, 1 mM PMSF, 1 % digitonin) at a final concentration of 1 mg/mL and incubated at 4 °C for 30 min. Lysates were cleared by centrifugation at 14,000 g for 10 min at 4 °C and applied to affinity matrices. For FLAG immunoprecipitations, anti-FLAG agarose affinity resin (Sigma-Aldrich) and for immuoprecipitations of $MIC10^{BioID2}$, anti-HA agarose affinity resin (Sigma-Aldrich) were used. For protein A and EPEA isolations, human-IgG sepharose (MP Biomedicals) or purified EPEA nanobody, respectively, were coupled to CNBr-Activated sepharose 4B (GE Healthcare) according to the manufacturers protocol. Affinity columns for Tim21 and Tim23 immunoisolations were prepared by crosslinking protein A-sepharose beads to Tim21 or Tim23 antisera. Protein lysates were incubated with affinity resins for 1 hour at 4 °C on an end-over-end shaker. Unbound proteins were removed by centrifugation (100 x g, 1 min, 4 °C) through a minicolumn fitted with a filter. The beads were washed 10 times with W-buffer (25 mM Tris/pH7.4, 150 mM NaCl, 1 mM EDTA, 10 %(w/v) Glycerol, 0.3 % (w/v) Digitonin, 1mM PMSF). Samples were eluted with 0.1M glycine (pH 2.8), except in the case of EPEA isolation (W-buffer + 0.5 mg/ml EPEA peptide for 10 min at RT), protein A isolation (cleaved overnight at 4 °C with 0.4 mg/mL acetylated tobacco etch virus (AcTEV; Thermo Fisher Scientific) protease), or native elution of $MIC10^{FLAG}$ (W-buffer + 5 μg/mL FLAG peptide (Sigma)).

2.4.4. *In vitro* mitochondrial import

Radiolabeled precursor proteins were synthesized using rabbit reticulocyte lysate (Promega) in the presence of [^{35}S]methionine. Isolated mitochondria were diluted in import buffer for yeast (250 mM sucrose, 10 mM MOPS/KOH pH 7.2, 80 mM KCl, 2 mM KH2PO4, 5 mM MgCl2, 5 mM methionine, 2 mM ATP, 2 mM NADH and 3 % BSA supplemented with 5 mM creatin phosphate and 0.1 mg/mL creatine kinase for TIM22 substrates). Import reactions were initiated by addition of 2 % or 5 % lysate for TIM23 substrates and TIM22 substrates respectively. Samples were incubated with radiolabelled proteins for the indicated times. To stop the reaction, membrane potential was dissipated on ice using 8 mM antimycin A, 1 mM valinomycin and 10 mM oligomycin. Non-imported

proteins were removed by Proteinase K (20 μg/mL) treatment for 10 minutes on ice. 2mM PMSF was added to inactivate Proteinase K for 10 minutes on ice. Mitochondria were collected, washed with SEM buffer (250 mM sucrose, 1 mM EDTA, 20 mM MOPS, pH 7.2) and used for SDS-PAGE analyses or BN-PAGE analyses. Results were visualized using digital autoradiography. Quantifications were performed using ImageQuant TL (GE Healthcare) using rolling ball background subtraction.

2.4.5. Generating and isolating the TOM-TIM23 supercomplex

For arresting the supercomplex, Prec-sfGFP was imported in isolated mitochondria as described before. After import, mitochondria were pelleted for 10 min, 16,000 x g, 4 °C and washed once with SEM. Mitochondria were solubilized in digitonin-containing buffer as prescribed before. For affinity purification, Strep-Tactin sepharose beads (IBA) were pre-incubated with purified GFP nanobody for 1 h at RT and washed with 2X buffer (40 mM HEPES/KOH pH 7.4, 300 mM NaCl, 40 % glycerol, 0.2 mM EDTA). Cleared mitochondrial lysate was incubated for 1 h at 4 °C on a rotating wheel. Beads were washed with W-buffer as prescribed before (see 2.4.3) followed by elution with 7.5 mM desthiobiotin in wash buffer. Samples were analysed by SDS-PAGE and western blotting.

2.4.6. *In organello* biotinylation

Adapted from (Rhee et al., 2013). For biotinylation, 1 mg of mitochondria were centrifuged for 5 min at 13200 rpm and 4 °C and the pellet resuspended in 1 mL buffer (THE for human mitochondria, SEM for yeast mitochondria). This was aliquoted into 2 x 500 μL (positive and negative sample), to the positive-sample 500 μM biotin-phenol were added and to the negative-sample the equivalent amount of buffer. Both samples incubated 10 min at 25 °C and 400 rpm before addition of H_2O_2 (final concentration of 1 mM) and incubation for 1 min. The samples were centrifuged for 5 min at 13200 rpm, the supernatant was discarded and the pellet resuspended in 600 μL quenching solution (10 mM NaN_3, 10 mM Na-Ascorbat, 5 mM Trolox) followed by again centrifugation. These step was repeated three times. Subsequently, the pellet was resuspended in 500 μL extraction buffer (20 mM Tris/HCl pH 7.4, 50 mM NaCl, 0.5 mM EDTA, 10% glycerol, 1% Triton X-100, 1 mM PMSF) and incubate short time at rt. After centrifugation for 10 min at 13200 rpm the supernatant was loaded on equilibrated containing 80 μL slurry matrix material and incubate for 30 min on an end-over-end shaker. The columns were centrifuged for 1 min at 1000 g and washed 10x with 400 μL washing buffer (20

mM Tris/HCl pH 7.4, 50 mM NaCl, 0.5 mM EDTA, 10% glycerol, 0.5% Triton X-100, 1 mM PMSF) and dried for 2 min at 2000 g. For elution, depending on column material, either 2 mM D-Biotin (2 x 40 μL, incubation for 5 min at rt), 0.1 M glycin pH 2.8 (2 x 40 μL, incubation for 5 min at rt) or hot SDS sample buffer with 5 mM desthiobiotin (80 μL, incubation for 5 min at 95 °C). All samples were analysed by SDS-PAGE.

2.4.7. *In vivo* biotinylation of HEK-cells

For *in vivo* biotinylation of HEK-cells as published (Roux, Kim, Burke, & May, 2018), those were grown on a 14 cm TC-plate. To start proteinbiosynthesis of modified proteins, the cells were induced for at least 12 h with tetracyclin (final concentration of 1 *mu*g/mL). 500 μM biotin phenol in DMEM-medium was added to the cells and incubate for 30 min at 37 °C before addition of H_2O_2 (final concentration of 1 mM) for 1 min at rt. The cells were washed twice with 10 mL quenching solution (see *in organello* biotinylation) and once with PBS. 10 mL quenching solution were added and the cells were collected by gently pipetting followed by centrifugation for 5 min at 2000 rpm. The pellet was frozen for at least 0 min at -80°C. Subsequently, the cell pellets were lysed by thawing on ice, followed by addition of 400 μL fresh RIPA lysis buffer (0.5% Na-deoxycholat, 5 mM Trolox, 50 mM Tris/HCl pH 7.4, 150 mM NaCl, 0.1% SDS, 1% Triton X-100, 1 mM PMSF, 10 mM NaN_3, 10 mM Na-ascorbate, protease-cocktail) and incubation for 5 min on ice. The lysates were clarified by centrifugation for 10 min at 13000 rpm. The supernatant was loaded on the columns and incubated for 30 min on an end-over-end-shaker. The flow-through was removed for 30 sec at 100 g and the beads washed 2x with RIPA lysis buffer, 1x with 2 M urea in 10 mM Tris/HCl pH 8.0 and again 2x with RIPA lysis buffer. For elution, depending on column material, either 2 mM D-Biotin (2 x 75 μL, incubation for 5 min at rt), 0.1 M glycin pH 2.8 (2 x 75 μL, incubation for 5 min at rt) or hot SDS sample buffer with 5 mM desthiobiotin (2x 125 μL, incubation for 5 min at 95 °C). All samples were analysed by SDS-PAGE.

2.4.8. Measurement of mitochondrial membrane potential

Mitochondrial membrane potential in human cells was assessed using the fluorescent dye Tetramethylrhodamine-methylester (TMRM). Cells were incubated for 30 min at 37°C with staining solution (0.1 μM TMRM in DMEM) and subsequently washed, harvested and then fixed for 10 min in 2 % PFA in PBS. Cells were then measured in PBS supplemented with 10 % FBS, using a BD-Canto flow cytometer (Becton Dick-

inson), with excitation at 488 nm and detection with a 570 ± 10 nm emission filter. Mitochondrial membrane potential in yeast was measured using a potential-sensitive dye 3,3â-dipropylthiadicarocyanine iodide (DiSC3(5)). Mitochondria were diluted in a buffer containing 600 mM sorbitol, 1 % (wt/vol) BSA, 10 mM MgCl2 and 20 mM KPi (pH7.4) to a concentration of 166 μg/mL. Changes in fluorescence were assessed with an F-7000 fluorescence spectrophotometer (Hitachi, JP), at room temperature, with excitation of 622 nm, emission at 670 nm and slits of 5 nm. After reaching a stable signal, components were added to the cuvette in the following order: 500 μL of buffer, DiSC3(5), 15 μg of mitochondria, 1 μM valinomycin (to compare relative differences in membrane potential, the difference in fluorescence before and after addition of valinomycin was used).

2.4.9. TCA precipitation of *Saccharomyces cerevisiae*

In order to verify the transformation, a TCA precipitation was performed. Therefore, one colony per culture was inoculated in 4 mL YNB-ura medium with 1% raffinose. After growing over night each culture was split into two and to one half 1% galactose was added. The cells were pelleted for 2 min at 13200 rpm and resuspended in 300 μL PBS. 100 μL TCA were added and mixed well. Cells were frozen for 20 min at -80 °C and thawed at rt. After centrifugation for 15 min at 13200 rpm and 4 °C the supernatant was discarded and the pellet was washed with 500 μL cold 80% acetone and centrifuged again for 15 min at 13200 rpm and 4 ° and dried for 15 min at rt. Subsequently, the pellet was resuspended in 150 μ 1x pellucid Laemmli and incubated for 20 min at 30 °C. Next, 50 μL 4x Laemmli (+ 1% β-Mercaptoethanol) were added and incubated for 5 min at 95 °C. The samples were analysed by SDS-PAGE.

2.4.10. SDS-PAGE

Denaturing SDS-PAGE was performed similar as described by Laemmli (1970). For this, gels with 0.1% SDS were used with a stacking gel containing 4% acrylamide (37.5:1 ratio of acrylamide to bisacrylamide), 80 mM Tris/HCl pH 6.8 and a separating gel containing 14 or 16% acrylamide, 385 mM Tris/HCl pH 8.8. Experiments were done using running buffer containing 190 mM glycine, 25 mM Tris/HCl pH 6.8 and 0.1% SDS (w/v). Before loading, samples were incubated for 5 min at 95 °C in SDS sample buffer and run in a custom-made midi gel system at 25 mA or 30 mA per gel respectively.

2.4.11. Western blotting and immunodecoration

Proteins were transferred to polyvinylidene fluoride (PVDF) membranes after SDS-PAGE by semi-dry blotting using PREQLAB chambers. The membranes were activated in ethanol and washed in transfer buffer (20 mM Tris, 150 mM glycine, 0.02% SDS (w/v), 20% ethanol). Next, the membrane was placed on top of three Whatman papers soaked in transfer buffer, the gel was placed on the membrane and topped with three additional Whatman papers. Blotting was done for 2.5 h at 250 mA. Subsequently, the membranes were stained with coomassie R-250, destained with methanol and blocked in 5% milk in TBS-T for 1 h at rt. After that, the membranes were washed with TBS-T and incubated with the primary antibody for 1 h at rt oder over night at 4 °C. The membranes were washed 3x for 10 min each with TBS-T and 1:10000 diluted HRP coupled secondary antibody was added and incubated for 1 h at rt. After another 3 washing steps in TBS-T, ECL was added and the signals were detected using x-ray films.

2.4.12. Coomassie Brilliant Blue staining

Proteins in SDS gels and PFDV membranes were stained using a solution containing 2.5 g/mL Coomassie Brilliant Blue R-250, 40% (w/v) ethanol and 10% acetic acid at room temperature for 5 minutes (PVDF) oder 1 h (gels). Washing with 30% ethanol, 10% acetic acid reduced background staining.

2.4.13. Colloidal Coomassie staining

Colloidal coomassie staining for subsequent MS analysis was performed similar as described by Neuhoff *et al.* (1988). In order to stain acrylamide gels which were used for MS analysis, gels were fixed at least 60 min in 40% (v/v) ethanol and 10% acetic acid. After washing with MilliQ water for 2 times, the gels were stained at least over night with a dye solution containing 0.1% (w/v) Coomassie Brilliant Blue G250, 2% (w/v) ortho-phosphoric acid, 10% (w/v) ammonium sulfate and 20% (v/v) methanol. Background staining was removed with 1% (v/v) acetic acid.

2.4.14. Mass-spectrometry

2.4.14.1. Sample preparation for mass spectrometry

Samples were separated on 4-12% NuPAGE Novex Bis-Tris Minigels (Invitrogen). After staining with Coomassie blue, each lane was sliced into 23 equdistand slices. To per-

form protein digestion, gel slices were washed, reduced with DTT and alkylated with 2-iodoacetamide followed by digestion with En7dopeptidase Trypsin (sequencing grade, Promega) overnight. The extracted peptide mix was dried in a SpeedVac and resuspended in 2% acetonitrile/0.1% formic acid/ (v:v) to be analysed by nanoLC-MS/MS as described previously (Atanassov & Urlaub, 2013).

Sample preparation and data analysis were performed by Thierry Wasselin and Christof Lenz of the Bioanalytical Mass Spectrometry Group at the Max-Planck Institute for Biophysical Chemistry in Göttingen.

3. Results

3.1. Deletion of MIC10 alters inner mitochondrial membrane morphology

3.1.1. Generation of MIC10 knock-out using the CRISPR/Cas9 system

The MICOS complex is crucial for forming and maintaining cristae junctions. Since initial studies in mammalian cells revealed MIC60 being essential for proper inner mitochondrial membrane morphology (John et al., 2005) it could also be shown that the same is observed for Mic10 in yeast (Alkhaja et al., 2012; von der Malsburg et al., 2011; Harner et al., 2011). The most insight about the function and necessity of Mic10 in mitochondrial ultrastructure come from various studies in yeast *S. cerevisiae* (Friedman et al., 2015; Barbot et al., 2015; Milenkovic & Larsson, 2015; Bohnert et al., 2015). So far, only studies of MICOS in knock-down cells were published and revealed an impact of the individual subunits on the mitochondrial membrane ultrastructure (Li et al., 2016). To investigate the necessity of the MICOS complex and the unique morphology of the mitochondrial inner membrane for proper functionality of mitochondria in the mammalian system, a MIC10$^{-/-}$ cell-line using the CRISPR/Cas9 system was generated. Therefore a MIC10 specific guide RNA was identified by online software prediction tools and cloned. The system is based on the guide RNA targeting the genomic locus of interest using the bacterial Cas9 nuclease, it induced a double-stranded breake (P. Horvath & Barrangou, 2010; Ran et al., 2013), which resulted in the recruitment of the cell's DNA repair machinery. The repair mechanism is very error-prone, leading mostly to a disrupted gene which results in a loss of protein expression (Ran et al., 2013).

To achieve this, for MIC10 specific primers were designed targeting the first exon of the gene and cloned into the CRISPR/Cas9 vector pX458. The cloned plasmid was transiently transfected into HEK293T-REx cells and single cells expressing the additional GFP-protein from the plasmid were sorted. To confirm the deletion of the protein, western-blot analysis of cell lysates with antibody against MIC10 was performed and

the clone missing the protein signal was used for further studies. To verify the knock-out on a genomic level, genomic DNA was isolated and PCR amplification of the open reading frame (ORF) of the MIC10 gene (EXON1) was carried out (Fig.3.1). The initial CRISPR induced double strand break at the designed target region led to multiple incorrect inserted base pairs (bp) after the first 18 bp of the ORF during the repair event. This resulted in an shortened protein after 126 bp by a premature stop codon. Thus, transcription and translation of this altered ORF led to a completely different protein after the first 6 amino-acids and no biosynthesis of a functional MIC10 is taking place in these cells.

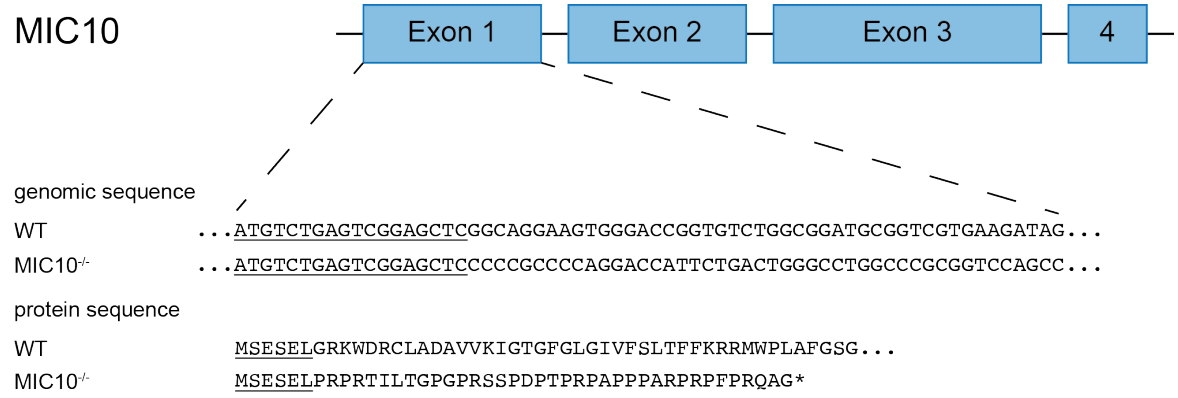

Figure 3.1.: CRISPR/Cas9 mediated knock-out leads to cancellation of WT MIC10 sequence in the first exon.
Sequencing of isolated genomic DNA from WT and MIC10$^{-/-}$ cells revealed a failed repair attempt after CRISPR/Cas9 treatment, thus leading to an abolition of the WT MIC10 sequence after the first 18 nucleotides.

3.1.2. Ablation of MIC10 affects mitochondrial inner membrane morphology

In yeast, deletion of Mic10 leads to a loss in cristae junctions, due to which the inner membrane loses its unique shape with distinct sections. Therefore resulting in onion-like shaped rings of the inner membrane (von der Malsburg et al., 2011; Alkhaja et al., 2012). To assess the ultrastructure in mitochondria from the MIC10$^{-/-}$ cells, an electron microscopy analysis was carried out in collaboration with Daniel C. Jans and Stefan Jakobs of the Max Planck institute for Biophysical Chemistry in Göttingen. Cells were fixed with glutaraldehyde and embedded in agarose, sections of WT and MIC10$^{-/-}$ cells were analysed using transmission electron microscopy. Whereas the WT cells displayed proper cristae junctions and distinctly long-shaped cristae, the deletion of MIC10 in

HEK-cells resulted in loss of cristae junctions, no formation of precise cristae and only ring-shaped inner mitochondrial membrane could be observed (Fig. 3.2) as shown for *mic10*Δ cells in yeast and MEF cells treated with shRNA against MIC10.

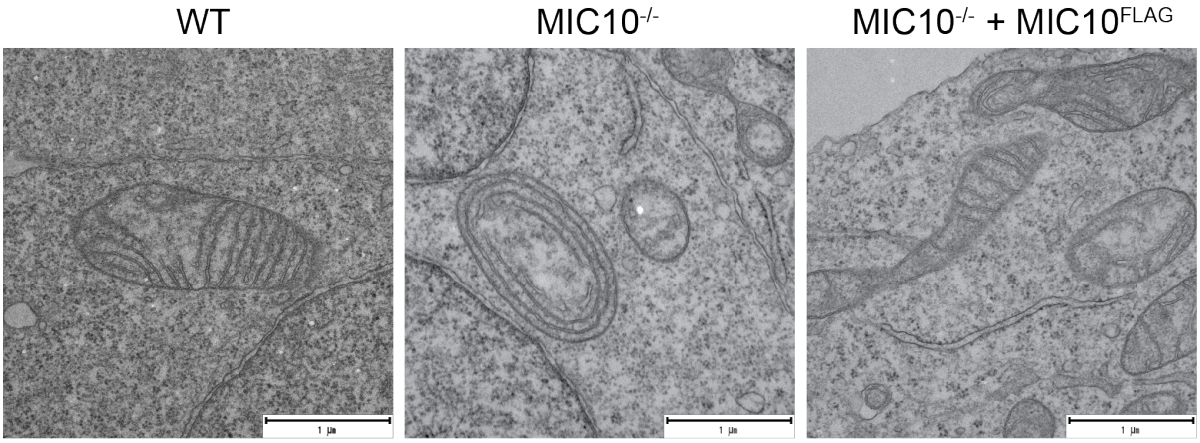

Figure 3.2.: Ablation of MIC10 leads to loss of cristae junctions and alteration of mitochondrial morphology.
WT, MIC10$^{-/-}$ and MIC10$^{-/-}$ cells expressing MIC10^{FLAG} were analysed using transmission electron microscopy to asses inner mitochondrial membrane morphology. Scale bar 1 μm. Courtesy of Daniel C. Jans and Stefan Jakobs.

To confirm that the observed morphological phenotype was based on the absence of MIC10 and was not an off-target effect of the CRISPR-approach, MIC10$^{-/-}$ cells were transfected with a MIC10^{FLAG} coding vector and the mitochondrial structure analysed. Bringing back the protein in the background of the knock-out could rescue the morphological phenotype (Fig. 3.2). This proved that also in mammalian cells MIC10 is crucial for maintaining and forming cristae junctions, thus important for proper inner mitochondrial membrane formation. For further investigation of the effect of alteration in the inner membrane structure, a cell proliferation assay was performed. For this purpose, 50,000 cells of WT and MIC10$^{-/-}$ were seeded and grown for three days on media containing either glucose or galactose. Cells were counted using a Neubauer chamber. However, neither growth on glucose nor galactose displayed a difference in cell proliferation after loss of MIC10 (Fig 3.3).

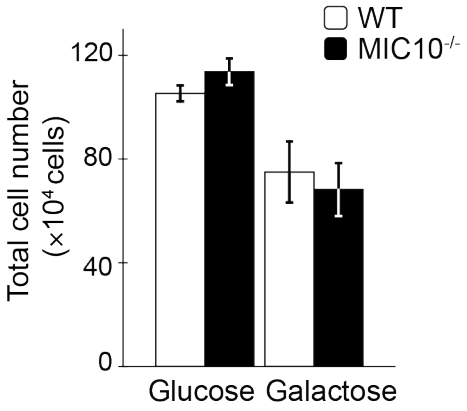

Figure 3.3.: Ablation of MIC10 does not influence cell proliferation.
Cell proliferation assay of WT and MIC10$^{-/-}$ cells grown in media containing either glucose or galactose. (mean ± SEM; n=3)

3.1.3. MIC10$^{-/-}$ mitochondria showed altered protein levels for MIC13

In spite of loosing their unique inner morphology, mitochondria lacking MIC10 seem to be able to maintain their function to not influence cell growth and health. To assess whether there is an impact of the altered morphology on the protein level, mitochondria from WT and MIC10$^{-/-}$ were isolated and steady state levels of various inner mitochondrial membrane proteins were evaluated by western-blot analysis (Fig. 3.4).

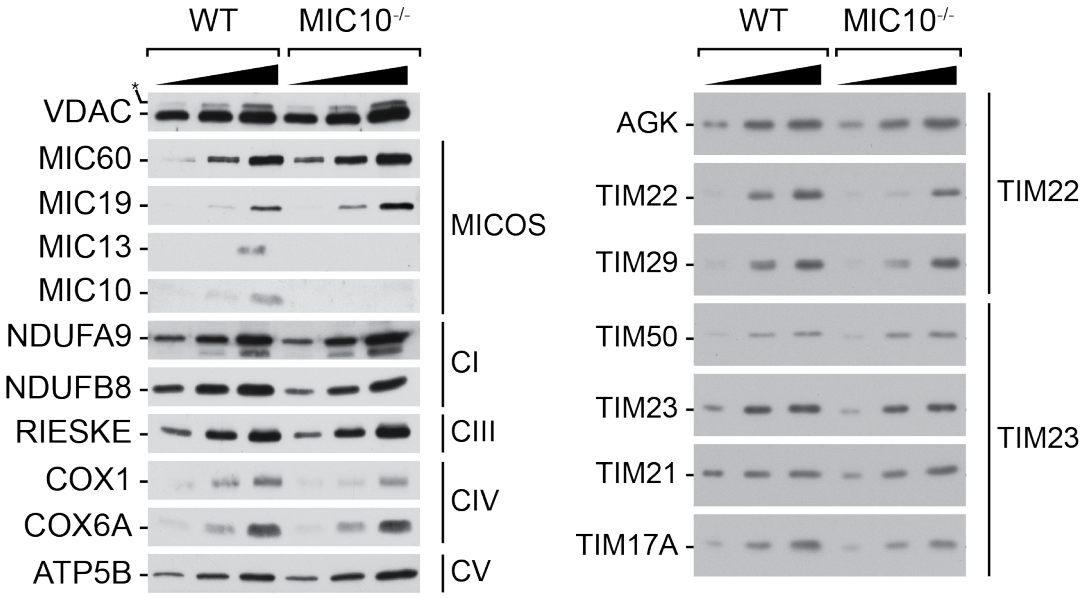

Figure 3.4.: MIC10$^{-/-}$ exhibits minor changes in protein steady state levels.
Mitochondria isolated from WT and MIC10$^{-/-}$ cells were analysed by western blot probing with various antibodies against MICOS, OXPHOS and translocases of the inner membrane.

Probing with antibodies against various MICOS components revealed that MIC60 and

MIC19, as part of the MIC60 subcomplex (Friedman et al., 2015), were slightly more abundant in the MIC10$^{-/-}$ cells then in the WT cells, whereas MIC13 was not present anymore in the MIC10$^{-/-}$ mitochondria. Thus led to the conclusion, that indeed the MIC60 subcomplex is able to function independently from the MIC10 subcomplex and upon loss of MIC10, MIC13 as an assembly factor of those two subcomplexes was not required anymore. Expression of MIC10^{FLAG} in MIC10$^{-/-}$ cells could rescue the protein levels of MIC10 and MIC10 (Fig. 3.5).

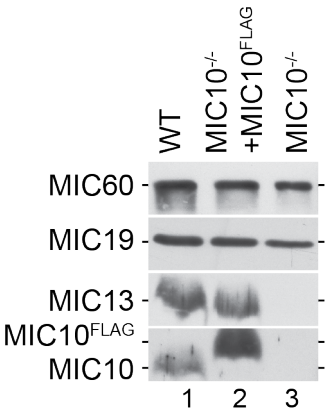

Figure 3.5.: MIC10^{FLAG} expression rescues MIC10$^{-/-}$ phenotype.
MIC10$^{-/-}$ were transiently transfected with a MIC10^{FLAG} coding vector and protein expression was assesed using western blot analysis.

Interestingly, only COX1 as part of the complex IV was affected of the OXPHOS machinery and its level slightly decreased, whereas COX6A as part of the same complex was not affected. Additionally, subunits of complex 1 (NDUFA9, NDUFB8), complex III (RIESKE) and complex V (ATP5B) were unaffected. Furthermore, translocase component TIM21 of the TIM23 complex did not show an effect upon the absence of MIC10. However, probing for components of the TIM22 complex revealed a slight decrease in TIM29 and an even more pronounced decrease in TIM22, two core components of the translocase. An effect of MIC10 ablation on the function of the TIM22 complex was confirmed by co-workers (Callegari et al., 2019).

To assess additional potential effects of a changed inner membrane structure, mitochondrial membrane potential was measured using the fluorescent dye tetramethylrhodamin methylester (TMRM). Being generated by proton pumps of the OXPHOS, it is essential for various mitochondrial functions, for example energy storage during oxidative phosporylation, protein import into mitochondria (Zorova et al., 2018). Furthermore, it is an indicator for mitochondrial health. To that end, cells were incubated for 30 min with a staining solution containing the dye and afterwards fixed with paraformaldehyde (PFA). The uptake of the membrane potential sensitive dye was measured using fluorescent activated flow cytometry and the fluorescent intensity of 10,000 cells was recorded.

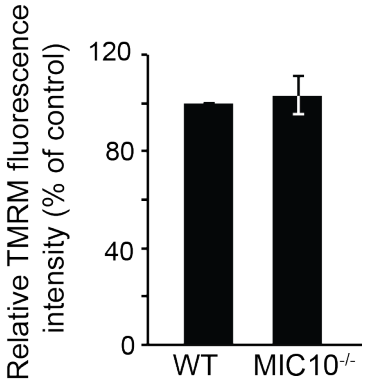

Figure 3.6.: Deletion of MIC10 does not result in an alteration of membrane potential.
WT and MIC10$^{-/-}$ cells were stained with membrane potential sensitive dye TMRM. After fixation the fluorescence of 10,000 cells was measured using flow cytometry. (mean ± SEM, n=6)

Compared to the WT cells, MIC10$^{-/-}$ cells did not display a change in fluorescent intensity (Fig. 3.6), thus the membrane potential was not affected despite the loss of cristae junctions. This lead to the conclusion that even though no distinct cristae are formed, the respiratory chain seem to operate appropriately to maintain mitochondrial function.

3.1.4. Respiration rate of MIC10$^{-/-}$ cells

Since COX1 levels in MIC10$^{-/-}$ mitochondria were reduced, this finding was indicative of an effect on the mitochondrial respiratory chain, although mitochondrial membrane potential was unaffected.

To adress a malfunction of respiration in the MIC10$^{-/-}$ cells, the amount and activity of complex IV was addressed using a complex IV Human Specific Activity Microplate Assay Kit. Cells were solubilized and applied to the provided plate to immunocapture complex IV. To colorimetrically asses the activity, reduced cytochrome *c* was added, whose oxidation by the complex can be measured by an absorbance at 500 nm. Subsequently, the amount of enzyme complex was assessed by adding a complex IV specific antibody conjugated with alkaline phosphatase. The phosphatase reacts with the substrate and changed it from colorless to yellow at 405 nm. The changes is colour time and complex IV amount dependent, thus can also be assessed colorimetrically. This analysis revealed, that indeed the overall amount of complex IV was reduced by nearly 50 %. However, the CIV activity in MIC10$^{-/-}$ cells was nearly at WT level and only reduced by about 10 % (Fig. 3.7 A).

To examine the entire OXPHOS activity, oxygen consumption measurements of whole cells using an OROBOROS2k system were performed. In this setup, the amount of

aqueous oxygen in the sample solution is evaluated by a Clark-type polarographic sensor inside the chamber and the specially designed software DatLab compute the oxygen uptake of the cells accordingly.

To pursue this analysis, WT and MIC10$^{-/-}$ cells were grown on DMEM media containing galactose and harvested. A cell suspension of 1 million cells in DMEM with galactose was transferred to the measuring chamber and the amount of oxygen over time in this suspension was monitored. The oxygen uptake of the cells without further addition resembled the basal respiration of cells. Oligomycine was added to block the proton channel of complex V, thus inhibiting the proton flow and slowing down the ATP synthesis and oxygen consumption. This state is termed "leaky respiration" seeing that only leaked protons can be used in the reaction of ADP to ATP. Subsequently, the protonophor carbonyl cyanide m-chlorophenyl hydrazone (CCCP) was added to uncouple the protein gradient and stimulate the maximum capacity of the respiratory chain (ETC). The measurements revealed that the overall oxygen consumption in MIC10$^{-/-}$

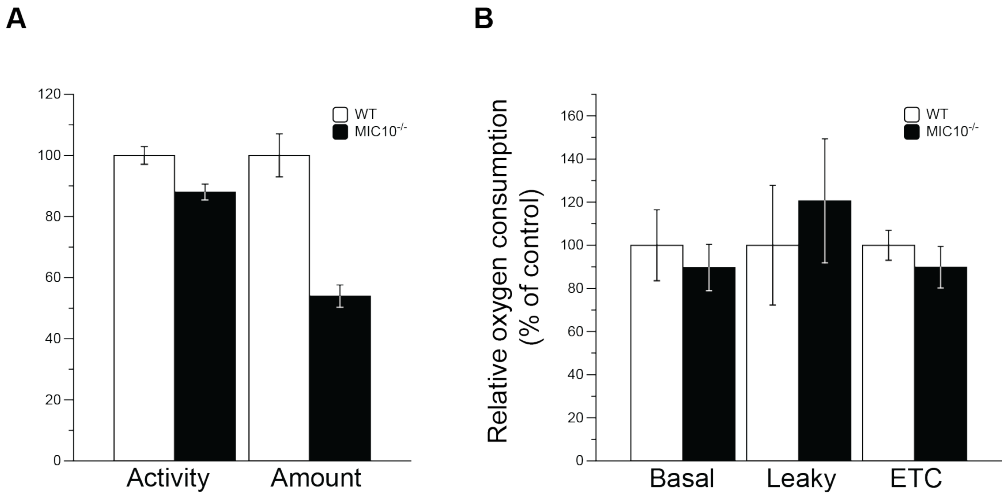

Figure 3.7.: Respirational activity is not affected in MIC10$^{-/-}$ cells.
A Enzyme activity and relativ amount of cytochrome C oxidase (CIV) of WT and MIC10$^{-/-}$ cells were measured by a Complex IV Human Specific Activity Microplate Essay Kit. (n=4, mean ± SEM)
B Relative oxygen consumption of WT and MIC10$^{-/-}$ cells using the OROBOROS. Basal respiration was measured in DMEM media containing glucose. Addition of oligomycin resulted in leaky respiration, full capacity of the electron transfer chain (ETC) was addressed by addition of CCCP. (n=3, mean ± SEM)

cells was not significantly reduced compared to WT cells (Fig 3.7 B), reflecting the findings of the complex IV activity assay. Hence, the ablation of MIC10$^{-/-}$ led to a reduced amount of complex IV, nevertheless the activity was not significantly affected and mi-

tochondrial respiration functions were at nearly full capacity.

In conclusion, this data set confirmed the necessity for human MIC10 to be present to build and maintain cristae junctions. Despite altering the unique morphological structure of the inner mitochondrial membrane, protein levels of various complexes with miscellaneous functionality and respirational activity did not seem to be affected.

3.2. Proximity labelling: A powerful tool to investigate transient interactions

In order to fully understand the mechanisms in cells, it is crucial to investigate the location of proteins and enzymes and their interactions amongst each other. Therefore, mainly two techniques were used: microscopy and mass spectrometry (MS). With microscopy it is possible to provide spatiotemporal information of living cells, but only about a small number of proteins at the same time. In contrast, MS is capable of detecting thousands of endogenous proteins simultaneously, for which lysed samples purified with immunprecipitation isolation are needed. Nevertheless, only the core complex is purified, providing no information about weak or transient interactions with other complexes and location. One approach to address transient interactions is to first perform a spatially restricted enzymatic labelling of specific proteins in living cells and to subsequently analyse the purified proteins with MS. Therefore, labelling substrates that are not harmful for the living cell are needed to preserve all membranes, complexes and spatial relationships during the tagging, and likewise an enzyme that covalently tags its neighbours, but no further proteins. Furthermore, the tagging process shall not be dependent on strong intermolecular interactions between enzyme and interactor.

Since mitochondria undergo permanent fission and fusion, thus being highly dynamic organelles, it only seems natural that not all protein-protein interactions are quite strong but only transient, nevertheless they are still important. MICOS for example seems to be involved in many diverse interactions with proteins of different mitochondrial compartments like the TOM and SAM-complex of the outer mitochondrial membrane (C. Ott et al., 2012; von der Malsburg et al., 2011) or the F_1F_o-ATPase in the cristae tip (Rampelt et al., 2017; Rampelt & van der Laan, 2017). Therefore it is highly likely that it has also some yet undetected transient interactions with protein complexes involved in various mitochondrial functions. To assess these further mutual interactors, a proximity labelling approach was performed.

A substrate that fulfils the proposed requirements is biotin. To date, two major enzymes are used to utilize this approach and activate biotin for tagging, an enhanced ascorbate C peroxidase (APEX) (Rhee et al., 2013) and a promiscuous biotin ligase (BirA*, BioID) (Roux, Kim, Raida, & Burke, 2012). Both enzymes were fused to the C-terminus of MIC10 and individual labelling experiments were performed. The biotin labelled proteins were isolated and analysed by mass-spectrometry.

3.2.1. Biotin-labelling using an enhanced ascorbate C peroxidase

APEX is derived from the ascorbate peroxidase (APX), a class I peroxidase which naturally occurs as a homodimer (Mandelman, Jamal, & Poulos, 1998). Because oligomeric tags can peturb the natural localization and function of a protein, a monomeric homologue was created (Martell et al., 2012). Three mutations (K14D, E112K and W41F) led to a predominantly monomeric peroxidase. As a positive side-effect, APEX shows an improved activity in Michaelis-Menten kinetics, approximately a 8-fold enhancement over WT-APX in terms of $\frac{k_{cat}}{K_M}$. Additionally not just L-ascorbate, but also nitrogen-containing compounds like diaminobenzidine (DAB) can be used as a substrate and various phenol derivatives can be oxidized to phenoxyl radicals. The advantage of radicals is their short lifetime (<1 ms), their small labelling radius (<20 nm) and their reactivity with electron-rich amino-acids like Tyr, Trp, His and Cys.

APEX utilizes a common porphyrin-based radical as a compound I intermediate, as observed in many other peroxidases (e.g. HRP) and uses small organic substrates. Although it has a high sequence identity with the well-investigated cytochrome *c* peroxidase (C*c*P), it does not share its anomalous features of building a protein-based radical as a compound I intermediate and the usage of protein substrates (Sharp, Mewies, Moody, & Raven, 2003). The oxidation of the substrate via APEX is achieved by means of a compound I intermediate, which is subsequently reduced by the substrate (HS) in two sequential single-electron-transfer steps:

$$\mathrm{APEX} + \mathrm{H_2O_2} \xrightarrow{\mathrm{k_1}} \mathrm{Compound\ I} + \mathrm{H_2O}$$

$$\mathrm{Compound\ I} + \mathrm{HS} \xrightarrow{\mathrm{k_2}} \mathrm{Compound\ II} + \mathrm{S^\bullet}$$

$$\mathrm{Compound\ II} + \mathrm{HS} \xrightarrow{\mathrm{k_3}} \mathrm{APEX} + \mathrm{S^\bullet} + \mathrm{H_2O}$$

where $S^\bullet$ is the one-electron oxidized form of the substrate (Raven, Lad, Sharp, Mewies, & Moody, 2004). This reaction takes place at the central haem c unit of the peroxidase.

In order to use it for enzymatic tagging, APEX can be targeted to a designated region, e.g. the mitochondrial matrix by fusing it to specifc targeting signals. Furthermore, to get more specific labeling, it can also be fused to single proteins. Biotin phenol is used as a tagging substrate to obtain reactive phenoxyl radicals. Only proteins in close vicinity to the APEX domain are proposed get biotinylated, and in addition, phenoxyl radicals are reported to not be membrane permeable, so biotinylation is compartment-specific (Rhee et al., 2013).

Already in previous work (Müller, 2014) a MIC10^{APEX} fusion construct was generated, stably transfected in HEK293T-REx cells, characterized and biotinylation protocols optimized. Mitochondrial localization was confirmed by incubating PFA fixed cells with antibodies against the APEX-tag and cyclophilin as mitochondrial marker and analysis via fluorescent microscopy (Fig. 3.8 A). To determine the right sub-mitochondrial lo-

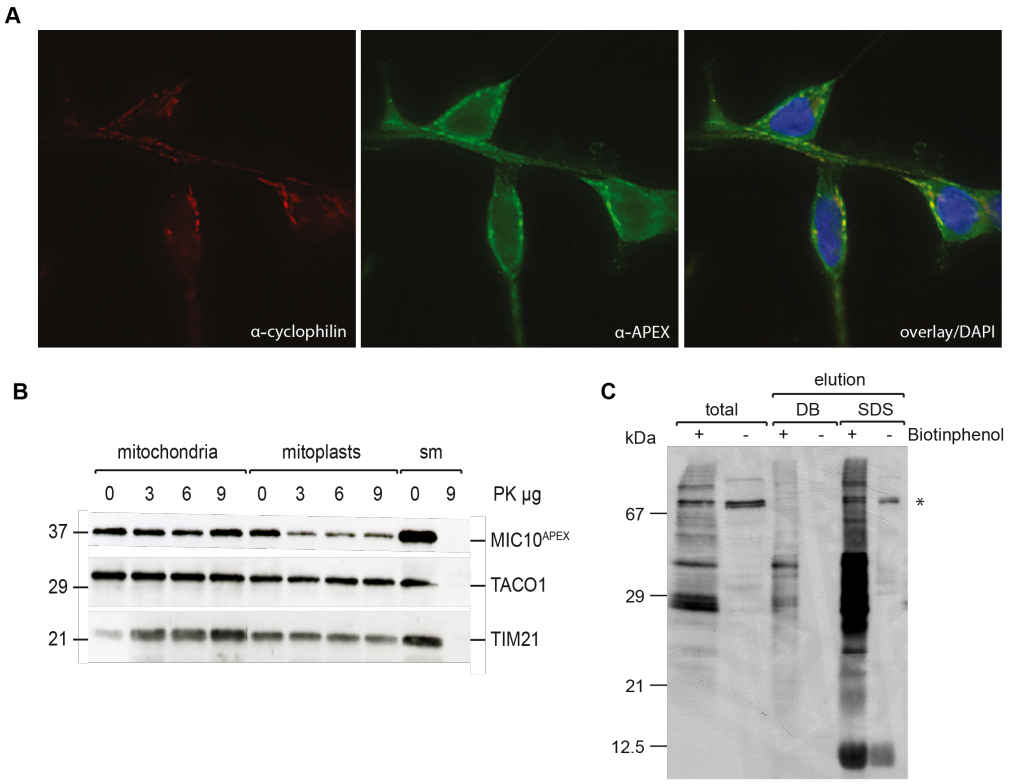

Figure 3.8.: Stable transfected MIC10^{APEX} cell-line.
A PFA fixed cells were permeabilized with Triton X-100 and incubated with α-cyclophilin as a mitochondrial marker and α-APEX. After applying fluorescent secondary antibodies DAPI staining was performed and the samples were analysed with fluorescent microscopy.
B Analysis of submitochondrial localization of MIC10^{APEX} by western-blotting confirmed the exposure of the enzyme to the IMS. Sm indicates sonicated mitochondria.
C *In vivo* biotinylation followed by affinity chromatography on streptavidin beads and western-blot analysis with SA-HRP confirmed functionality of the APEX. DB indicates elution with desthiobiotin, SDS indicates elution with SDS Laemmli buffer and heating at 95° C.

calization of the enzyme, MIC10^{APEX} mitochondria were tested for the accessibility of protease to the tag in mitoplasts and in intact mitochondria. Analysing the samples on western blot revealed that the enzyme is facing the IMS (Fig. 3.8 B). Functionality of the fusion construct was assessed by inducing labelling with H_2O_2 in isolated MIC10APEX

mitochondria supplemented with or without biotin phenol. Labelled proteins were enriched by incubation with streptavidin beads. To investigate milder elution conditions, a first elution step with desthiobiotin containing buffer was performed followed by incubation with SDS containing laemmli buffer at 95 °. Western blot analysis confirmed successful biotinylation and isolation of proteins (Fig. 3.8 C).

In this work, an *in organello* labelling approach with subsequent Mass-Spectrometry analysis of WT and MIC10^{APEX} was performed as published (Rhee et al., 2013). Therefore, isolated mitochondria were labelled with biotinphenol and after solubilisation, biotinylated proteins were isolated using streptavidin beads. Samples were prepared for MS analysis by SDS-PAGE and subsequent trypsin digestion. To assess enrichment of proteins within the achieved dataset, peptide count of proteins in WT and MIC10^{APEX} samples were compared and an at least two-fold higher peptide count in the MIC10^{APEX} sample was accounted as an enrichment of the protein. Subsequently, the data was analysed via bioinformatic tools for subcellular localisation (Fig. 3.9).

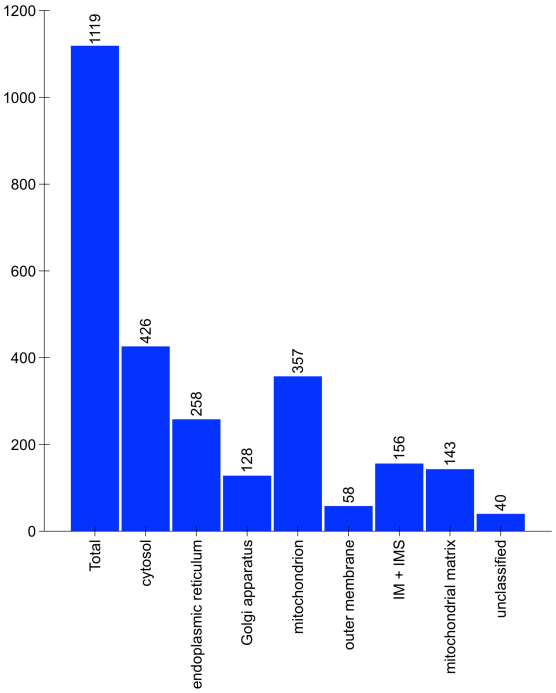

Figure 3.9.: MIC10^{APEX} Mass Spectrometry results classified according to subcellular compartments.
Proteins with peptide counts at least two-fold enriched in MIC10^{APEX} over WT sample were categorized into cellular compartments using the on-line bioinformatic tool on the website webgestalt.org.

Of the 1119 proteins enriched in the dataset, most of these were cytosolic, but furthermore a high number of proteins of the endoplasmic reticulum were found to be enriched. 32 % of the toal amount of enriched proteins were mitochondrial. Within this fraction, proteins of all mitochondrial compartments could be detected, although proteins located in the IMM and IMS represented the majority of labelled proteins. Besides all known

components of the MICOS complex and as well as published interactors like SAMM50, a large portion of matrix-located proteins, mainly mitochondrial ribosomal constituents, were obtained. These findings suggested, that the radical form of biotin-phenol was able to cross the mitochondrial membranes. Moreover, the total amount of enriched mitochondrial proteins covered nearly 40 % of the whole mitochondrial proteome, whereas its highly unlikely that MIC10 was interacting with such a large subset of proteins. This demonstrated, that not only MICOS interacting proteins were biotinylated, but that the active biotinphenol radical was more reactive than anticipated and most likely also labelled proteins that were not in direct vicinity to the protein of interest and even in the same compartment. Hence, a less reactive method for proximity labelling was needed and a different approach of activating biotin by using a promiscuous biotin-ligase was taken.

3.2.2. BioID: a milder form of proximity labelling

Since the proximity labelling using the APEX-approach seemed to lead to a high amount of background labelling, a second approach was adapted using a promiscuous bioting ligase. First introduced as a labeling technique in 2012 with a modified version of the biotin-ligase of *Escherichia coli* (Roux et al., 2012), the ligase termed first BirA* and later BioID activates the biotin by coupling AMP to the carboxyl-group of biotin, forming a biotinyl-AMP (bioAMP) and thus making it reactive against primary amines (e.g. lysines). Whereas the wild-type BirA releases the bioAMP only upon reaction with a specific biotin acceptor tag (BAT) (Beckett, Kovaleva, & Schatz, 1999) and being higly specific in labelling, a mutation in the BioID (R118G) led to a lower affinity to biotin but also to bioAMP, hence promoting a promiscuous release of the reactive biotin species. The estimated labelling range is $\tilde{1}0$ to 15 nm (Kim et al., 2014) and could be successfully applied to investigations in many different organisms, even labelling in living mice for tumor xenograft sutdies is possible (Chan et al., 2014; Uezu et al., 2016), also a split version of BioID (Schopp & Béthune, 2018) is availabble by now. Furthemore, a smaller and more active version was found in 2016 (Kim et al., 2016). This enzyme called BioID2 was the mutated biotin-ligase of *Aquifex aeolicus* and lacked the DNA-binding domain of the *E. coli* version of the enzyme, thus being smaller in size (27 kD versus 35 kD) and, as tests revealed, also more efficient in labelling.

To purify biotinylated proteins, one takes advantage of the high affinity of biotin to streptavidin ($K_D = 10^{-14}$ M) (Green, 1963), one of the strongest non-covalent affinity between two molecules. Subsequently, proteins were typically analysed via mass-

spectrometry after either liquid on-bead trypsin digestion or in-gel digestion (Roux et al., 2018).

3.2.2.1. Expression of MIC10^{BioID2}

To compare the different proximity labeling approaches, the enzyme BioID2 was fused to MIC10 using the commercially available vector for human expression of BioID2-HA with a pcDNA3 backbone. After transient transfection, the expression and mitochondrial localisation of MIC10^{BioID2} was verified with immunfluorescent staining of fixed U2OS cells using HA-antibody for detection of the fusion protein and mito-tracker as a mitochondrial marker (Fig. 3.10 A).

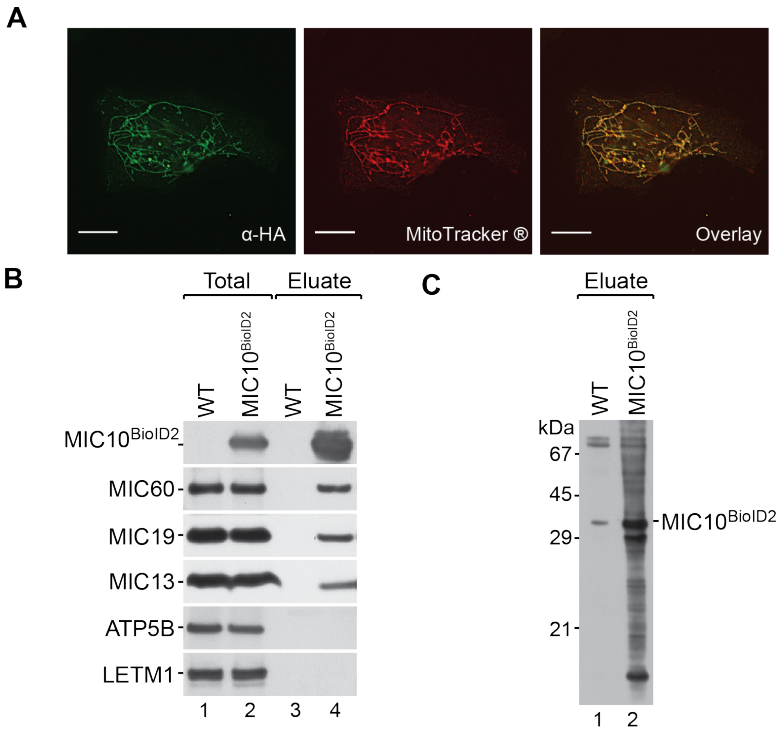

Figure 3.10.: Function of transient transfected MIC10^{BioID2} was verified by immunostaining and immuno-precipitation.
A Cells were incubated with MitoTracker.Subsequently fixation using PFA was followed by permeabilisation with Triton X-100 and incubation with α-HA antibody. After applying fluorescent secondary antibodies DAPI staining was performed and the samples were analysed with fluorescent microscopy.
B Transient transfected cells with MIC10^{BioID2} were solubilized using digitonin and incubated with HA-beads. After glycine elution, interaction partners were analysed by SDS-PAGE and immunoblotting with indicated antibodies.
C Cells transiently expressing MIC10^{BioID2} were supplied with excess biotin for 24 h. After solubilisation, the cell lysate was incubated with streptavidin beads and biotinylated proteins were detected on western blot after elution with SA-HRP.

To adress the functional incorporation of the fusion protein into MICOS, an immunoprecipitation of WT and transient transfected MIC10^{BioID2} using anti-HA beads was performed (Fig. 3.10 B). Western blot analysis revealed that the fusion-construct was able to co-isolate components of the MICOS, therefore it was functional incorporated. Furthermore, the function of the promiscuous biotin-ligase needed to be confirmed. Therefore, transient transfected MIC10^{BioID2} cells as well as non-transfected cells were supplemented for 24 h with 50 μM biotin. Subsequently, to enrich the biotinylated proteins for western-blot analysis, the cells were lysed and incubated with streptavidin beads. Upon analysis of the eluate sample with immunoblotting using HRP coupled streptavidin, a pattern of biotinylated proteins in the MIC10^{BioID2} sample could be observed (Fig. 3.10 C).

Hence, MIC10^{BioID2} was successful incorporated into MICOS and able to biotinylate proteins in close vicinity.

3.2.2.2. Identification of biotinylated proteins marked by MIC10^{BioID2} via mass-spectrometry

To analyse biotin-labelled proteins via Mass-Spectrometry, eluted proteins of WT and MIC10^{BioID2} cells after streptavidin-immunoprecipitation were sent to the proteomics service facility of the UMG (Hennig Urlaub and Christof Lenz) and analyzed by mass-spectrometry. To identify enriched proteins in the MIC10^{BioID2}-sample, the average peptide count was calculated and compared to the WT-sample. Enriched proteins were analysed via an online-bioinformatics tool (webgestalt.org)(Fig. 3.11) to sort them into their subcellular fractions.

To identify possible interactors of MICOS, only mitochondrial proteins were considered. Since in this analysis no cytosolic negative control was included and one cannot be sure whether non-mitochondrial biotinylated proteins were labelled due to close proximity and interactions with MIC10 or during the biosynthesis and transport to mitochondria of the fusion protein. The list of 86 mitochondrial annotated proteins was further manually curated and narrowed down to 37 proteins with published mitochondrial localization (Fig. 3.12).

As expected, among the enriched proteins nearly the whole MICOS complex was obtained, only with MIC13 and MIC26 absent. Additionally, proteins involved in mitochondrial membrane organization and known interactors with MICOS, like OPA1 and TMEM11, could be enriched (Barrera et al., 2016). Components of the SAM-complex SAMM50, DNJAC11 and MTX2 together with TOMM70, as part of the protein transport of the outer membrane, have been previously reported to interact with MICOS

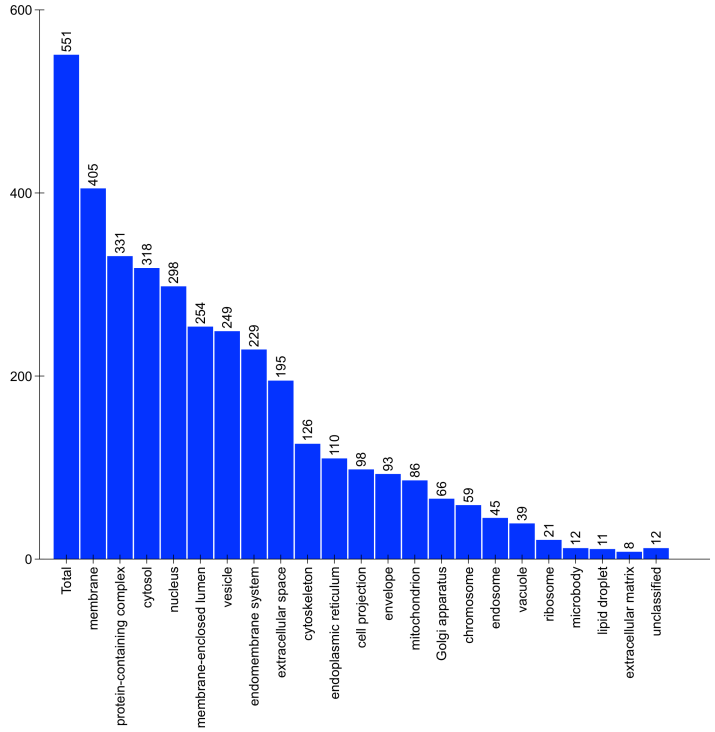

Figure 3.11.: Bioinformatical analysis of MIC10$^{\mathbf{BioID2}}$ mass spectrometry results.
Enriched proteins of the MIC10$^{\mathrm{BioID2}}$ sample were categorized for cellular localisation using the webgestalt.org online bioinformatics tool.

through MIC60 (Zerbes et al., 2012; Xie et al., 2007; Körner et al., 2012). These could also be isolated in this labelling approach, indicating that MIC10$^{\mathrm{BioID2}}$ was indeed able to label MICOS interactors. Since various interactions could be observed between the IM located MICOS and OM located proteins, also further functional interactions to proteins involved in mitochondrial fission and fusion MFF1 and DNM1L are possible and would need further rectification in future studies. In addition, the porins VDAC2 and VDAC3 were found enriched in the dataset, but no experimental evidence is published so far that confirmed an interaction of MICOS with this protein family. In yeast it was reported that MICOS interacts with components of complex V of the OXPHOS machinery (Rampelt et al., 2017; Rampelt & van der Laan, 2017), so the enrichment of ATP5F1A, ATP5F1B and ATP5F1C as part of the human complex V could hint towards a similar interaction in the human system. Further OXPHOS components were NDUFS1 (complex I) and UQCRC2 (complex III), though no direct interactions to these with MICOS has been reported so far. Whether these are novel direct interactors of MICOS or background labelling would need further experimental assessment.

In addition, the Carrier protein family detected are predicted substrates of the TIM22-complex with TIM29 as one of the core components of the translocase. Recent studies based on this finding could demonstrate an impact of a lack of MIC10 in a knock-out mutant on the proper functionality of the TIM22-complex (Callegari et al., 2019), thus

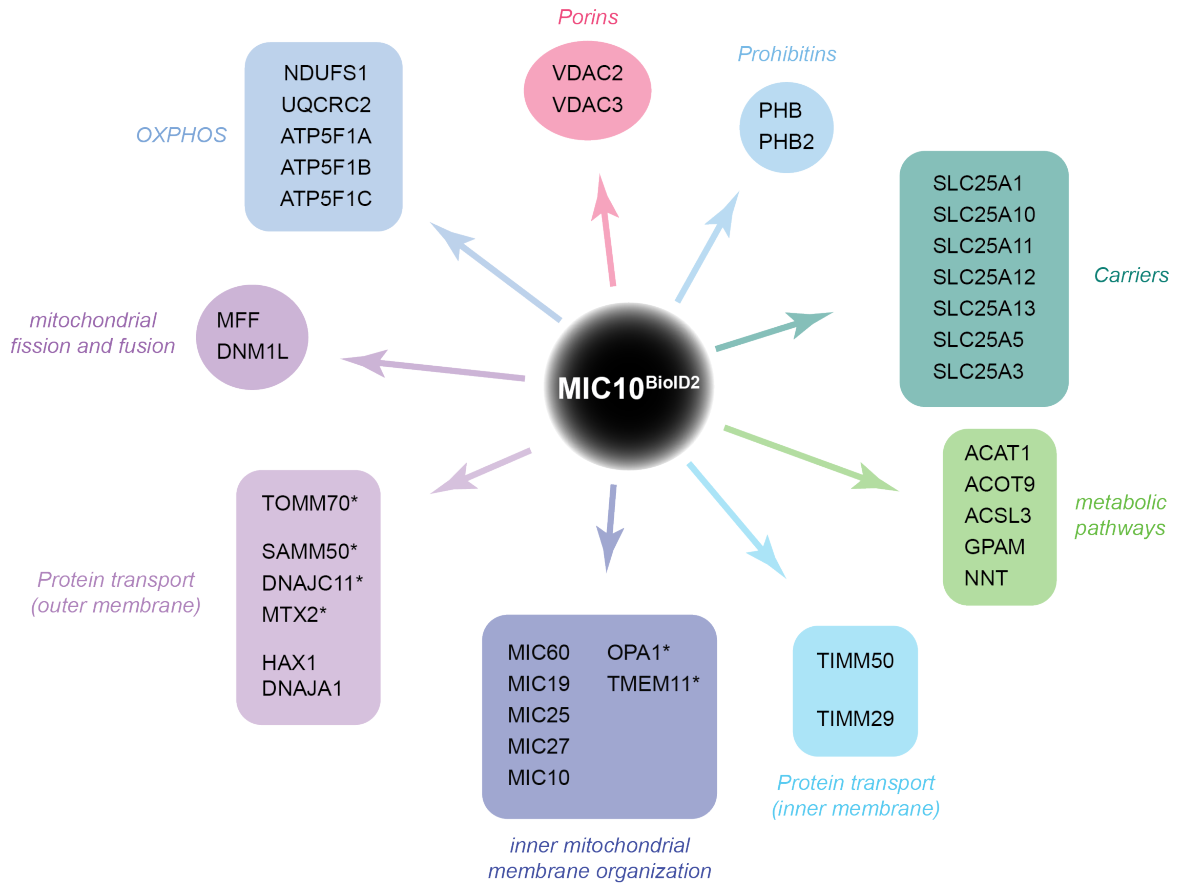

Figure 3.12.: MIC10 induced biotinylated mitochondrial proteins obtained by mass spectrometry analysis.
Biotinylated proteins isolated after labelling of WT and MIC10^{BioID2} cells were analysed by mass-spectrometry. Results of obtained mitochondrial proteins enriched in the MIC10^{BioID2} sample were grouped according to their reported function. Published interactors with MICOS were labelled with a *.

confirmed the finding in this analysis. Moreover, TIM50, a component of the TIM23 complex, was also enriched. However, no functional connection between MIC10 and TIM23 has been discovered so far. Additionally, in contrast to the labelling using the enhanced ascorbate C peroxidase (see chapter 3.2.1), no mitochondrial matrix-located proteins could be detected, thus leading to the conclusion that the reactive Biotin-AMP was not able to freely cross the inner membrane, hence the labelling was compartment specific.

To conclude, proximity labelling via biotin using a promiscuous biotin ligase is a powerful tool to investigate for novel and transient interaction partners of a protein of interest. Using the enhanced ascorbate C peroxidase APEX for labelling approaches seem at first glance more promising, having a significant shorter time of labelling and

also the possibility of performing time-dependent labelling experiments. But the analysis revealed, that the highly reactive biotin phenol radical led to a high amount of unspecific labelling, thus needing a rigid set-up of control samples to narrow down the dataset to proteins with a high probability of interacting with the target protein. Furthermore, not being compartment specific and apparently able to cross the inner mitochondrial membrane even more controls are needed. In contrast, with a quite simple experimental set-up of one tagged protein of interest with BioID2 in the closed environment of the intermembrane space within mitochondria, a quite specific dataset of labelled proteins after *in vivo* biotinylation and analysis of whole cell samples could be achieved. Thus providing directions for possible future studies.

3.3. Alteration of the inner mitochondrial morphology affects precursor protein import in *S. cerevisiae*

The MICOS complex has been extensively studied in yeast where it has been found to have a large interaction network. Several interaction partners are components of the mitochondrial translocase machineries such as the TOM and SAM complexes. MICOS is also required for the import of MIA substrates (von der Malsburg et al., 2011). Contacts between the inner and outer mitochondrial membrane are important for the presequence pathway since the TOM and TIM23 complexes must form transient supercomplexes to allow efficient precursor handover. Therefore one aim of this work was to characterise whether MICOS has a role for the import of presequence containing proteins. Previous studies concluded that upon Mic60 deletion, not only the membrane morphology is affected but also the import of precursor proteins is dependent on proper MICOS functionality, due to its interaction with the TOM complexes and Mia40 (von der Malsburg et al., 2011). Although a clear reduction in imported proteins could be observed, the data is not conclusive since the mitochondrial membrane potential $\Delta\Psi$ is significantly decreased in *mic60*Δ mitochondria, thus affecting the membrane potential dependent imports of proteins. A clear distinction of whether there is a functional connection of MICOS to the translocase machinery or the observed phenotype is due to secondary effects of altered inner mitochondrial membrane morphology cannot be made.

To assess this question from a different point of view, a characterisation of MICOS on protein import was carried out using a *mic10*Δ strain.Tthis strain has been characterised before (von der Malsburg et al., 2011; Alkhaja et al., 2012), but under the reported conditions, no interactions between MICOS and TIM23 were detected (von der Malsburg et al., 2011).

3.3.1. Deletion of Mic10 does not effect translocase components

To determine whether steady state levels of translocase components were affected in mitochondria lacking Mic10, cells were grown on non-fermentable media, mitochondria were isolated and western-blot analysis was performed probing for various components of diverse mitochondrial protein complexes (Fig. 3.13). In contrast to the findings in mammalian cells which displayed a complete loss of MIC13, the yeast homologue Mic12 is only reduced, but still present in *mic10*Δ cells. However, the levels of Mic19 remain consistent. This verifies that the Mic60-subcomplex is unaffected.

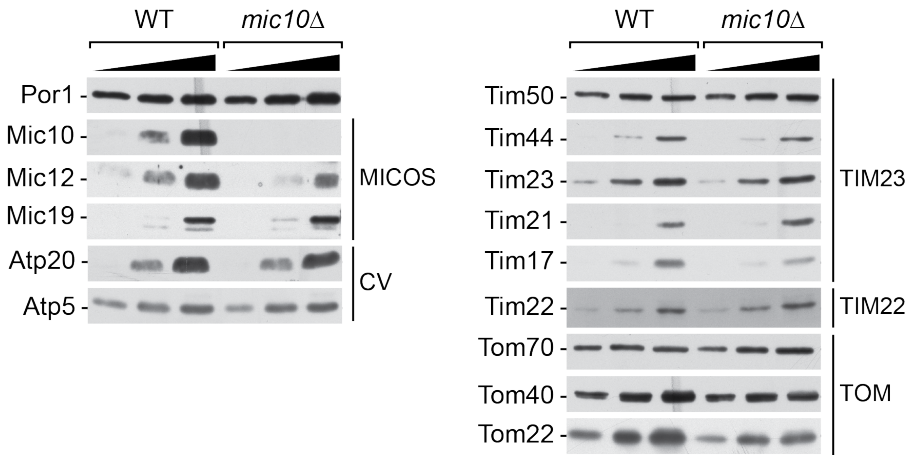

Figure 3.13.: Protein levels of translocase components are not affected in *mic10*Δ. Mitochondria were isolated from WT and *mic10*Δ cells after growth on non-fermentable media and subsequently analysed on western-blot using various antibodies against proteins of interest.

Furthermore, protein levels of complex V components Atp5 and Atp20 are not affected, as reported (Alkhaja et al., 2012). Detection of Tim22 revealed no reduction in TIM22 complex levels, therefore not resembling the findings in human isolated mitochondria of MIC10$^{-/-}$. Moreover, constituents of the presequence translocase TIM23 are not reduced in protein level, although Tim17 levels are slightly reduced. Levels of TOM-complex components Tom70 and Tom40 are unaltered upon Mic10 deletion, only the receptor protein Tom22 displays a minor decrease in protein levels. Since steady state analysis of protein levels did not reveal any major changes in the *mic10*Δ strain, a closer look was taken into a MICOS-translocase interaction.

3.3.2. Ablation of Mic10 influences the activity of the TIM23 complex

Based on the observation that import of precursor-containing proteins was impared in *mic60*Δ mitochondria (von der Malsburg et al., 2011), the question arose, whether in yeast indeed there might be a functional interaction between MICOS and the TIM23-complex.

To investigate for protein-protein interactions, an immunoprecipitation using IgG-sepharose, coupled with antibody against Tim21 or Tim23, was performed. Isolated WT and *mic10*Δ mitochondria were solubilized in a digitonin containing buffer and incubated with the beads. After elution at low pH, western blot analysis was performed.

The Tim21, Tim23 and Tim44 proteins were co-isolated, verifying the success of the

isolation of the translocase complex (Fig. 3.14). Furthermore, Mic60 and Mic10 could be co-purified with both Tim21 and Tim23. Interestingly, the interaction of Mic60 and Tim21/Tim23 is Mic10 independent, since the interaction is maintained in the *mic10*Δ sample. Therefore, Tim21/Tim23 seem to interact with the MICOS complex through Mic60, but whether it is the only direct interaction partner would need further investigation.

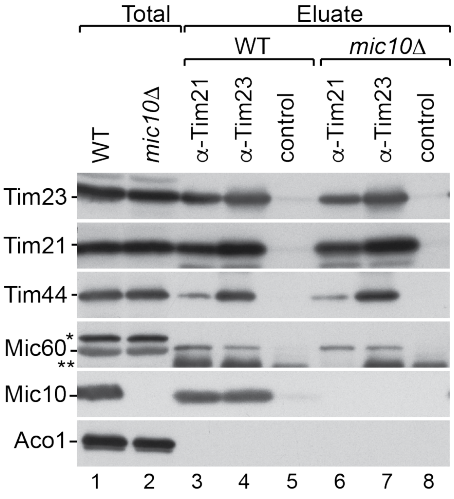

Figure 3.14.: MICOS interacts with the TIM23 complex.
Digitonin solubilized mitochondria of WT and *mic10*Δ were used for immunoprecipitation of Tim21 and Tim23.* indicates cross reaction of the antibody.

To assess, if there is a functional influence of MICOS on the translocation of presequence-containing proteins, import experiments of radiolabelled matrix proteins $F_1\beta$ and Atp14 along with inner mitochdrial membrane sorted Ina22 and Atp4 into *mic10*Δ mitochondria were carried out, with all four proteins being substrates of the TIM23 complex.

Translocation via the TIM23 complex requires mitochondrial membrane potential. To ascertain, that the isolated WT and *mic10*Δ mitochondria have equivalent membrane potentials, measurements were made using the potential sensitive dye 3,3'-dipropylthiadicarocyanine iodide ($DiSC_3(5)$) (Fig. 3.15 A and B). The quenching of the dye as it is taken up into mitochondria reflects the membrane potential, and comparison of the quenching in the *mic10*Δ sample compared to the WT displayed no significant potential phenotype.

For the import assays, precursor proteins were synthesized *in vitro* in the presence of [^{35}S] methionine and added to WT and *mic10*Δ mitochondria resuspended in import buffer. After stopping the import reaction by dissipating the membrane potential $\Delta\Psi$ using AVO (antimycin, valinomycin and oligomycin), samples were treated with proteinase K (pK) to digest non-imported precursor proteins. Import was monitored by assessing levels of the processed precursor (mature protein) at increasing time points. Quantification of mature imported protein was carried out after analysis by SDS-PAGE

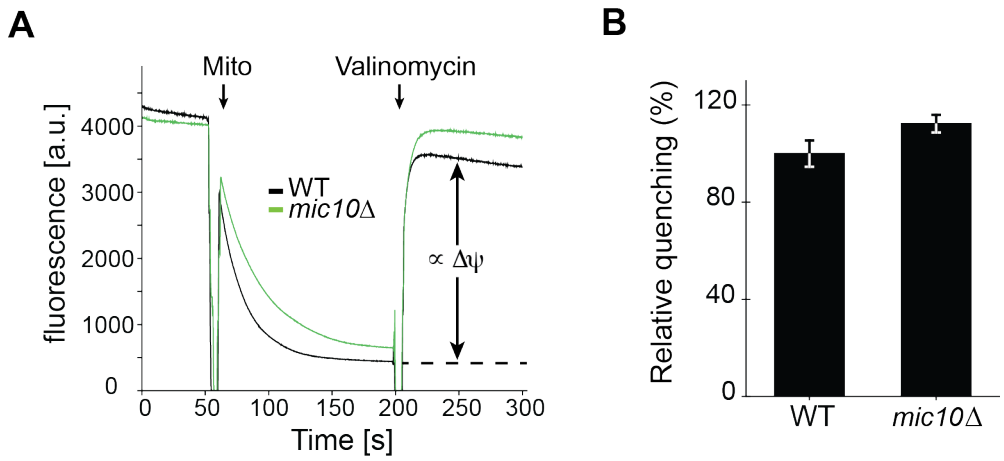

Figure 3.15.: Membrane potential in *mic10*Δ is not reduced.
AMembrane potential ΔΨ was assessed by adding WT (black line) or *mic10*Δ mitochondria to the fluorophore DiSC3(5).ΔΨ was dissipated using valinomycin and the amount of fluorophore quenching was determined. Arrow indicates parameter quantified in (B).
B Relative fluorophore quenching was determined from three independent experiments and quantified as indicated in (A). (mean ± SEM)

and digital autoradiography. In this study, a reduction of import efficiency could be observed in mitochondria from *mic10*Δ cells.

The highest reduction of imported precursor proteins could be observed using the matrix-proteins $F_1\beta$ and Atp14 as substrates Both exhibit a 50-60 % reduction ath the 15 min time point in *mic10*Δ mitochondria (Fig. 3.16). The radiolabelled precursor proteins, Ina22 and Atp4, sorted into the inner mitochondrial membrane by the Tim21 containing $TIM23^{SORT}$ complex, were also imported into mitochondria. Again, a defect of 40 % and 20 % respectively could be observed.

As no impact on the steady state level of individual translocase proteins could be observed in *mic10*Δ mitochondria, the amount and composition of the functional translocase complex needed to be assessed in the deletion strain, to determine whether MICOS affects formation of the TOM-TIM23 supercomplex during precursor handover and if the MICOS interaction is strengthened upon supercomplex formation. Therefore, a recently published Method (Gomkale, 2018) to isolate the TOM-TIM23 supercomplex was used. In this assay, a modified precursor protein fused to a superfolded GFP moiety sfGFP (Prec-sfGFP) was *in vitro* imported into isolated mitochondria. The sfGFP acts as a blocking moiety and stalls the precursor protein in the TOM and TIM23 complex while being imported (Fig. 3.17 A), thus enabling the isolation of the translocase supercomplex using GFP nanobodies.

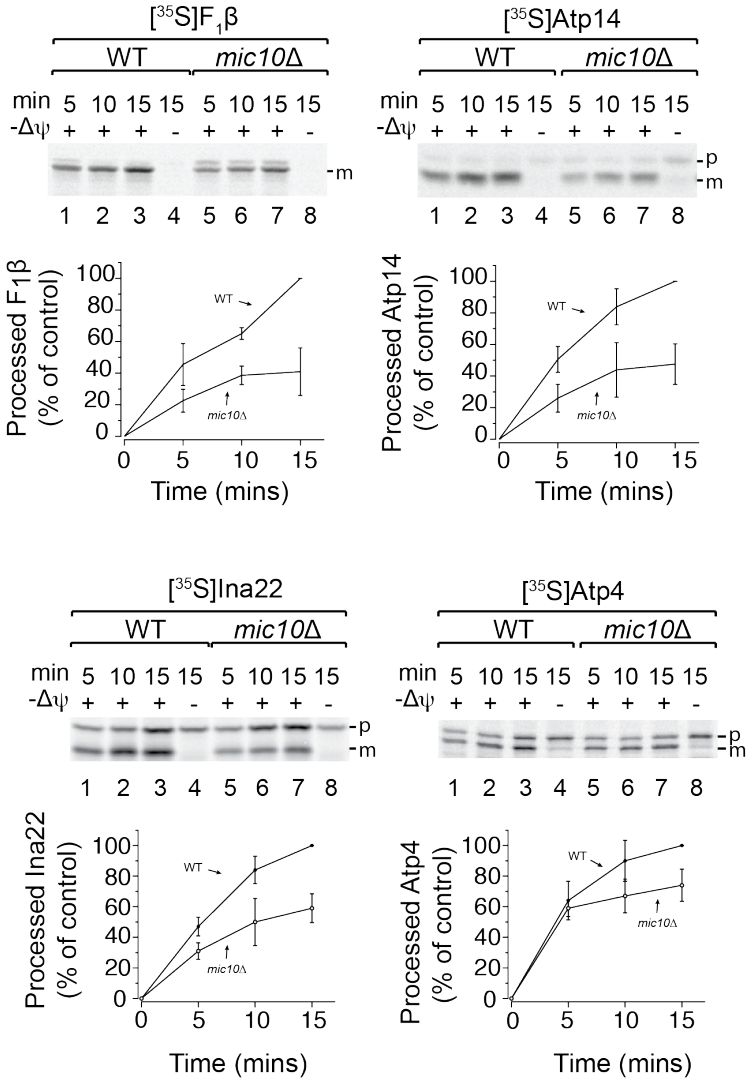

Figure 3.16.: Deletion of *mic10* reduces the amount of imported precursor proteins.
Radiolabelled precursor proteins were imported into isolated WT and *mic10*Δ mitochondria for the indicated time in the presence or absence of membrane potential (ΔΨ). Proteinase K treated samples were analysed by SDS-PAGE. Graph indicates quantification of at least 3 independent experiments, therefore import of precursor proteins in WT at 15 min was set to 100 %. p, precursor; m, mature; mean ± SEM.

Western-Blot analysis revealed that in *mic10*Δ mitochondria the composition of the translocase supercomplex is largely unchanged (Fig. 3.17 B). Probing with antibodies against GFP confirmed, that both WT and *mic10*Δ imported the Prec-GFP with the same efficiency and could also be isolated in equal amounts. Isolated amounts of Tim50, Tim23, Tim21 and Tim17 all components of the TIM23-complex where the same in both samples. Also, Tom40 as part of the TOM-complex was present in identical amounts. Only Tom22, a receptor protein of the TOM-complex was slightly reduced already in the total sample of the *mic10* deletion strain, conclusive with steady state analysis and subsequently co-isolated in lower amounts (Fig. 3.13). Interestingly, Mic10 could not be isolated together with the TOM-TIM23 supercomplex, in contrast to isolation of the TIM23 complex using endogenous antibodies against Tim21 and Tim23 (Fig. 3.14 C).

This lad to the conclusion that the import defect in mitochondria lacking Mic10

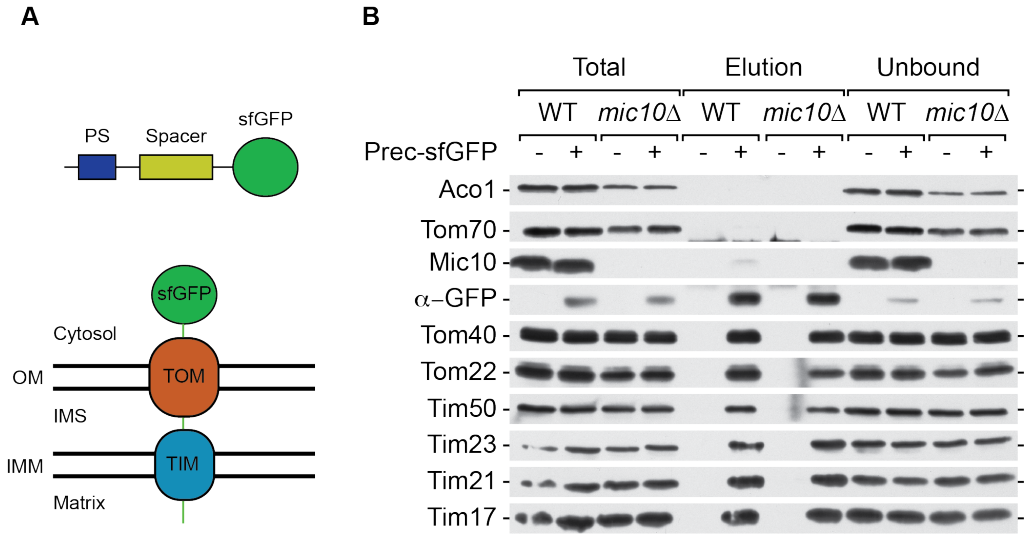

Figure 3.17.: The TOM-TIM23 supercomplex does not exhibit an altered composition upon *Mic10* deletion.
A Overview of supercomplex generation using a precursor and a spacer protein fused to sfGFP as blocking moiety.
B TOM-TIM23 supercomplex generated by importing a modified precursor protein with sfGFP (Prec-sfGFP) into WT and *mic10*Δ mitochondria. Mitochondria were solubilized in digitonin containing buffer and the formed supercomplex was isolated using GFP nanobodies (nb).

does not stem from an altered composition of the translocase supercomplex, nor the amount of translocase proteins. The reduced amount of the receptor protein Tom22 suggests that the reduced import could derive from impaired recognition of presequence-containing proteins on the outer mitochondrial membrane and not from a more inefficient translocation through the inner membrane. However, since *mic10*Δ mitochondria have a vastly altered cristae morphology, it is possible that the disruption of cristae junctions also impacts in the translocation of presequence-containing precursors.

To verify, that the observed import phenotype in MICOS altered mitochondria is derived from a functional association between MICOS and the TIM23-complex, imports into membrane morphology altered mitochondria with an intact MICOS complex were performed. Therefore, an *atp20*Δ strain was used. Atp20 is required for dimerisation of the ATPase. Dimerisation is responsible for the membrane curving properties of the ATPase which generates cristae tips (Paumard et al., 2002). As published (Alkhaja et al., 2012; Paumard et al., 2002), this strain also lacks cristae and has the typical onion-shaped ring structure of the inner membrane, although the MICOS complex is unaffected.

Using the same radiolabelled presequence-containing precursor proteins revealed that

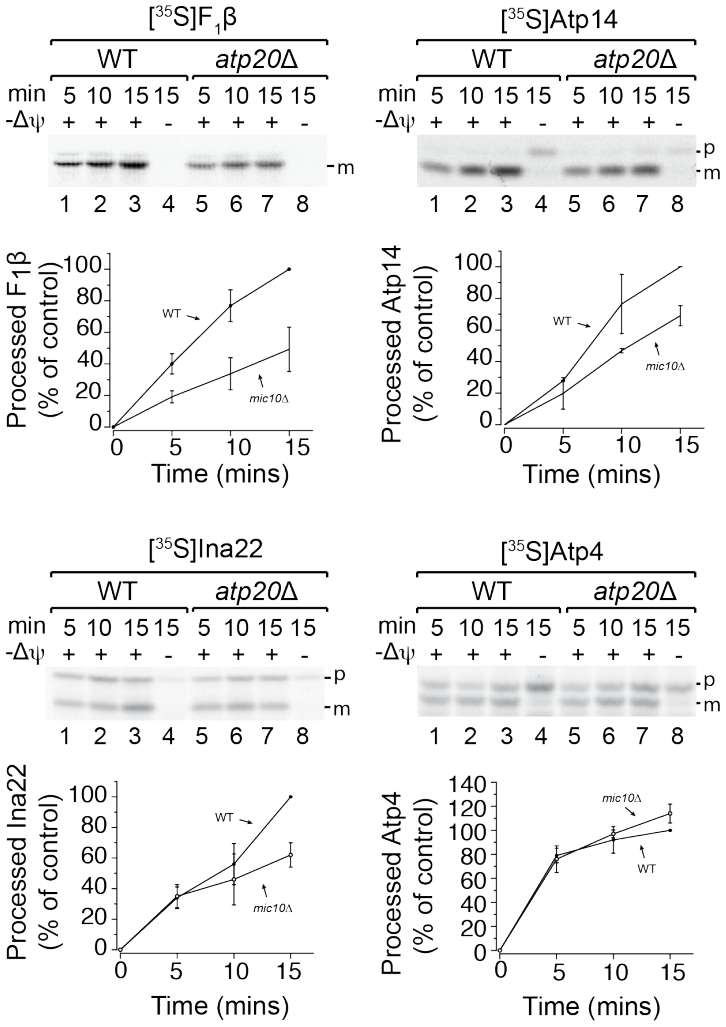

Figure 3.18.: Import into *atp20*Δ mitochondria is also affected.
Radiolabelled precursor proteins were imported into isolated WT and *atp20*Δ mitochondria for the indicated time points in the presence or absence of membrane potential (ΔΨ). Proteinase K treated samples were analysed by SDS-PAGE. Graph indicates quantification of at least 3 independent experiments, therefore import of precursor proteins in WT at 15 min was set to 100 %. p, precursor; m, mature; mean ± SEM.

the import in *atp20*Δ mitochondria is reduced for most of the tested proteins (Fig. 3.18). Matrix targeted precursor protein $F_1\beta$ displayed a reduction of imported proteins of over 50 % at 15 min time point, whereas Atp14 of the same mitochondrial compartment is imported with around 30 % less efficiency. Furthermore, proteins sorted into the inner mitochondrial membrane via the $TIM23^{SORT}$ complexes are also affected, assessed by a 40 % reduction in importing Ina22 after 15 min. Surprisingly, only import Atp4, also a protein located in the IMM, is not reduced upon the loss of Atp20 and an altered mitochondrial ultrastructure These results show that altered cristae morphology can indeed impact on the efficiency of translocation via the TIM23-pathway.

Thus, the import defect observed in Mic10 deficient cells likely does not stem from a functional deficit between MICOS and TIM23, but from the altered morphology of the inner mitochondrial membrane in *mic10*Δ cells, considering a similar phenotype could be observed in *atp20*Δ mitochondria.

3.3.3. MICOS does not interact with the carrier translocase in yeast

To determine whether MICOS interacts with the TIM22-complex in yeast, a TIM22-complex isolation was performed using a Tim18^{ZZ} strain. The complex was isolated by incubating digitonin solubilised WT and *mic10*Δ mitochondria with IgG-Sepharose. Proteins were eluted via TEV-cleavage of the ZZ-tag on the beads, thus resulting in a low possibility of eluting non-specifically bound proteins.

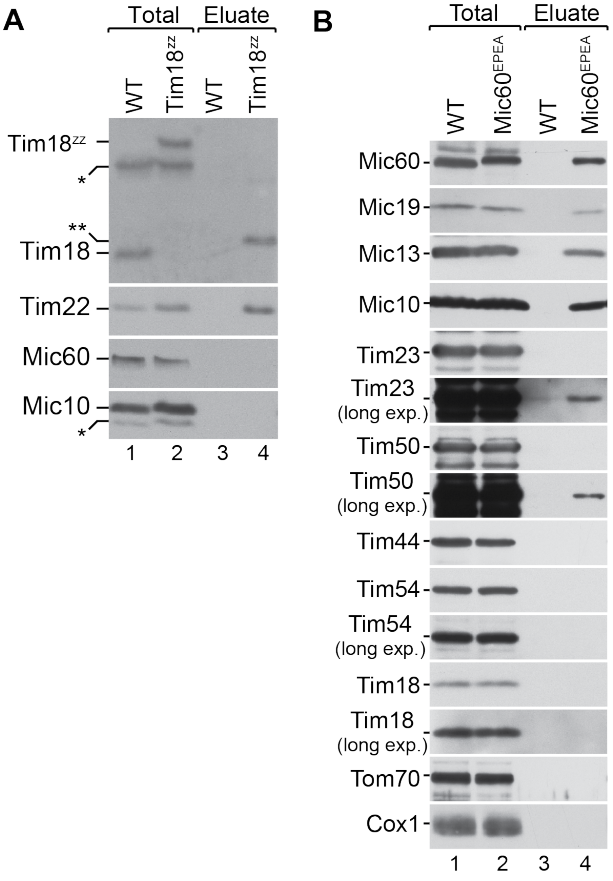

Figure 3.19.: TIM22 and MICOS cannot be co-isolated.
A TIM22 complex isolation using the Tim18^{ZZ} strain. Digitonin solubilized mitochondria were incubated with IgG sepharose. For elution, TEV-protease was added to the beads and the eluate analysed on western blot. * indicates cross-reaction with the antibody, ** the size of Tim18^{ZZ} after TEV-protease cleavage.
B WT and Mic60^{EPEA} mitochondria solubilized in digitonin were incubated with EPEA nano bodies coupled to CNBr-activated sepharose. After eluution with 2x EPEA peptide samples were analysed on SDS-PAGE.

Interestingly, neither Mic60 nor Mic10 could be co-isolated with Tim18 (Fig. 3.19 A). Thus neither subcomplexes seem to interact with the TIM22 complex, which is in contrast to findings in mammalian cells (see 3.1.3.). To verify these findings, a yeast strain expressing a genomically integrated Mic60 fused to an EPEA tag was generated. A Mic60^{EPEA} isolation was performed to assess if the interaction could be detected from a MICOS isolation (Fig. 3.19 B). Although the MICOS complex could be isolated, Tim18 was not co-purified.

In human cells the functional interaction of MICOS and the TIM22-complex was demonstrated by importing radiolabelled carrier proteins, which are transported by the

TIM22-complex, in WT and MIC10$^{-/-}$ mitochondria (Callegari et al., 2019). To exclude a MICOS/TIM22 interaction in yeast, a similar approach was undertaken in *S. cerevisae*, involving the import and assembly of the ADP/ATP carrier Aac1, a known substrate of the yeast TIM22 complex. Therefore, radiolabelled AAC was imported into isolated WT and *mic10*Δ mitochondria. After mild digitonin solubilisation to maintain intact protein complexes, the samples were analysed using digital autoradiography after Blue-Native PAGE separation of the complexes. The assembly of AAC was neither affected by the absence of Mic10 (Fig. 3.20 A) nor Atp20 (Fig. 3.20 B).

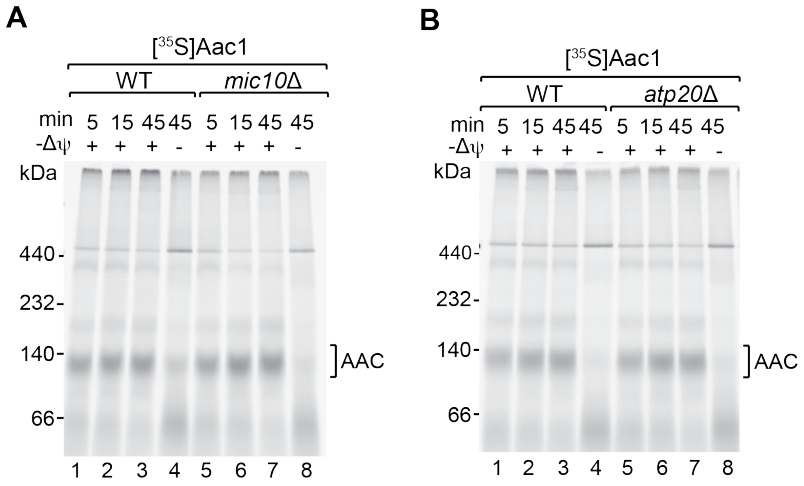

Figure 3.20.: AAC assembly is not affected by altered inner mitochdondrial membrane morphology.
Radiolabelled Aac1 was imported in WT and *mic10*Δ (A) or *atp20*Δ (B) mitochondria for indicated time in the presence ore absence of membrane potential (ΔΨ). Samples were analysed with BN-PAGE and digital autoradiography.

This finding demonstrates that the MICOS-TIM22 interaction observed in human is not conserved in yeast and is therefore likely specific to higher eukaryotes. Furthermore it could be proved that protein import by the TIM22 complex is not dependent on inner mitochondrial membrane morphology and precursor protein handover likely solely relies on soluble TIM chaperones in the IMS.

In conclusion, in *S. cerevisiae* there seems to be a spacial connection between MICOS and the TIM23-complex, but no specific functional co-dependency between these two distinct complexes could be observed. Furthermore, the intact inner mitochondrial membrane morphology seems to be crucial for efficient precursor protein import via the TIM23-complex. On the other hand the TIM22 carrier pathway is not affected by the absence of the Mic10 subcomplex and does not appear to require proper inner

mitochondrial membrane morphology.

These findings build upon the previously reported results by vonderMalsburg:2011fa where presequence import was investigated in a *mic60*Δ strain. In this case, the results were inconclusive due to the reduced mitochondrial membrane potential of *mic60*Δ mitochondria. Here, it is evident that the role of MICOS for maintaining mitochondrial ultrastructure is essential for efficient translocation via the TIM23 pathway. The observation that Mic10 is dispensable for carrier import is consistent with von der Malsburg which show that Mic60 is also dispensable for import via the TIM22 pathway, suggesting that MICOS and cristae ultrastructure play less of a role for the carrier import in yeast.

4. Discussion

Mitochondria have a unique inner membrane structure, consisting of a inner boundary membrane and cristae, which are connected by the cristae junctions. Over the years different proteins and protein complexes were found to be crucial for building and maintaining this structure. In bakers yeast *S. cerevisiae* the tips of the cristae are stabilized by the formation of the F_1F_oATPase dimers (Paumard et al., 2002; van der Laan et al., 2012). Furthermore, the GTP-binding portein Mgm1(yeast)/OPA1(human) (Meeusen et al., 2006; DeVay et al., 2009; Frezza et al., 2006) are also reported to have an impact on inner mitochondrial membrane topology. Since knock-down studies revealed MIC60/Mitofilin and its yeast homologue Mic60/Fcj1 being crucial for proper cristae junction formation (John et al., 2005; Rabl et al., 2009), a deletion of Mic10 in yeast displayed the same phenotype (von der Malsburg et al., 2011; Harner et al., 2011; S. Hoppins et al., 2011; Alkhaja et al., 2012) and a human homologue was identified (Alkhaja et al., 2012). It was also shown, that the oligomerization of Mic10, induced by the characteristical glycin rich GXGXGXG motif in both transmembrane regions plays a mayor role in the membrane shaping ability (Barbot et al., 2015). Considering that deletion of further MICOS components only led to less severe alteration of the inner mitochondrial membrane (Harner et al., 2011; von der Malsburg et al., 2011; S. Hoppins et al., 2011), Mic60 and Mic10 are considered the core components of MICOS. However, experimental data on the mammalian MIC10 are scarce and only knock-down experiments in mouse embryonic fibroblasts (MEF) cells found it to be involved in cristae formation and stabilisation (Li et al., 2016).

4.1. MIC10 is involved in cristae junction formation and stabilisation

Using the CRISPR/Cas9 system, a widely used approach to genetically modify human cells, a MIC10$^{-/-}$ cell line was generated to investigate the function of MIC10 and its influence on mitochondrial function and membrane morphology. Analysis on the genomic and protein level could proof, that the approach was a success and no MIC10

was further expressed. A clear impact on mitochondrial morphology was evident after electron-microscopy of these cells, displaying the ring-like structure of inner membrane as in yeast *mic10*Δ and *mic60*Δ as well as in MIC60 deficient human cells, confirming MIC10 fulfilling the same role in cristae junction formation and stabilisation as its yeast homologue. The observed phenotype is specific for MIC10, since protein levels of MIC60 and other components of the MICOS complex, excluding MIC13, are not reduced and can be reversed by reexpressing MIC10 from a plasmid. Furthermore, processing of OPA1, a reported regulator of cristae and cristae junction morphology, is not affected (Data not shown).

4.2. Altering the inner membrane morphology does not impact on mitochondrial function

Cristae are believed to be needed to enlarge the surface of the inner mitochondrial membrane, with the cristae junctions to function as a barrier between IMS and cristae, thus creating highly specialized sub-compartments of different protein contents to maximise the efficiency of mitochondrial functions like ATP production via respiration. Thus, disturbing the morphology is expected to display defects in mitochondrial bioenergetics. Indeed, it was shown that yeast cells lacking Mic60 or Mic10 display a reduced oxygen consumption, reduced growth under conditions demanding a high mitochondrial activity and in terms of lacking Mic60 also reduced membrane potential.

However, this seemed not to be the case in mammalian cells. Ablation of the human MIC10 did not revealed to have an impact on cell growth and mitochondrial health seemed not be affected, as the mitochondrial membrane potential is unchanged compared to control cells. In contrast, down-regulation of MIC60 led to a decreased cell number after 48 h of treatment, increased membrane potential and apoptosis (John et al., 2005). Furthermore, overall oxygen consumption was not significantly altered. Although taking a closer look on complex IV revealed that the amount of complex IV was reduced to nearly 50 %, the complex IV specific activity remained nearly unchanged. Assessing protein levels of complex IV constituents revealed a slight reduction of the mitochondrial encoded subunit COX1, but no effect on the nuclear encoded COX6A. It was shown that assembly of complex IV via MITRAC is dependent on TIM21 (Mick et al., 2012), however no reduction of TIM21 was found on the protein level after deletion of MIC10. The translocation activity of the TIM23 complex was unaffected and therefore a secondary effect of MIC10 deletion via the TIM23 complex is highly unlikely. Studies in MEF cells

could show that the MIC60 together with MIC19 plays a role in mitochondrial DNA organization and translation of mitochondrial encoded proteins is impaired in MIC60 knock-down cells (Li et al., 2016). Still, whether the observed translation deficiency was due to a disruption of the MICOS complex, alteration of the inner mitochondrial morhpology or specifically linked to ablation of MIC60 remains unclear. For MIC10$^{-/-}$ an of the effect on mitochondrial translation is not reported so far and should be adressed in the future.

In conclusion, it could be shown that MIC10 is involved in forming and maintaining proper mitochondrial ultrastructure in mammalian cells, however the general mitochondrial function and health is not affected by the change in inner mitochondrial membrane morphology. Since some of the various phenotypes observed in already MIC60 deficient cells could not be reproduced in cells lacking MIC10 proved further that the MIC60 subcomplex can interact independently from the MIC10 subcomplex and is not only required for proper mitochondrial ultrastructure but is involved in assorted mitochondrial functions by so far unknown mechanisms.

4.3. Unveiling novel MICOS interaction partners via proximity labelling

In general, biological functions are carried out by proteins as components of complexes, organelles or other assemblies. Although the human genome project provided information of plenty of proteins encoded in the genome, the arrangement, organization and function of these proteins is largely unknown. Several biochemical techniques have been developed and are constantly evolved to characterise protein location and to identify there function and interactions. Biochemical approaches like immunoprecipitation and cross-linking are established to uncover protein-protein interactions. To identify associated proteins, Mass-Spectrometry is the method widely used to analyse a large dataset of proteins. In the classical approach, a sample is lysed using mild detergent conditions followed by immunoprecipitation of the protein of interest. However, many crucial protein interactions are only weak and transient (Nooren & Thornton, 2003), therefore arduous to maintain during even mild purification and washing steps. An idea to overcome these boundaries is either cross-linking or proximity labelling to label proteins of close vicinity with a purifiable tag. Such a broadly used tag is biotin, its strength being usable in living cells and preserving membranes, complexes and spatial relationships. Moreover, both soluble and insoluble proteins tagged with biotin can be purified with

efficient high-stringency using streptavidin while minimizing the background without loosing proteins during the process.

Since its first introduction in 2012, two main means of enzymatic activation of biotin are used, BioID (Roux et al., 2012) and APEX (Rhee et al., 2013). While the general concept is equivalent in both attempts, they differ in their initial activation step. BioID utilize endogenous biotin with labelling times around 18-24 h in a proximity of estimated 10 nm, although exact confirmations of these radius is still ongoing. Publications revealed that it can be applied to a great variety of cellular proteins not only in cultured cells, but also in yeast, protozoa, embryonic stem cells and in living mice (Trinkle-Mulcahy, 2019). The functionally related method APEX was originally designed to provide high-resolution images for cellular structures by electron-microscopy (Martell et al., 2012) but was later adapted for proximity labelling in living cells. Using biotin-phenol as a substrate the labelling is radical driven, thus only short labelling time is needed (around 1 min) and enables the utilization of biotin-labelling in a time-dependent manner to investigate complex dynamics. Although due to the higher hydrophobicity of biotin-phenol compared with biotin, there is a possibility of affecting the bioviability of the substrate in every cellular compartment. Both reactive biotin species biotin-AMP and the biotin-phenol radical are proposed to be compartment specific and not able to cross cellular membranes, although the latter is controversial discussed in the field.

In this study, both techniques were applied to attempt to investigate interaction partners of a mitochondrial inner membrane protein complex, MICOS. The enzymes BioID2 and APEX were both fused to MIC10 and expressed in HEK293T-REx cells and correct localisation of the enzyme in the IMS could be confirmed. Since the labelling times using APEX were remarkably short, the labelling was carried out *in organello* in isolated mitochondria to reduce possible background from whole cell labelling, nevertheless over 50 % of the 1119 biotinylated proteins were not mitochondrial. Although mitochondrial purification was performed by sequential centrifugation, the mitochondrial fraction still contained membranes of the endoplasmic reticulum and the golgi apparatus. Furthermore, background localisation of $MIC10^{APEX}$ in the cytosol could not be excluded by immunofluorescence microscopy due to background staining of the antibody, thus biotinylation outside mitochondria was not completely unexpected. Concentrating on the mitochondrial fraction, a striking number of 357 mitochondrial located proteins could be isolated, with the majority resided in the inner mitochondrial membrane or the inter membrane space. Moreover, roughly the same amount of matrix proteins was found enriched, including 62 out of 67 mitochondrial ribosomal constituents. In conclusion, the

biotin-phenol radical indeed seemed to have crossed the inner mitochondrial membrane and entered the mitochondrial matrix. Whether this is due to possible side-effects of the highly reactive H_2O_2 treatment or the radical despite different proposals is possible to cross the inner mitochondrial membrane remains unclear. Nevertheless, the APEX approach seemed not favourable for the desired purpose without the implementation of rigorous controls such as matrix-located APEX and APEX on the outer mitochondrial membrane facing the cytosol, as the active labelling species appeared to be more reactive than anticipated.

However, the BioID approach already resulted in a more distinct biotinylation pattern after western-blot analysis and $MIC10^{BioID2}$ and wild-type MIC10 could be clearly detected by probing for biotinylated proteins with HRP-coupled streptavidin. Mass-spectrometry analysis after *in vivo* labelling revealed 551 biotinylated proteins enriched, only 50 % of the enriched proteins using the APEX approach despite the fact that in this analysis whole cell lysates were analysed. As expected, most proteins were non-mitochondrial, due to the fact that the fully synthesised protein has a certein dwell time within the cytosol with the BioID enzyme already active before it is fully imported into mitochondria. To additionally search for mutual interaction partners outside of mitochondria, a cytosolic control would need to be implemented to be able to identify background labelling. Focusing on the labelled mitochondrial proteins, a subset of 37 biotinylated proteins could be identified, apart from known MICOS components published interactors were found on this list, such as constituents of the mitochondrial intermembrane space bridging (MIB) complex (Barrera et al., 2016) and proteins involved in inner mitochondrial membrane organization (Zerbes et al., 2012; Xie et al., 2007; Körner et al., 2012). TIM29, a constituent of the carrier translocase TIM22 and an assortment of its substrates were found to be mutual novel interactors. Further investigations could prove that indeed the TIM22 complex is a novel interactor of the MICOS complex and they share a functional connection (Callegari et al., 2019).

These findings confirm that this approach indeed was able to label interacting partners of MICOS. Surprisingly, not every constituent of an interacting protein complex could be labelled. MIC13 and MIC26 could not be identified by mass-spectrometry and likewise TIM29 is the only labelled component of the TIM22 complex, although it could be clearly shown that MIC10 interacts additionally with TIM22 and AGK. This demonstrates, that there is a limitation of proteins being accessible for labelling with biotin-AMP. However, using BioID analysis provided already without further control labelling experiments a manageable set of proteins for further investigations. Nevertheless, further analysis

would need to be done to provide a definite answer whether proteins interact with each other.

In conclusion, proximity biotinylation is a powerful tool to screen for mutual interaction partners. BioID is a more sensitive approach which is able to provide even with little controls a solid list of interaction partners, although the reactivity seems not to be high enough to label all proteins in vicinity. Whereas APEX is also able to provide a time-resolution of protein interactions, the background labelling of non-interacting proteins is significantly higher and more stringent labelling controls are needed.

4.4. MICOS interacts with the TIM23-complex

The impact of MICOS on mitochondrial ultrastructure in yeast have been studied thoroughly. Furthermore, MICOS via Mic60 seems to be involved in various other mitochondrial functions, like phospholipid metabolism (Harner et al., 2014; Aaltonen et al., 2016). Moreover, it was reported that loss of Mic60 has an impact on protein translocation into mitochondria (von der Malsburg et al., 2011). However, this data is not quite conclusive since also the membrane potential is affected in this strain, which is the mayor driving force of precursor-containing protein translocation. Nevertheless, a possible interaction of MICOS and the translocase machinery is likely, considering the TOM and TIM23 complex need to be in close spatial proximity for efficient precursor handover and MICOS is proved to be involved in forming contact sites between the outer and inner mitochondrial membrane. Therefore this study was designed to have a closer look on a mutual MICOS/translocase interaction and characterize protein translocation in a *mic10*Δ strain.

So far, a direct interaction of MICOS to constituents of the TIM23 complex could not be observed. Performing a Tim21 and Tim23 immunoprecipitation, MICOS components Mic60 and Mic10 could be co-isolated. Additionally, specific amounts of TIM23 components were co-purified by a reversed experiment where MICOS is isolated via Mic60$^{\mathrm{EPEA}}$. This correlates with the finding of enriched TOM-TIM23 supercomplex clusters at cristae junctions (Gold et al., 2014; Harner et al., 2011), thus an interaction between these two distinct protein complexes is likely. Interestingly, the interaction is also maintained in a *mic10*Δ strain, indicating that the interaction is Mic60 mediated and independent from the Mic10 subcomplex. This is supported by numerous findings of MICOS interacting with further translocase complexes SAM and TOM via Mic60 (von der Malsburg et al., 2011; C. Ott et al., 2012; Körner et al., 2012; Xie et al., 2007; Zerbes et al., 2012).

In contrast, no interactions between MICOS and the carrier translocase TIM22 were found in yeast, neither in TIM22 isolations nor in MICOS purifications. Interestingly, its contrary in mammalian cells. Although whether MICOS interacts with the TIM23 complex in human is still controversial, a clear interaction to the TIM22-complex could be established (Callegari et al., 2019)

4.5. Inner mitochondrial ultrastructure affects import of precursor-containing proteins in yeast

Past studies of protein import into MICOS deficient mitochondria revealed a decrease in protein translocation via TIM23 and Mia40 in *mic60*Δ. However, also membrane potential was deficient, thus the observed phenotype is likely an indirect effect (von der Malsburg et al., 2011). Translocation via Mia40 in *mic10*Δ mitochondria was not impaired. Since no protein import experiments with precursor-containing proteins have been performed so far, radiolabelled substrates of the TIM23 complex were used in this study to explore possible connection of MICOS to protein translocation.

Importing precursor proteins into isolated WT and *mic10*Δ revealed a decrease from 20 % (Atp4) to 60 % ($F_1\beta$) upon loss of Mic10. To rule out secondary effects, membrane potential measurements in *mic10*Δ mitochondria were performed and proofed to be equivalent to the control. Due to accumulation of the TOM-TIM23 supercomplex at cristae junctions and thus close vicinity to MICOS, a functional interaction between these two is likely and might be the basis of the observed phenotype. However, isolating translocase-arrested TOM-TIM23 supercomplex unveiled no change in the composition of the complex in *mic10*Δ mitochondria. Surprisingly, also no Mic10 was found to be isolated together with the supercomplex. This led to the conclusion that MICOS interacts with different pool of TIM23 complex, which is likely since both the TOM and the TIM23 complex were found to be associated with other complexes in an independent manner (Qiu et al., 2013; Mehnert et al., 2014; Kulawiak et al., 2013).

Similar to *mic10*Δ, *atp20*Δ also displayed an altered mitochondrial inner membrane morphology (Alkhaja et al., 2012; Paumard et al., 2002). Performing the same import experiments as in *mic10*Δ revealed that precursor-containing protein translocation is not functionally linked to MICOS, but to the membrane morphology. Thus, it could be proved that precursor handover indeed is mediated by close proximity of the outer and the inner mitochondrial membrane and proper mitochondrial ultrastructure is important for efficient precursor translocation. The connection of MICOS to the TIM23-complex

however seemed just to be spatial, lacking a direct influence on their respective function.

4.6. Carrier import via TIM22 does not depend on proper mitochondrial morphology in yeast

The TIM22 carrier translocase is specialized in insertion of hydrophobic, multi transmembrane domain proteins with internal targeting signals. Typically, these substrates are either metabolite carriers which possess 6 transmembrane spanes or four transmembrane spanning components if the different translocases such as Tim23, Tim22 and Tim17. Handover from the TOM complex to the TIM22 complex is mediatet by small TIM chaperones in the IMS to stabilize the hydrophobic parts of the substrates while being transportet through the aqueous IMS. However, the exact mechanism how the TOM complex and the TIM22 complex interact with each other is not known. To date, no direct interactions between components of the TOM complex have been reported to constituents of the TIM22 complex, although recent studies revealed an interaction of Porin with carrier precursors followed by recruitment of the TIM22 complex (Ellenrieder et al., 2019).

In contrast to translocation of TIM23 dependent proteins, import of the carrier protein Aac1 as a substrate of the TIM22 complex was unaffected by the altered inner mitochondrial membrane morphology in *mic10*Δ and *atp20*Δ mitochondria. This is solified by the finding that the handover from the TOM complex to the TIM22 complex is facilitated by the soluble small TIM chaperons in the IMS (Koehler et al., 1998; Weinhäupl et al., 2018), thus not relying on close proximity of both translocases and therefore proper mitochondrial morphology. Although the small TIM chaperones are conserved in the mammalian system, the human TIM22 complex itself harbours metazoan-specific constituents and its architecture is poorly conserved betwween human and yeast. Furthermore, in human cells lacking MIC10 the TIM22 complex facilitated import is impaired in contrast to the findings in yeast (Callegari et al., 2019). It has been shown that in human mitochondria the small TIM chaperones are more closely associated to the inner mitochondrial membrane and are not present as a soluble complex in the IMS. Moreover, TOM40 as constituent of the TOM complex has been found to interact with the TIM22 complex via TIM29.

Combining these findings revealed that the mechanism of precursor handover from the TOM complex to the TIM22 complex is opposite from human to yeast. Whereas in the mammalian system MICOS and TIM22 work synergistically to drive translocation via

close spatial connection of the outer and the inner mitochondrial membrane, in yeast the transport through the IMS is independent from outer and inner mitochondrial membrane contact sites and MICOS and solely relies on the soluble TIM chaperones.

5. Conclusion and future perspective

MICOS is an essential multisubunit protein complex responsible for forming and maintaining inner mitochondrial ultrastructure. By generation of a MIC10 knock-out cell line in mammalian cells it was proven that the human MIC10 protein is essential for maintaining inner mitochondrial membrane structure similar to its yeast homologue. Although the cell growth and membrane potential in addition to oxygen consumption of mitochondria were not impaired, a specific reduction in the amounts of complex IV were detected. Whether this is caused by a potential phenotype in mitochondrial translation or has a diverse cause would need to be assessed in further studies. Strikingly, there was also a reduction in the levels of components of the TIM22 complex and its substrates.

In the second part of the study it was shown that proximity biotinylation, mediated via a promiscuous biotin ligase, is a feasible approach to investigate novel interaction partners. In contrast, using the APEX approach for biotin labelling led to a high amount of background labelling and there was poor compartment specificity of the reactive labelling substrate. Aside from known interactors, a number of mutual novel interaction partners were found. Out of these, the carrier TIM22 complex was proved in further studies to functionally interact with the MICOS complex. To confirm interplay of MICOS to other proteins found in this study, additional biochemical analysis would need to be done.

It was shown in the past that loss of Mic60 in yeast has an impact on protein translocation, a direct link between MICOS and the translocases of the inner membrane could not be established so far. In this study Mic60 and Mic10 were co-isolated with Tim21 and Tim23 in a Mic10 independent manner. Import of precursor-containing substrates of the TIM23 complex in *mic10*Δ mitochondria demonstrated a reduction in import efficiency. This defect however could also be reproduced in *atp20*Δ mitochondria, which has a similar defect in mitochondrial morphology. Thus, precursor import via the TIM23 complex is linked to inner mitochondrial membrane morphology. The function of the association between MICOS and the TIM23 complex would need to be assessed in future studies. In contrast, carrier translocation via the TIM22 complex proved to be unaffected by the altered inner mitochondrial ultrastructure in yeast and is less reliant on contacts between the inner and outer mitochondrial membrane.

A. Appendix

A.1. Abbreviations

AAC	ADP/ATP carrier
APEX	enhanced ascorbate peroxidase
APS	ammonium peroxosulfate
ATP	adenosine triphosphate
AVO	Antimycin A, valinomycin, oligomycin micture
BN-PAGE	blue native polyacrylamid gel electrophoresis
bp	base pairs
BSA	bovine serum albumine
BTS	biotinylation targeting signal
Cas9	CRISPR associated protein 9
CK	creatine kinase
CP	Creatine phosphate
COX	cytochrome *c* oxidase
CRISPR	clustered regularly interspaced short palindromic repeats
DMSO	Dimethylsulfoxid
DNA	deoxyribonucleic acid
dNTP	2'-deoxynucleoside-5'-triphosphate
DTT	dithiothreitol
E. coli	escherichia coli
EDTA	ethylenediaminetetraacetic acid
EM	electron microscopy
ER	endoplasmic reticulum
ERMIONE	ER mitochondria organizing network
ERMES	ER-mitochondria encounter structure
EtBr	Ethidium bromide
FCS	fetal calf serum
FMN	flavin mononucleotide
HEK	human embryonic kidney

HEPES	4-(2-hydroxyethyl)-1-piperazineethanesulfonic acid
HRP	Horseradish peroxidase
IBM	inner boundary membrane
IgG	immunoglobulin G
IMM	inner mitochondrial membrame
IMS	intermembrane space
kDa	kilodalton
LB	lysogeny broth
LC	Liquid chromatography
MALDI	matrix-assisted laser desorption ionization
MIA	Mitochondrial intermembrane space assembly machinery
MICOS	mitochondrial contact site and cristae organizing system
MIM	mitochondrial import complex
MITRAC	mitochondrial translation regulation assembly intermediate of cytochrome *c* oxidase
MOPS	morpholinopropanesulfonic acid
MPP	mitochonrial processing peptidase
MS	mass-spectrometry
MTS	mitochondrial targeting signal
NADH	nicotinamide adenine dinucleotide (reduced)
Nb	nano body
OD	optical density
OM	outer mitochondrial membrane
ORF	open reading frame
PAGE	polyacrylamide gel electrophoresis
PAM	presequence translocase assosiated motor
PBS	phosphate buffered saline
P_i	inorganic phosphate
PCR	polymerase chain reaction
PEG	polyethylene glycol
PK	proteinase K
PMSF	phenylmethylsulphonylfluoride
PVDF	polyvinylidene fluoride
RNA	ribonucleic acid
rpm	rotations per minute
S. cerevisiae	*Saccharomyces cerevisiae*
SAM	sorting and assembly machinery of the outer membrane
SA-HRP	streptavidin coupled to horseradish peroxidase

SEM buffer	sucrose/EDTA/MOPS buffer
SDS	sodium dodecyl sulfate
SDS-PAGE	sodium dodecyl sulfate-polyacrylamide gel electrophoresis
sfGFP	super folder green fluorescent protein
TAE	Tris/Acetate/EDTA buffer
TCA	Tricarboxylic acid
TEMED	Tetramethylethylendiamine
TIM22	carrier translocase of the inner mitochondrial membrane
TIM23	presequence translocase of the inner mitochondrial membrane
TOM	translocase of the outer mitochondrial membrane
WT	wild type
YPG	Yeast Extract, peptone, glucose
$\Delta\Psi$	membrane potential

A.2. List of Figures

A.3. List of Tables

References

Aaltonen, M. J., Friedman, J. R., Osman, C., Salin, B., di Rago, J.-P., Nunnari, J., ... Tatsuta, T. (2016, June). MICOS and phospholipid transfer by Ups2-Mdm35 organize membrane lipid synthesis in mitochondria. *The Journal of Cell Biology*, *213*(5), 525–534.

Abe, Y., Shodai, T., Muto, T., Mihara, K., Torii, H., Nishikawa, S., ... Kohda, D. (2000, March). Structural basis of presequence recognition by the mitochondrial protein import receptor Tom20. *Cell*, *100*(5), 551–560.

Alavian, K. N., Beutner, G., Lazrove, E., Sacchetti, S., Park, H.-A., Licznerski, P., ... Jonas, E. A. (2014, July). An uncoupling channel within the c-subunit ring of the F1FO ATP synthase is the mitochondrial permeability transition pore. *Proceedings of the National Academy of Sciences of the United States of America*, *111*(29), 10580–10585.

Alkhaja, A. K., Jans, D. C., Nikolov, M., Vukotic, M., Lytovchenko, O., Ludewig, F., ... Deckers, M. (2012, January). MINOS1 is a conserved component of mitofilin complexes and required for mitochondrial function and cristae organization. *Molecular biology of the cell*, *23*(2), 247–257.

Amutha, B., & Pain, D. (2003, March). Nucleoside diphosphate kinase of Saccharomyces cerevisiae, Ynk1p: localization to the mitochondrial intermembrane space. *The Biochemical journal*, *370*(Pt 3), 805–815.

Arnold, I., Pfeiffer, K., Neupert, W., Stuart, R. A., & Sch a gger, H. (1998, December). Yeast mitochondrial F1F0-ATP synthase exists as a dimer: identification of three dimer-specific subunits. *The EMBO Journal*, *17*(24), 7170–7178.

Arselin, G., Giraud, M.-F., Dautant, A., Vaillier, J., Brèthes, D., Coulary-Salin, B., ... Velours, J. (2003, April). The GxxxG motif of the transmembrane domain of subunit e is involved in the dimerization/oligomerization of the yeast ATP synthase complex in the mitochondrial membrane. *European journal of biochemistry*, *270*(8), 1875–1884.

Atanassov, I., & Urlaub, H. (2013, October). Increased proteome coverage by combining PAGE and peptide isoelectric focusing: comparative study of gel-based separation approaches. *PROTEOMICS*, *13*(20), 2947–2955.

Backes, S., Hess, S., Boos, F., Woellhaf, M. W., Gödel, S., Jung, M., ... Herrmann, J. M. (2018, April). Tom70 enhances mitochondrial preprotein import efficiency by binding to internal targeting sequences. *J. Cell Biol.*, *217*(4), 1369–1382.

Balsa, E., Marco, R., Perales-Clemente, E., Szklarczyk, R., Calvo, E., Landázuri, M. O., & Enriquez, J. A. (2012, September). NDUFA4 is a subunit of complex IV of the mammalian electron transport chain. *Cell Metabolism*, *16*(3), 378–386.

Barbot, M., Jans, D. C., Schulz, C., Denkert, N., Kroppen, B., Hoppert, M., ... Meinecke, M. (2015, May). Mic10 oligomerizes to bend mitochondrial inner membranes at cristae junctions. *Cell Metabolism*, *21*(5), 756–763.

Barrera, M., Koob, S., Dikov, D., Vogel, F., & Reichert, A. S. (2016, October). OPA1 functionally interacts with MIC60 but is dispensable for crista junction formation. *FEBS Letters*, *590*(19), 3309–3322.

Becker, T., Böttinger, L., & Pfanner, N. (2012, March). Mitochondrial protein import: from transport pathways to an integrated network. *Trends in Biochemical Sciences*, *37*(3), 85–91.

Beckett, D., Kovaleva, E., & Schatz, P. J. (1999, April). A minimal peptide substrate in biotin holoenzyme synthetase-catalyzed biotinylation. *Protein science : a publication of the Protein Society*, *8*(4), 921–929.

Benz, R. (1994, June). Permeation of hydrophilic solutes through mitochondrial outer membranes: review on mitochondrial porins. *Biochimica et biophysica acta*, *1197*(2), 167–196.

Bohnert, M., Rehling, P., Guiard, B., Herrmann, J. M., Pfanner, N., & van der Laan, M. (2010, July). Cooperation of stop-transfer and conservative sorting mechanisms in mitochondrial protein transport. *Current biology : CB*, *20*(13), 1227–1232.

Bohnert, M., Wenz, L.-S., Zerbes, R. M., Horvath, S. E., Stroud, D. A., von der Malsburg, K., ... van der Laan, M. (2012, October). Role of mitochondrial inner membrane organizing system in protein biogenesis of the mitochondrial outer membrane. *Molecular biology of the cell*, *23*(20), 3948–3956.

Bohnert, M., Zerbes, R. M., Davies, K. M., Mühleip, A. W., Rampelt, H., Horvath, S. E., ... van der Laan, M. (2015, May). Central role of Mic10 in the mitochondrial contact site and cristae organizing system. *Cell Metabolism*, *21*(5), 747–755.

Bömer, U., Meijer, M., Maarse, A. C., Hönlinger, A., Dekker, P. J., Pfanner, N., & Rassow, J. (1997, May). Multiple interactions of components mediating preprotein translocation across the inner mitochondrial membrane. *The EMBO Journal*, *16*(9), 2205–2216.

Bornhövd, C., Vogel, F., Neupert, W., & Reichert, A. S. (2006, May). Mitochondrial membrane potential is dependent on the oligomeric state of F1F0-ATP synthase supracomplexes. *Journal of Biological Chemistry*, *281*(20), 13990–13998.

Boyer, P. D. (1997). The ATP synthase–a splendid molecular machine. *Annual review of biochemistry*, *66*(1), 717–749.

Boyle, G. M., Roucou, X., Nagley, P., Devenish, R. J., & Prescott, M. (1999, June). Identification of subunit g of yeast mitochondrial F1F0-ATP synthase, a protein required for maximal activity of cytochrome c oxidase. *European journal of biochemistry*, *262*(2), 315–323.

Brix, J., Dietmeier, K., & Pfanner, N. (1997, August). Differential recognition of preproteins by the purified cytosolic domains of the mitochondrial import receptors Tom20, Tom22, and Tom70. *Journal of Biological Chemistry*, *272*(33), 20730–20735.

Callegari, S., Müller, T., Schulz, C., Lenz, C., Jans, D. C., Wissel, M., ... Deckers, M. (2019). A MICOS-TIM22 association promotes mitochondrial carrier import in human mitochondria. *Journal of Molecular Biology*, 1–55 (submitted).

Callegari, S., Richter, F., Chojnacka, K., Jans, D. C., Lorenzi, I., Pacheu-Grau, D., ... Rehling, P. (2016, December). TIM29 is a subunit of the human carrier translocase required for protein transport. *FEBS Letters*, *590*(23), 4147–4158.

Capaldi, R. A. (1990). Structure and function of cytochrome c oxidase. *Annual review of biochemistry*, *59*(1), 569–596.

Chacinska, A., Guiard, B., Müller, J. M., Schulze-Specking, A., Gabriel, K., Kutik, S., & Pfanner, N. (2008, October). Mitochondrial biogenesis, switching the sorting pathway of the intermembrane space receptor Mia40. *Journal of Biological Chemistry*, *283*(44), 29723–29729.

Chacinska, A., Koehler, C. M., Milenkovic, D., Lithgow, T., & Pfanner, N. (2009, August). Importing mitochondrial proteins: machineries and mechanisms. *Cell*, *138*(4), 628–644.

Chacinska, A., Pfannschmidt, S., Wiedemann, N., Kozjak, V., Sanjuán Szklarz, L. K., Schulze-Specking, A., ... Pfanner, N. (2004, October). Essential role of Mia40 in import and assembly of mitochondrial intermembrane space proteins. *The EMBO Journal*, *23*(19), 3735–3746.

Chan, P.-K., Srikumar, T., Dingar, D., Kalkat, M., Penn, L. Z., & Raught, B. (2014, December). BioID data of c-MYC interacting protein partners in cultured cells and xenograft tumors. *Data in brief*, *1*, 76–78.

Chatzispyrou, I. A., Guerrero-Castillo, S., Held, N. M., Ruiter, J. P. N., Denis, S. W., IJlst, L., ... Houtkooper, R. H. (2018, November). Barth syndrome cells display widespread remodeling of mitochondrial complexes without affecting metabolic

flux distribution. *BBA - Molecular Basis of Disease*, *1864*(11), 3650–3658.

Cipolat, S., Martins de Brito, O., Dal Zilio, B., & Scorrano, L. (2004, November). OPA1 requires mitofusin 1 to promote mitochondrial fusion. *Proceedings of the National Academy of Sciences*, *101*(45), 15927–15932.

Cipolat, S., Rudka, T., Hartmann, D., Costa, V., Serneels, L., Craessaerts, K., ... De Strooper, B. (2006, July). Mitochondrial rhomboid PARL regulates cytochrome c release during apoptosis via OPA1-dependent cristae remodeling. *Cell*, *126*(1), 163–175.

Collinson, I. R., van Raaij, M. J., Runswick, M. J., Fearnley, I. M., Skehel, J. M., Orriss, G. L., ... Walker, J. E. (1994, September). ATP synthase from bovine heart mitochondria. In vitro assembly of a stalk complex in the presence of F1-ATPase and in its absence. *Journal of Molecular Biology*, *242*(4), 408–421.

Curran, S. P., Leuenberger, D., Oppliger, W., & Koehler, C. M. (2002, March). The Tim9p-Tim10p complex binds to the transmembrane domains of the ADP/ATP carrier. *The EMBO Journal*, *21*(5), 942–953.

Daithankar, V. N., Farrell, S. R., & Thorpe, C. (2009, June). Augmenter of liver regeneration: substrate specificity of a flavin-dependent oxidoreductase from the mitochondrial intermembrane space. *Biochemistry*, *48*(22), 4828–4837.

Darshi, M., Mendiola, V. L., Mackey, M. R., Murphy, A. N., Koller, A., Perkins, G. A., ... Taylor, S. S. (2011, January). ChChd3, an inner mitochondrial membrane protein, is essential for maintaining crista integrity and mitochondrial function. *The Journal of biological chemistry*, *286*(4), 2918–2932.

Davies, K. M., Strauss, M., Daum, B., Kief, J. H., Osiewacz, H. D., Rycovska, A., ... Kühlbrandt, W. (2011, August). Macromolecular organization of ATP synthase and complex I in whole mitochondria. *Proceedings of the National Academy of Sciences of the United States of America*, *108*(34), 14121–14126.

Davis, A. J., Alder, N. N., Jensen, R. E., & Johnson, A. E. (2007, February). The Tim9p/10p and Tim8p/13p complexes bind to specific sites on Tim23p during mitochondrial protein import. *Molecular biology of the cell*, *18*(2), 475–486.

De los Rios Castillo, D., Zarco-Zavala, M., Olvera-Sanchez, S., Pardo, J. P., Juarez, O., Martinez, F., ... Flores-Herrera, O. (2011, July). Atypical cristae morphology of human syncytiotrophoblast mitochondria: role for complex V. *The Journal of biological chemistry*, *286*(27), 23911–23919.

Demishtein-Zohary, K., Marom, M., Neupert, W., Mokranjac, D., & Azem, A. (2015, June). GxxxG motifs hold the TIM23 complex together. *The FEBS journal*,

282(11), 2178–2186.

DeVay, R. M., Dominguez-Ramirez, L., Lackner, L. L., Hoppins, S., Stahlberg, H., & Nunnari, J. (2009, September). Coassembly of Mgm1 isoforms requires cardiolipin and mediates mitochondrial inner membrane fusion. *The Journal of Cell Biology*, *186*(6), 793–803.

Dimmer, K. S., & Rapaport, D. (2012, April). Unresolved mysteries in the biogenesis of mitochondrial membrane proteins. *Biochimica et biophysica acta*, *1818*(4), 1085–1090.

Ding, C., Wu, Z., Huang, L., Wang, Y., Xue, J., Chen, S., ... Chen, S. (2015, October). Mitofilin and CHCHD6 physically interact with Sam50 to sustain cristae structure. *Nature Publishing Group*, 1–11.

Dudek, J., Rehling, P., & van der Laan, M. (2013, February). Mitochondrial protein import: common principles and physiological networks. *Biochimica et biophysica acta*, *1833*(2), 274–285.

Ellenrieder, L., Dieterle, M. P., Doan, K. N., Mårtensson, C. U., Floerchinger, A., Campo, M. L., ... Becker, T. (2019, March). Dual Role of Mitochondrial Porin in Metabolite Transport across the Outer Membrane and Protein Transfer to the Inner Membrane. *Molecular Cell*, *73*(5), 1056–1065.e7.

Endo, T., Yamano, K., & Kawano, S. (2011, March). Structural insight into the mitochondrial protein import system. *Biochimica et biophysica acta*, *1808*(3), 955–970.

Esaki, M., Kanamori, T., Nishikawa, S.-i., Shin, I., Schultz, P. G., & Endo, T. (2003, December). Tom40 protein import channel binds to non-native proteins and prevents their aggregation. *Nature Structural Biology*, *10*(12), 988–994.

Eubel, H. (2003, September). New Insights into the Respiratory Chain of Plant Mitochondria. Supercomplexes and a Unique Composition of Complex II. *PLANT Physiol.*, *133*(1), 274–286.

Fawcett, D. W. (1981). *The Cell* (2nd ed.). W. B. Saunders Co., Philadelphia.

Feng, Y., Madungwe, N. B., & Bopassa, J. C. (2018, September). Mitochondrial inner membrane protein, Mic60/mitofilin in mammalian organ protection. *Journal of Cellular Physiology*, *234*(4), 3383–3393.

Fillingame, R. H., & Divall, S. (1999). Proton ATPases in bacteria: comparison to Escherichia coli F1F0 as the prototype. *Novartis Foundation symposium*, *221*, 218–29– discussion 229–34.

Frey, T. G., & Mannella, C. A. (2000, July). The internal structure of mitochondria. *Trends in Biochemical Sciences*, *25*(7), 319–324.

Frezza, C., Cipolat, S., Martins de Brito, O., Micaroni, M., Beznoussenko, G. V., Rudka, T., ... Scorrano, L. (2006, July). OPA1 controls apoptotic cristae remodeling independently from mitochondrial fusion. *Cell*, *126*(1), 177–189.

Friedman, J. R., Mourier, A., Yamada, J., McCaffery, J. M., & Nunnari, J. (2015). MICOS coordinates with respiratory complexes and lipids to establish mitochondrial inner membrane architecture. *eLife*, *4*, 621.

Friedman, J. R., & Nunnari, J. (2014, January). Mitochondrial form and function. *Nature*, *505*(7483), 335–343.

Gabaldón, T., & Huynen, M. A. (2004, December). Shaping the mitochondrial proteome. *Biochimica et biophysica acta*, *1659*(2-3), 212–220.

Gavin, P. D., Prescott, M., Luff, S. E., & Devenish, R. J. (2004, May). Cross-linking ATP synthase complexes in vivo eliminates mitochondrial cristae. *Journal of Cell Science*, *117*(Pt 11), 2333–2343.

Gebert, N., Gebert, M., Oeljeklaus, S., von der Malsburg, K., Stroud, D. A., Kulawiak, B., ... Wiedemann, N. (2011, December). Dual Function of Sdh3 in the Respiratory Chain and TIM22 Protein Translocase of the Mitochondrial Inner Membrane. *Molecular Cell*, *44*(5), 811–818.

Genova, M. L., & Lenaz, G. (2011, September). New developments on the functions of coenzyme Q in mitochondria. *BioFactors (Oxford, England)*, *37*(5), 330–354.

Gilkerson, R. W., Selker, J. M. L., & Capaldi, R. A. (2003, July). The cristal membrane of mitochondria is the principal site of oxidative phosphorylation. *FEBS Letters*, *546*(2-3), 355–358.

Giraud, M.-F., Paumard, P., Soubannier, V., Vaillier, J., Arselin, G., Salin, B., ... Velours, J. (2002, September). Is there a relationship between the supramolecular organization of the mitochondrial ATP synthase and the formation of cristae? *Biochimica et biophysica acta*, *1555*(1-3), 174–180.

Glick, B. S., Beasley, E. M., & Schatz, G. (1992, November). Protein sorting in mitochondria. *Trends in Biochemical Sciences*, *17*(11), 453–459.

Gödiker, J., Grüneberg, M., DuChesne, I., Reunert, J., Rust, S., Westermann, C., ... Marquardt, T. (2018, April). QIL1-dependent assembly of MICOS complex-lethal mutation in C19ORF70 resulting in liver disease and severe neurological retardation. *Journal of human genetics*, *123*, 157.

Gold, V. A. M., Ieva, R., Walter, A., Pfanner, N., van der Laan, M., & Kühlbrandt, W. (2014, June). Visualizing active membrane protein complexes by electron cryotomography. *Nature communications*, *5*(1), 4129.

Gomkale, R. (2018). *Insights into mitochondrial presequence and carrier import pathways* (Unpublished doctoral dissertation). Universtiy of Göttingen.

Gornicka, A., Bragoszewski, P., Chroscicki, P., Wenz, L.-S., Schulz, C., Rehling, P., & Chacinska, A. (2014, December). A discrete pathway for the transfer of intermembrane space proteins across the outer membrane of mitochondria. *Molecular biology of the cell*, *25*(25), 3999–4009.

Gray, M. W., Burger, G., & Lang, B. F. (1999, March). Mitochondrial evolution. *Science*, *283*(5407), 1476–1481.

Green, N. M. (1963, December). Avidin. 1. The use of (14-C)biotin for kinetic studies and for assay. *The Biochemical journal*, *89*(3), 585–591.

Guarani, V., McNeill, E. M., Paulo, J. A., Huttlin, E. L., Fröhlich, F., Gygi, S. P., ... Harper, J. W. (2015). QIL1 is a novel mitochondrial protein required for MICOS complex stability and cristae morphology. *eLife*, *4*, 40.

Hackenbrock, C. R. (1968, May). Ultrastructural bases for metabolically linked mechanical activity in mitochondria. II. Electron transport-linked ultrastructural transformations in mitochondria. *The Journal of Cell Biology*, *37*(2), 345–369.

Harner, M., Körner, C., Walther, D., Mokranjac, D., Kaesmacher, J., Welsch, U., ... Neupert, W. (2011, October). The mitochondrial contact site complex, a determinant of mitochondrial architecture. *The EMBO Journal*, *30*(21), 4356–4370.

Harner, M., Unger, A.-K., Izawa, T., Walther, D. M., Özbalci, C., Geimer, S., ... Neupert, W. (2014, January). Aim24 and MICOS modulate respiratory function, tafazzin-related cardiolipin modification and mitochondrial architecture. *eLife*, *3*, e01684.

Hatefi, Y. (1985). The mitochondrial electron transport and oxidative phosphorylation system. *Annual review of biochemistry*, *54*(1), 1015–1069.

Hawlitschek, G., Schneider, H., Schmidt, B., Tropschug, M., Hartl, F. U., & Neupert, W. (1988, June). Mitochondrial protein import: identification of processing peptidase and of PEP, a processing enhancing protein. *Cell*, *53*(5), 795–806.

Hofmann, S., Rothbauer, U., Mühlenbein, N., Baiker, K., Hell, K., & Bauer, M. F. (2005, October). Functional and mutational characterization of human MIA40 acting during import into the mitochondrial intermembrane space. *Journal of Molecular Biology*, *353*(3), 517–528.

Hoppins, S., Collins, S. R., Cassidy-Stone, A., Hummel, E., DeVay, R. M., Lackner, L. L., ... Nunnari, J. (2011, October). A mitochondrial-focused genetic interaction map reveals a scaffold-like complex required for inner membrane organization in

mitochondria. *The Journal of Cell Biology*, *195*(2), 323–340.

Hoppins, S. C., & Nargang, F. E. (2004, March). The Tim8-Tim13 complex of Neurospora crassa functions in the assembly of proteins into both mitochondrial membranes. *Journal of Biological Chemistry*, *279*(13), 12396–12405.

Horvath, P., & Barrangou, R. (2010, January). CRISPR/Cas, the immune system of bacteria and archaea. *Science*, *327*(5962), 167–170.

Horvath, S. E., & Daum, G. (2013, October). Lipids of mitochondria. *Progress in lipid research*, *52*(4), 590–614.

Hulett, J. M., Lueder, F., Chan, N. C., Perry, A. J., Wolynec, P., Likić, V. A., ... Lithgow, T. (2008, February). The transmembrane segment of Tom20 is recognized by Mim1 for docking to the mitochondrial TOM complex. *Journal of Molecular Biology*, *376*(3), 694–704.

Huynen, M. A., Mühlmeister, M., Gotthardt, K., Guerrero-Castillo, S., & Brandt, U. (2016, January). Evolution and structural organization of the mitochondrial contact site (MICOS) complex and the mitochondrial intermembrane space bridging (MIB) complex. *BBA - Molecular Cell Research*, *1863*(1), 91–101.

Jans, D. C., Wurm, C. A., Riedel, D., Wenzel, D., Stagge, F., Deckers, M., ... Jakobs, S. (2013, May). STED super-resolution microscopy reveals an array of MINOS clusters along human mitochondria. *Proceedings of the National Academy of Sciences of the United States of America*, *110*(22), 8936–8941.

John, G. B., Shang, Y., Li, L., Renken, C., Mannella, C. A., Selker, J. M. L., ... Zha, J. (2005, March). The mitochondrial inner membrane protein mitofilin controls cristae morphology. *Molecular biology of the cell*, *16*(3), 1543–1554.

Jores, T., Klinger, A., Groß, L. E., Kawano, S., Flinner, N., Duchardt-Ferner, E., ... Rapaport, D. (2016, June). Characterization of the targeting signal in mitochondrial β-barrel proteins. *Nature communications*, *7*(1), 12036.

Kang, Y., Baker, M. J., Liem, M., Louber, J., McKenzie, M., Atukorala, I., ... Stojanovski, D. (2016, August). Tim29 is a novel subunit of the human TIM22 translocase and is involved in complex assembly and stability. *eLife*, *5*, 313.

Kang, Y., Fielden, L. F., & Stojanovski, D. (2018, April). Mitochondrial protein transport in health and disease. *Seminars in cell & developmental biology*, *76*, 142–153.

Kang, Y., Stroud, D. A., Baker, M. J., De Souza, D. P., Frazier, A. E., Liem, M., ... Stojanovski, D. (2017, August). Sengers Syndrome-Associated Mitochondrial Acylglycerol Kinase Is a Subunit of the Human TIM22 Protein Import Complex. *Molecular Cell*, *67*(3), 457–470.e5.

Kiebler, M., Pfaller, R., Söllner, T., Griffiths, G., Horstmann, H., Pfanner, N., & Neupert, W. (1990, December). Identification of a mitochondrial receptor complex required for recognition and membrane insertion of precursor proteins. *Nature*, *348*(6302), 610–616.

Kim, D. I., Jensen, S. C., Noble, K. A., Kc, B., Roux, K. H., Motamedchaboki, K., & Roux, K. J. (2016, April). An improved smaller biotin ligase for BioID proximity labeling. *Molecular biology of the cell*, *27*(8), 1188–1196.

Kim, D. I., KC, B., Zhu, W., Motamedchaboki, K., Doye, V., & Roux, K. J. (2014, June). Probing nuclear pore complex architecture with proximity-dependent biotinylation. *Proceedings of the National Academy of Sciences*, *111*(24), E2453–E2461.

Koehler, C. M., Jarosch, E., Tokatlidis, K., Schmid, K., Schweyen, R. J., & Schatz, G. (1998, January). Import of mitochondrial carriers mediated by essential proteins of the intermembrane space. *Science*, *279*(5349), 369–373.

Komiya, T. (1997, July). Binding of mitochondrial precursor proteins to the cytoplasmic domains of the import receptors Tom70 and Tom20 is determined by cytoplasmic chaperones. *EMBO J.*, *16*(14), 4267–4275.

Koob, S., Barrera, M., Anand, R., & Reichert, A. S. (2015a, September). Data supporting the role of the non-glycosylated isoform of MIC26 in determining cristae morphology. *Data in brief*, *4*, 135–139.

Koob, S., Barrera, M., Anand, R., & Reichert, A. S. (2015b, July). The non-glycosylated isoform of MIC26 is a constituent of the mammalian MICOS complex and promotes formation of crista junctions. *Biochimica et biophysica acta*, *1853*(7), 1551–1563.

Körner, C., Barrera, M., Dukanovic, J., Eydt, K., Harner, M., Rabl, R., ... Reichert, A. S. (2012, June). The C-terminal domain of Fcj1 is required for formation of crista junctions and interacts with the TOB/SAM complex in mitochondria. *Molecular biology of the cell*, *23*(11), 2143–2155.

Kozjak-Pavlovic, V., Ross, K., Benlasfer, N., Kimmig, S., Karlas, A., & Rudel, T. (2007, June). Conserved roles of Sam50 and metaxins in VDAC biogenesis. *EMBO reports*, *8*(6), 576–582.

Krause, F., Reifschneider, N. H., Goto, S., & Dencher, N. A. (2005, April). Active oligomeric ATP synthases in mammalian mitochondria. *Biochem. Biophys. Res. Commun.*, *329*(2), 583–590.

Krüger, V., Becker, T., Becker, L., Montilla-Martinez, M., Ellenrieder, L., Vögtle, F.-N., ... Meisinger, C. (2017, November). Identification of new channels by system-

atic analysis of the mitochondrial outer membrane. *The Journal of Cell Biology*, *216*(11), 3485–3495.

Kulawiak, B., Höpker, J., Gebert, M., Guiard, B., Wiedemann, N., & Gebert, N. (2013, May). The mitochondrial protein import machinery has multiple connections to the respiratory chain. *Biochimica et biophysica acta*, *1827*(5), 612–626.

Lackey, S. W. K., Taylor, R. D., Go, N. E., Wong, A., Sherman, E. L., & Nargang, F. E. (2014, August). Evidence supporting the 19 β-strand model for Tom40 from cysteine scanning and protease site accessibility studies. *The Journal of biological chemistry*, *289*(31), 21640–21650.

Lamond, A. I. (2002). *Molecular Biology of Cell* (4th ed., Vol. 3). Shock.

Lenaz, G., & Genova, M. L. (2010, April). Structure and organization of mitochondrial respiratory complexes: a new understanding of an old subject. *Antioxidants & redox signaling*, *12*(8), 961–1008.

Li, H., Ruan, Y., Zhang, K., Jian, F., Hu, C., Miao, L., ... Song, Z. (2016, March). Mic60/Mitofilin determines MICOS assembly essential for mitochondrial dynamics and mtDNA nucleoid organization. *Cell Death and Differentiation*, *23*(3), 380–392.

Lill, R. (2009, August). Function and biogenesis of iron-sulphur proteins. *Nature*, *460*(7257), 831–838.

Mandelman, D., Jamal, J., & Poulos, T. L. (1998, December). Identification of two electron-transfer sites in ascorbate peroxidase using chemical modification, enzyme kinetics, and crystallography. *Biochemistry*, *37*(50), 17610–17617.

Mannella, C. A. (2006, February). The relevance of mitochondrial membrane topology to mitochondrial function. *Biochimica et biophysica acta*, *1762*(2), 140–147.

Martell, J. D., Deerinck, T. J., Sancak, Y., Poulos, T. L., Mootha, V. K., Sosinsky, G. E., ... Ting, A. Y. (2012, November). Engineered ascorbate peroxidase as a genetically encoded reporter for electron microscopy. *Nature Biotechnology*, *30*(11), 1143–1148.

Martin, J., Mahlke, K., & Pfanner, N. (1991, September). Role of an energized inner membrane in mitochondrial protein import. Delta psi drives the movement of presequences. *Journal of Biological Chemistry*, *266*(27), 18051–18057.

Meeusen, S., DeVay, R., Block, J., Cassidy-Stone, A., Wayson, S., McCaffery, J. M., & Nunnari, J. (2006, October). Mitochondrial inner-membrane fusion and crista maintenance requires the dynamin-related GTPase Mgm1. *Cell*, *127*(2), 383–395.

Mehnert, C. S., Rampelt, H., Gebert, M., Oeljeklaus, S., Schrempp, S. G., Kochbeck,

L., ... van der Laan, M. (2014, September). The mitochondrial ADP/ATP carrier associates with the inner membrane presequence translocase in a stoichiometric manner. *The Journal of biological chemistry*, *289*(39), 27352–27362.

Meisinger, C., Pfanner, N., & Truscott, K. N. (2006). Isolation of yeast mitochondria. *Methods in molecular biology (Clifton, N.J.)*, *313*, 33–39.

Melin, J., Kilisch, M., Neumann, P., Lytovchenko, O., Gomkale, R., Schendzielorz, A., ... Schulz, C. (2015, August). A presequence-binding groove in Tom70 supports import of Mdl1 into mitochondria. *Biochimica et biophysica acta*, *1853*(8), 1850–1859.

Michaud, M., Gros, V., Tardif, M., Brugière, S., Ferro, M., Prinz, W. A., ... Jouhet, J. (2016, March). AtMic60 Is Involved in Plant Mitochondria Lipid Trafficking and Is Part of a Large Complex. *Current Biology*, *26*(5), 627–639.

Mick, D. U., Dennerlein, S., Wiese, H., Reinhold, R., Pacheu-Grau, D., Lorenzi, I., ... Rehling, P. (2012, December). MITRAC links mitochondrial protein translocation to respiratory-chain assembly and translational regulation. *Cell*, *151*(7), 1528–1541.

Mick, D. U., Fox, T. D., & Rehling, P. (2011, January). Inventory control: cytochrome c oxidase assembly regulates mitochondrial translation. *Nature reviews. Molecular cell biology*, *12*(1), 14–20.

Milenkovic, D., & Larsson, N.-G. (2015, May). Mic10 Oligomerization Pinches off Mitochondrial Cristae. *Cell Metabolism*, *21*(5), 660–661.

Milenkovic, D., Ramming, T., Müller, J. M., Wenz, L.-S., Gebert, N., Schulze-Specking, A., ... Chacinska, A. (2009, May). Identification of the signal directing Tim9 and Tim10 into the intermembrane space of mitochondria. *Molecular biology of the cell*, *20*(10), 2530–2539.

Mishra, P., & Chan, D. C. (2014, October). Mitochondrial dynamics and inheritance during cell division, development and disease. *Nature reviews. Molecular cell biology*, *15*(10), 634–646.

Model, K., Meisinger, C., & Kühlbrandt, W. (2008, November). Cryo-electron microscopy structure of a yeast mitochondrial preprotein translocase. *Journal of Molecular Biology*, *383*(5), 1049–1057.

Mokranjac, D., & Neupert, W. (2015, December). Cell biology: Architecture of a protein entry gate. *Nature*, *528*(7581), 201–202.

Mueller, S. J., & Reski, R. (2015). Mitochondrial Dynamics and the ER: The Plant Perspective. *Frontiers in cell and developmental biology*, *3*(551), 78.

Müller, T. (2014). *Targeted biotinylation of mitochondrial proteins for the identification of transient interactions* (Unpublished doctoral dissertation). University of Göttingen.

Muñoz-Gómez, S. A., Slamovits, C. H., Dacks, J. B., Baier, K. A., Spencer, K. D., & Wideman, J. G. (2015, June). Ancient homology of the mitochondrial contact site and cristae organizing system points to an endosymbiotic origin of mitochondrial cristae. *Current biology : CB*, *25*(11), 1489–1495.

Nijtmans, L. G. J., Taanman, J.-W., Muijsers, A. O., Speijer, D., & Van den Bogert, C. (1998, June). Assembly of cytochrome-c oxidase in cultured human cells. *European journal of biochemistry*, *254*(2), 389–394.

Nooren, I. M. A., & Thornton, J. M. (2003, July). Diversity of protein-protein interactions. *The EMBO Journal*, *22*(14), 3486–3492.

Nunnari, J., & Suomalainen, A. (2012, March). Mitochondria: In Sickness and in Health. *Cell*, *148*(6), 1145–1159.

Olichon, A., Baricault, L., Gas, N., Guillou, E., Valette, A., Belenguer, P., & Lenaers, G. (2003, March). Loss of OPA1 perturbates the mitochondrial inner membrane structure and integrity, leading to cytochrome c release and apoptosis. *Journal of Biological Chemistry*, *278*(10), 7743–7746.

Osman, C., Voelker, D. R., & Langer, T. (2011, January). Making heads or tails of phospholipids in mitochondria. *J. Cell Biol.*, *192*(1), 7–16.

Ott, C., Dorsch, E., Fraunholz, M., Straub, S., & Kozjak-Pavlovic, V. (2015). Detailed analysis of the human mitochondrial contact site complex indicate a hierarchy of subunits. *PLOS ONE*, *10*(3), e0120213.

Ott, C., Ross, K., Straub, S., Thiede, B., Gotz, M., Goosmann, C., ... Kozjak-Pavlovic, V. (2012, February). Sam50 Functions in Mitochondrial Intermembrane Space Bridging and Biogenesis of Respiratory Complexes. *Molecular and Cellular Biology*, *32*(6), 1173–1188.

Ott, M., & Herrmann, J. M. (2010, June). Co-translational membrane insertion of mitochondrially encoded proteins. *Biochimica et biophysica acta*, *1803*(6), 767–775.

Pagliarini, D. J., Calvo, S. E., Chang, B., Sheth, S. A., Vafai, S. B., Ong, S.-E., ... Mootha, V. K. (2008, July). A mitochondrial protein compendium elucidates complex I disease biology. *Cell*, *134*(1), 112–123.

Palade, G. E. (1964, August). The Organization of Living matter. *Proceedings of the National Academy of Sciences*, *52*(2), 613–634.

Papic, D., Krumpe, K., Dukanovic, J., Dimmer, K. S., & Rapaport, D. (2011, August). Multispan mitochondrial outer membrane protein Ugo1 follows a unique Mim1-dependent import pathway. *J. Cell Biol.*, *194*(3), 397–405.

Paschen, S. A., Waizenegger, T., Stan, T., Preuss, M., Cyrklaff, M., Hell, K., ... Neupert, W. (2003, December). Evolutionary conservation of biogenesis of beta-barrel membrane proteins. *Nature*, *426*(6968), 862–866.

Paumard, P., Vaillier, J., Coulary, B., Schaeffer, J., Soubannier, V., Mueller, D. M., ... Velours, J. (2002, February). The ATP synthase is involved in generating mitochondrial cristae morphology. *The EMBO Journal*, *21*(3), 221–230.

Perocchi, F., Jensen, L. J., Gagneur, J., Ahting, U., von Mering, C., Bork, P., ... Steinmetz, L. M. (2006, October). Assessing systems properties of yeast mitochondria through an interaction map of the organelle. *PLoS genetics*, *2*(10), e170.

Popov-Celeketić, J., Waizenegger, T., & Rapaport, D. (2008, February). Mim1 functions in an oligomeric form to facilitate the integration of Tom20 into the mitochondrial outer membrane. *Journal of Molecular Biology*, *376*(3), 671–680.

Qiu, J., Wenz, L.-S., Zerbes, R. M., Oeljeklaus, S., Bohnert, M., Stroud, D. A., ... Becker, T. (2013, August). Coupling of mitochondrial import and export translocases by receptor-mediated supercomplex formation. *Cell*, *154*(3), 596–608.

Rabl, R., Soubannier, V., Scholz, R., Vogel, F., Mendl, N., Vasiljev-Neumeyer, A., ... Reichert, A. S. (2009, June). Formation of cristae and crista junctions in mitochondria depends on antagonism between Fcj1 and Su e/g. *The Journal of Cell Biology*, *185*(6), 1047–1063.

Rampelt, H., Bohnert, M., Zerbes, R. M., Horvath, S. E., Warscheid, B., Pfanner, N., & van der Laan, M. (2017, March). Mic10, a Core Subunit of the Mitochondrial Contact Site and Cristae Organizing System, Interacts with the Dimeric F1Fo-ATP Synthase. *Journal of Molecular Biology*.

Rampelt, H., & van der Laan, M. (2017, August). The Yin & Yang of Mitochondrial Architecture - Interplay of MICOS and F1Fo-ATP synthase in cristae formation. *Microbial Cell*, *4*(8), 236–239.

Rampelt, H., Wollweber, F., Gerke, C., de Boer, R., van der Klei, I. J., Bohnert, M., ... van der Laan, M. (2018, June). Assembly of the Mitochondrial Cristae Organizer Mic10 Is Regulated by Mic26–Mic27 Antagonism and Cardiolipin. *Journal of Molecular Biology*, *430*(13), 1883–1890.

Rampelt, H., Zerbes, R. M., van der Laan, M., & Pfanner, N. (2016, September). Role of the mitochondrial contact site and cristae organizing system in membrane

architecture and dynamics. *Biochimica et biophysica acta*.

Ran, F. A., Hsu, P. D., Wright, J., Agarwala, V., Scott, D. A., & Zhang, F. (2013, November). Genome engineering using the CRISPR-Cas9 system. *Nature protocols*, *8*(11), 2281–2308.

Raven, E. L., Lad, L., Sharp, K. H., Mewies, M., & Moody, P. C. E. (2004). Defining substrate specificity and catalytic mechanism in ascorbate peroxidase. *Biochemical Society symposium*(71), 27–38.

Renken, C., Siragusa, G., Perkins, G., Washington, L., Nulton, J., Salamon, P., & Frey, T. G. (2002, April). A thermodynamic model describing the nature of the crista junction: a structural motif in the mitochondrion. *Journal of structural biology*, *138*(1-2), 137–144.

Rhee, H.-W., Zou, P., Udeshi, N. D., Martell, J. D., Mootha, V. K., Carr, S. A., & Ting, A. Y. (2013, March). Proteomic mapping of mitochondria in living cells via spatially restricted enzymatic tagging. *Science*, *339*(6125), 1328–1331.

Richter, F., Dennerlein, S., Nikolov, M., Jans, D. C., Naumenko, N., Aich, A., ... Rehling, P. (2019, February). ROMO1 is a constituent of the human presequence translocase required for YME1L protease import. *J. Cell Biol.*, *218*(2), 598–614.

Rissler, M., Wiedemann, N., Pfannschmidt, S., Gabriel, K., Guiard, B., Pfanner, N., & Chacinska, A. (2005, October). The essential mitochondrial protein Erv1 cooperates with Mia40 in biogenesis of intermembrane space proteins. *Journal of Molecular Biology*, *353*(3), 485–492.

Roux, K. J., Kim, D. I., Burke, B., & May, D. G. (2018, February). BioID: A Screen for Protein-Protein Interactions. *Current protocols in protein science*, *91*, 19.23.1–19.23.15.

Roux, K. J., Kim, D. I., Raida, M., & Burke, B. (2012, March). A promiscuous biotin ligase fusion protein identifies proximal and interacting proteins in mammalian cells. *The Journal of Cell Biology*, *196*(6), 801–810.

Saddar, S., & Stuart, R. A. (2005, July). The yeast F(1)F(0)-ATP synthase: analysis of the molecular organization of subunit g and the importance of a conserved GXXXG motif. *Journal of Biological Chemistry*, *280*(26), 24435–24442.

Sakowska, P., Jans, D. C., Mohanraj, K., Riedel, D., Jakobs, S., & Chacinska, A. (2015, September). The oxidation status of Mic19 regulates MICOS assembly. *Molecular and Cellular Biology*, MCB.00578–15–16.

Sambrook, J., & Russel, D. W. (2001). *Molecular Cloning*. CSHL Press.

Saraste, M. (1999, March). Oxidative phosphorylation at the fin de siècle. *Science*,

283(5407), 1488–1493.

Schendzielorz, A. B., Schulz, C., Lytovchenko, O., Clancy, A., Guiard, B., Ieva, R., ... Rehling, P. (2017, January). Two distinct membrane potential-dependent steps drive mitochondrial matrix protein translocation. *The Journal of Cell Biology*, *216*(1), 83–92.

Schlossmann, J., Dietmeier, K., Pfanner, N., & Neupert, W. (1994, April). Specific recognition of mitochondrial preproteins by the cytosolic domain of the import receptor MOM72. *Journal of Biological Chemistry*, *269*(16), 11893–11901.

Schopp, I. M., & Béthune, J. (2018, April). Split-BioID - Proteomic Analysis of Context-specific Protein Complexes in Their Native Cellular Environment. *Journal of visualized experiments : JoVE*(134).

Schulz, C., Schendzielorz, A., & Rehling, P. (2015, May). Unlocking the presequence import pathway. *Trends in Cell Biology*, *25*(5), 265–275.

Sesaki, H., Southard, S. M., Yaffe, M. P., & Jensen, R. E. (2003, June). Mgm1p, a dynamin-related GTPase, is essential for fusion of the mitochondrial outer membrane. *Molecular biology of the cell*, *14*(6), 2342–2356.

Sharp, K. H., Mewies, M., Moody, P. C. E., & Raven, E. L. (2003, March). Crystal structure of the ascorbate peroxidase–ascorbate complex. *Nature Structural Biology*, *10*(4), 303–307.

Shiota, T., Imai, K., Qiu, J., Hewitt, V. L., Tan, K., Shen, H.-H., ... Endo, T. (2015, September). Molecular architecture of the active mitochondrial protein gate. *Science*, *349*(6255), 1544–1548.

Shiota, T., Mabuchi, H., Tanaka-Yamano, S., Yamano, K., & Endo, T. (2011, September). In vivo protein-interaction mapping of a mitochondrial translocator protein Tom22 at work. *Proceedings of the National Academy of Sciences of the United States of America*, *108*(37), 15179–15183.

Sickmann, A., Reinders, J., Wagner, Y., Joppich, C., Zahedi, R., Meyer, H. E., ... Meisinger, C. (2003, November). The proteome of Saccharomyces cerevisiae mitochondria. *Proceedings of the National Academy of Sciences*, *100*(23), 13207–13212.

Sideris, D. P., Petrakis, N., Katrakili, N., Mikropoulou, D., Gallo, A., Ciofi-Baffoni, S., ... Tokatlidis, K. (2009, December). A novel intermembrane space-targeting signal docks cysteines onto Mia40 during mitochondrial oxidative folding. *J. Cell Biol.*, *187*(7), 1007–1022.

Simbeni, R., Pon, L., Zinser, E., Paltauf, F., & Daum, G. (1991, June). Mitochondrial membrane contact sites of yeast. Characterization of lipid components and possi-

ble involvement in intramitochondrial translocation of phospholipids. *Journal of Biological Chemistry*, *266*(16), 10047–10049.

Sjuts, I., Soll, J., science, B. B. F. i. p., & 2017. (n.d.). Import of soluble proteins into chloroplasts and potential regulatory mechanisms. *frontiersin.org*.

Stojanovski, D., Pfanner, N., & Wiedemann, N. (2007, January). Import of proteins into mitochondria. *Methods Cell Biol.*, *80*, 783–806.

Strauss, M., Hofhaus, G., Schröder, R. R., & Kühlbrandt, W. (2008, April). Dimer ribbons of ATP synthase shape the inner mitochondrial membrane. *The EMBO Journal*, *27*(7), 1154–1160.

Tarasenko, D., Barbot, M., Jans, D. C., Kroppen, B., Sadowski, B., Heim, G., ... Meinecke, M. (2017, March). The MICOS component Mic60 displays a conserved membrane-bending activity that is necessary for normal cristae morphology. *The Journal of Cell Biology*.

Tatsuta, T., & Langer, T. (2017, January). Intramitochondrial phospholipid trafficking. *BBA - Molecular and Cell Biology of Lipids*, *1862*(1), 81–89.

Thomas, D., Bron, P., Weimann, T., Dautant, A., Giraud, M.-F., Paumard, P., ... Brèthes, D. (2008, October). Supramolecular organization of the yeast F1Fo-ATP synthase. *Biology of the cell*, *100*(10), 591–601.

Trinkle-Mulcahy, L. (2019). Recent advances in proximity-based labeling methods for interactome mapping. *F1000Research*, *8*.

Tzagoloff, A. (1995). Ubiquinol-cytochrome-c oxidoreductase from Saccharomyces cerevisiae. *Methods in enzymology*, *260*, 51–63.

Uezu, A., Kanak, D. J., Bradshaw, T. W. A., Soderblom, E. J., Catavero, C. M., Burette, A. C., ... Soderling, S. H. (2016, September). Identification of an elaborate complex mediating postsynaptic inhibition. *Science*, *353*(6304), 1123–1129.

van der Laan, M., Bohnert, M., Wiedemann, N., & Pfanner, N. (2012, April). Role of MINOS in mitochondrial membrane architecture and biogenesis. *Trends Cell Biol.*, *22*(4), 185–192.

van der Laan, M., Meinecke, M., Dudek, J., Hutu, D. P., Lind, M., Perschil, I., ... Rehling, P. (2007, October). Motor-free mitochondrial presequence translocase drives membrane integration of preproteins. *Nature Cell Biology*, *9*(10), 1152–1159.

van Wilpe, S., Ryan, M. T., Hill, K., Maarse, A. C., Meisinger, C., Brix, J., ... Pfanner, N. (1999, September). Tom22 is a multifunctional organizer of the mitochondrial preprotein translocase. *Nature*, *401*(6752), 485–489.

Velours, J., Dautant, A., Salin, B. e. n. e. d., Sagot, I., & Br e thes, D. (2009, October). Mitochondrial F1F0-ATP synthase and organellar internal architecture. *Int. J. Biochem. Cell Biol.*, *41*(10), 1783–1789.

Velours, J., Paumard, P., Soubannier, V., Spannagel, C., Vaillier, J., Arselin, G., & Graves, P. V. (2000, May). Organisation of the yeast ATP synthase F(0):a study based on cysteine mutants, thiol modification and cross-linking reagents. *Biochimica et biophysica acta*, *1458*(2-3), 443–456.

Vogel, F., Bornhövd, C., Neupert, W., & Reichert, A. S. (2006, October). Dynamic subcompartmentalization of the mitochondrial inner membrane. *The Journal of Cell Biology*, *175*(2), 237–247.

Vögtle, F.-N., Wortelkamp, S., Zahedi, R. P., Becker, D., Leidhold, C., Gevaert, K., ... Meisinger, C. (2009, October). Global analysis of the mitochondrial N-proteome identifies a processing peptidase critical for protein stability. *Cell*, *139*(2), 428–439.

Volkov, A. N., & van Nuland, N. A. J. (2012). Electron transfer interactome of cytochrome C. *PLoS computational biology*, *8*(12), e1002807.

von der Malsburg, K., Müller, J. M., Bohnert, M., Oeljeklaus, S., Kwiatkowska, P., Becker, T., ... van der Laan, M. (2011, October). Dual Role of Mitofilin in Mitochondrial Membrane Organization and Protein Biogenesis. *Developmental Cell*, *21*(4), 694–707.

Vukotic, M., Nolte, H., König, T., Saita, S., Ananjew, M., Krüger, M., ... Langer, T. (2017, August). Acylglycerol Kinase Mutated in Sengers Syndrome Is a Subunit of the TIM22 Protein Translocase in Mitochondria. *Molecular Cell*, *67*(3), 471–483.e7.

Wagner, K., Mick, D. U., & Rehling, P. (2009, January). Protein transport machineries for precursor translocation across the inner mitochondrial membrane. *Biochimica et biophysica acta*, *1793*(1), 52–59.

Wang, C., & Youle, R. J. (2009). The role of mitochondria in apoptosis*. *Annual review of genetics*, *43*(1), 95–118.

Weber, T. A., Koob, S., Heide, H., Wittig, I., Head, B., van der Bliek, A., ... Reichert, A. S. (2013). APOOL is a cardiolipin-binding constituent of the Mitofilin/MINOS protein complex determining cristae morphology in mammalian mitochondria. *PLOS ONE*, *8*(5), e63683.

Weinhäupl, K., Lindau, C., Hessel, A., Wang, Y., Schütze, C., Jores, T., ... Schanda, P. (2018, November). Structural Basis of Membrane Protein Chaperoning through

the Mitochondrial Intermembrane Space. *Cell*, *175*(5), 1365–1379.e25.

Weiss, H., Friedrich, T., Hofhaus, G., & Preis, D. (1991, May). The respiratory-chain NADH dehydrogenase (complex I) of mitochondria. *European journal of biochemistry*, *197*(3), 563–576.

Werner, S., & Neupert, W. (1972, February). Functional and biogenetical heterogeneity of the inner membrane of rat-liver mitochondria. *European journal of biochemistry*, *25*(2), 379–396.

Wiedemann, N., & Pfanner, N. (2017, June). Mitochondrial Machineries for Protein Import and Assembly. *Annual review of biochemistry*, *86*(1), 685–714.

Wiedemann, N., Truscott, K. N., Pfannschmidt, S., Guiard, B., Meisinger, C., & Pfanner, N. (2004, April). Biogenesis of the protein import channel Tom40 of the mitochondrial outer membrane: intermembrane space components are involved in an early stage of the assembly pathway. *Journal of Biological Chemistry*, *279*(18), 18188–18194.

Wittig, I., Velours, J., Stuart, R., & Schägger, H. (2008, May). Characterization of domain interfaces in monomeric and dimeric ATP synthase. *Molecular & cellular proteomics : MCP*, *7*(5), 995–1004.

Wong, E. D., Wagner, J. A., Scott, S. V., Okreglak, V., Holewinske, T. J., Cassidy-Stone, A., & Nunnari, J. (2003, February). The intramitochondrial dynamin-related GTPase, Mgm1p, is a component of a protein complex that mediates mitochondrial fusion. *The Journal of Cell Biology*, *160*(3), 303–311.

Xie, J., Marusich, M. F., Souda, P., Whitelegge, J., & Capaldi, R. A. (2007, July). The mitochondrial inner membrane protein mitofilin exists as a complex with SAM50, metaxins 1 and 2, coiled-coil-helix coiled-coil-helix domain-containing protein 3 and 6 and DnaJC11. *FEBS Letters*, *581*(18), 3545–3549.

Young, J. C., Hoogenraad, N. J., & Hartl, F. U. (2003, January). Molecular chaperones Hsp90 and Hsp70 deliver preproteins to the mitochondrial import receptor Tom70. *Cell*, *112*(1), 41–50.

Zerbes, R. M., Bohnert, M., Stroud, D. A., von der Malsburg, K., Kram, A., Oeljeklaus, S., ... van der Laan, M. (2012, September). Role of MINOS in Mitochondrial Membrane Architecture: Cristae Morphology and Outer Membrane Interactions Differentially Depend on Mitofilin Domains. *Journal of Molecular Biology*, *422*(2), 183–191.

Zerbes, R. M., Höß, P., Pfanner, N., van der Laan, M., & Bohnert, M. (2016, March). Distinct roles of Mic12 and Mic27 in the mitochondrial contact site and cristae

organizing system. *Journal of Molecular Biology*.

Zorova, L. D., Popkov, V. A., Plotnikov, E. Y., Silachev, D. N., Pevzner, I. B., Jankauskas, S. S., ... Zorov, D. B. (2018, July). Mitochondrial membrane potential. *Analytical Biochemistry*, *552*, 50–59.